A Planar Penning trap

Fernando Galve Conde

Institut für Physik

Johannes Gutenberg Universität, Mainz

A thesis submitted for the degree of

Doktor der Naturwissenschaften

Abstract

In this thesis I present theoretical and experimental results concerning the operation and properties of a new kind of Penning trap, the planar trap. It consists of circular electrodes printed on an isolating surface, with an homogeneous magnetic field pointing perpendicular to that surface. The motivation of such geometry is to be found in the construction of an array of planar traps for quantum informational purposes. The open access to radiation of this geometry, and the long coherence times expected for Penning traps, make the planar trap a good candidate for quantum computation. Several proposals for quantum 2-qubit interactions are studied and estimates for their rates are given.

An expression for the electrostatic potential is presented, and its features exposed. A detailed study of the anharmonicity of the potential is given theoretically and is later demonstrated by experiment and numerical simulations, showing good agreement.

Size scalability of this trap has been studied by replacing the original planar trap by a trap twice smaller in the experimental setup. This substitution shows no scale effect apart from those expected for the scaling of the parameters of the trap. A smaller lifetime for trapped electrons is seen for this smaller trap, but is clearly matched to a bigger misalignment of the trap's surface and the magnetic field, due to its more difficult hand manipulation.

I also give a hint that this trap may be of help in studying non-linear dynamics for a sextupolarly perturbed Penning trap.

Contents

CONTENTS

Chapter 1

Introduction

The search for a physical system having the properties required for quantum computing has been the philosopher's stone for quite some years, as can be seen from extensive literature (Cirac; Gershenfeld; Kane; Loss; Freedman; Makhlin; Tombesi). Apart from condensed-matter devices such as quantum dots, Josephson junctions,etc. and NMR (nuclear magnetic resonance), which has already achieved the factorisation of the number 15, storing devices such as optical traps and Paul and Penning traps seem to be good candidates for the short term research in the field, and have been proven to be so. The relatively good isolation of trapped particles from their environment is a major advantage and has given already enough results to the physics community so as to be regarded a promising branch. In the next section I'll discuss the panorama in both quantum computation and the branch of trap physics in the sense of usable techniques for developing a quantum processor.

1.1 Quantum Computing

Since the birth of computation as a science, mankind has seen the dawn of a new experience; till that moment mathematicians and natural scientists had always thought of solutions to their problems as entities which were eternally existing and only had to be found by the human mind, sometimes in an instantaneous flash of inspiration. With the introduction of the concept of the Turing machine (an equivalent process took place in pure mathematics and gave place to the

1. INTRODUCTION

famous Gödel's theorem(Gödel)) there came a new question and perspective: the way of getting to the solution of a mathematical problem is always, at least for us humans- and we are beginning to suspect that it is so in principle-, a physical process, the one in our brains, the transistors in a computer, the abacus, etc. A little bridge between the world of ideas and that of nature has been established.

To the question: "can this problem be solved?" there were, before computation, only two answers: yes or no. Now there can be another one: "who knows? a conceivable nowadays computer would need more than 20 times the age of the Universe for the solution". The example here makes us think what would happen if the Universe was to last less than the time needed for the best-ever-buildable-computer-for-this-universe to compute the answer of a given problem; and then the matter of principle comes: does the answer of that problem exist in the world of ideas but it's unaccessible?, or have we proven with the above argument that such solution exists not?

Not only a philosophical discussion can be raised at this point -i.e. "cognizability" in this reality- but mathematical proofs have been given by Gödel (in logical systems) Turing(Turing), and Chaitin(Chaitin) (in terms of computability as thought by Turing) concerning the undecidability of certain propositions inside a logical system of truths. I will not insist on these points since it is not the subject of my thesis, but these authors have demonstrated that a system of truths can never be complete and needs always a bigger system of truths including yours in order to complete this lack; and that's universal!

Of course there were always two type of scientists, those closer to the philosopher, the mystic, the Michelangelo,etc, and those closer to the engineer, at the service of the little king. Knowledge has always been a double-edged sword: on the one hand it gives wisdom to those who are able to apprehend it, and on the other, it gives power to crush the weak (let's not forget that ignorance is a kind of weakness). And that's precisely why any new scientific knowledge has first served war purposes, and after the war had ended, it has served the whole of mankind. An easy example has been the discovery in the past century of nuclear reactions and its energy liberating capacity. A new hint of this traditional reality can be seen to be coming with the advent of quantum computing and its capacity to uncover, when we manage to master its power, the cryptographic codes of the

enemy. An evidence to this fact is that all first-world governments are investing enormous amounts of money to this field, which is rather suspicious...

1.1.1 A little bit of history

Since the introduction by Turing of its ideal computing machine(1936)(Turing), a purely mathematical and abstract field, known as information theory, the concepts of logic, "mind", computability,etc. have been raised to a new category, that of a physical process. From that moment on, physicists have been working not only in the implementation of those ideas in order to physically manage their power, but also in the understanding of its significance in terms of physical laws and reality: is information a physical entity?

A relation between the information a physical system contains and its entropy was given by Shannon (1948s)(Shannon) and it was proved to be a fundamental relation. Since then, and after much effort, the science of information theory became well established, furthermore by the modern physical implementation of a computer, which has the universality of a Turing machine and proves its inherent power.

The birth of quantum mechanics, at the beginning of the past century, however, added a new window through which to look at reality in terms of a whole lot of new physical laws. The question then arose, whether this new aspect of physical processes would make any difference regarding information theory, and hence quantum information theory was born.

After Bell's analysis of the EPR (Einstein-Rosen-Podolsky) paradox in 1964(Bell), and its many experimental demonstrations in the 1970s, and also with the experiment by Aspect et al.(1982)(Aspect), an important fact became obvious: quantum mechanics allows for a new type of information encoding mechanism, entanglement. This fact can be exposed in another fashion: it had been demonstrated that quantum mechanics allows for a bigger amount of mutual information between systems than that in classical information theory. Of course this is a difference of principle and led, among other things, to the birth of a new way of formulating the principles of quantum mechanics in terms of the amount

1. INTRODUCTION

of information that quantum systems can exchange, i.e. physical systems became nothing more than information containers and physical states are *states of knowledge* (for a nice exposition of the idea see (Zeilinger)). That on the plane of theory, but in a much more practical view of things, entanglement meant that quantum mechanics might lead to a more powerful kind of computation than the classical one. Anyway, it was not clear at all at the beginning how a quantum system could be used to produce a better computation, since at the end of the process the physicist should have to collapse the quantum state of the computer into a chain of classical bits, thus apparently gaining nothing.

Benioff (1980)(Benioff) showed that a quantum Hamiltonian could, at least, mimic the operation of a universal Turing machine. An this was only the beginning. In 1985 Deutsch proposed a set of 2-state systems in a row, which after being applied a specific small set of operation, could be shown to develop *any* unitary evolution, and therefore the ability of this system as a quantum physical simulator(Deutsch). He also discussed how to produce Turing-like behaviour using the same ideas.

But it was in the 1990s that computational tasks were found which could be done more efficiently by a quantum computer than a classical one. The factorization of large integers by Shor's algorithm (1994)(Shor) based on a method for doing fast Fourier transforms (Coppersmith 1994(Coppersmith), and Deutsch 1994 unpublished) was one of them. Grover's algorithm (1997) for finding an element in a long list of elements(Grover), and Kitaev's algorithm for the Abelian stabilizer problem (1995) were others(Kitaev).

Having shown to the scientific community that quantum algorithms were possible and that some of them were much more efficient than their classical counterparts, added to the studies in quantum error correction, it was a matter of time that efforts were dedicated to the experimental implementation of those ideas.

Another important fact which I haven't discussed yet is the quest for a deeper understanding of the nature of quantum mechanics related to the measurement postulate. Since this postulate is an *ad hoc* one and no proof of principle of it has yet been given , despite the efforts of quite a variety of physicists, in terms of dynamical quantum laws, and given its relation to the main core of quantum computation -entanglement-, scientists have been avid to realize experimentally a

quantum computer. The search for a better understanding of the meaning of entanglement provided by a thorough experimentation and control of the quantum regime had begun.

The need for entanglement to be conserved during the operation of a quantum computer unveils a major experimental difficulty: the computer has to be sufficiently isolated from its environment! And I say "sufficiently" because, to the extent of my knowledge of physics, no system is really isolated from anything else in the universe (it's a known reality that the wave function of a system extends until infinity, and so is shared by the rest of objects in the universe). This transforms the task of building a quantum computer into the search for isolating methods. Such isolation has been only achieved in trapped particle systems, despite the success of fields such as NMR (nuclear magnetic resonance) in quantum-factorizing integers. And this is the main reason that trapped-particle physics is nowadays regarded as the best promising tool in order to implement quantum information ideas. It's clear, nevertheless, that operation of 100 qubits (a qubit is the quantum equivalent of a classical bit) in a controlled and useful way, is yet a subject for science fiction, but experimental implementation of up to 10 qubits seems to be accessible in the near future and may prove sufficient to understand the basics of this new tool.

In next section I will introduce the field of trap physics and it's relation to quantum computation, as well as its first successful realization of quantum gates.

1.2 Trap Physics

The history of trap physics began as the search to extend the lifetime of an electrical discharge (Penning, 1936). Its natural continuation followed by the invention of the so called Pennning trap by Hans Georg Dehmelt, and by the invention of the Paul trap by Wolfgang Paul, who shared the Nobel Prize in 1989 together with Norman F. Ramsey for their work on ion traps.

From that point on, traps have been used as instruments of precision for measuring quantities such as the g-factor(Werth), hyperfine structures, lifetimes of excited states, atomic clocks, inertial mass(Dyck; Blaum), atomic transition

1. INTRODUCTION

lines, etc. whose stringent results have confirmed quantum electrodynamics to a great degree of accuracy.

A Penning trap consists of an ideally quadrupolar electrostatic field together with an homogeneous magnetic field. The electrostatic field provides confinement in one spatial direction and the magnetic field in the remaining two. The magnetic field is required since Laplace's electrostatic equation doesn't permit absolute potential minima in the absence of free charges. A roundabout for this consists in alternating the sign of the complete potential and dispense with the magnetic field. The latter configuration is the definition of the Paul trap[1].

In Figure 1.1 we see typical schemes for both Paul and Penning configurations of an ion trap.
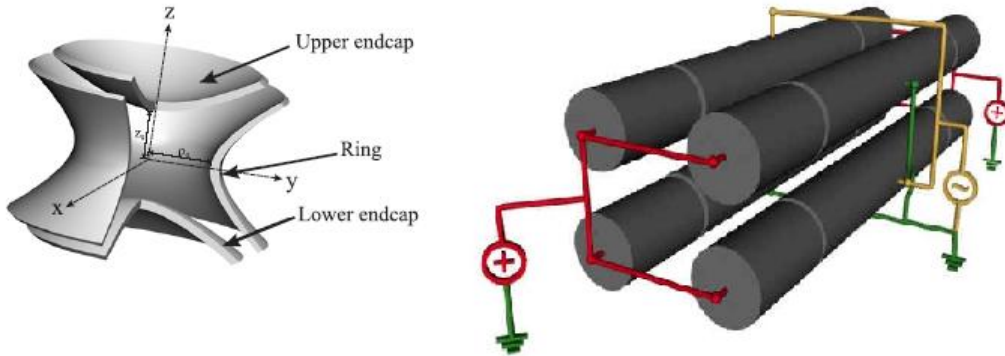
Figure 1.1: **Left**: Hyperbolical electrodes can be used with voltage V on endcaps and -V on ring electrode plus a magnetic field along z (Penning configuration). If the voltage signs are changed in time and the magnetic field removed, we have a Paul configuration. **Right**: Paul configuration with cylindrical electrodes. Note that static positive voltages are needed at the extremes for trapped particles not to be lost along the symmetry axis.

Special efforts have been dedicated along the years to improve the performance of traps, such as perfecting cooling methods, removing trap's electrodes

---

[1]There are other types of ion traps such as the Kingdon trap, but they are the most common. In addition, not only ion traps exist, but also traps for neutral particles such as the optical traps (also known as optical tweezers), which rely on dipolar forces produced by stationary laser light waves.

imperfections, increasing the accuracy of the detection methods and studying the effect of different radiations coupled to the motion of trapped particles.

Since the field of trap physics is broad enough to constitute in its own right a branch of physics, I will not try to summarize it but will take the main ideas for the operation of a Penning trap and elaborate from there our contribution to the field by showing how a planar Penning trap is similar to the standard but at the same time has some interesting features of its own.

As seen in Figure 1.1, a Penning trap consists of hyperbolical electrodes, ideally extending to infinity, which yield an electrostatic quadrupolar potential. Its stable eigendirection is usually named z and yields a unique eigenfrequency called ω_z. Confinement on the radial plane, perpendicular to z, is given by an homogeneous magnetic field $\vec{B} = B_z \hat{u}_z$. This further radial confinement yields another two eigenfrequencies called respectively reduced *cyclotron* (ω_+) and *magnetron* (ω_-). Figure 1.2 shows the trajectory of particle trapped in such configuration for the case of the three eigenfrequencies being similar in magnitude.

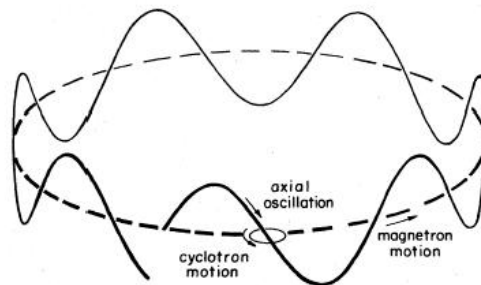Figure 1.2: Illustration of the three eigenmotions of a particle inside a Penning trap.

The system is equivalent to three independent harmonic oscillators. The independence of those oscillators occurs only in ideality, and the general situation is that all oscillators are coupled. If the stored particle has a non-zero spin its precession in the magnetic field has to be included. Several methods have been

developed in trap physics concerning these couplings, either for reducing their negative effects or for amplifying their positive counterparts.

1.2.1 Motion of one trapped particle

The equations of motion for a single particle trapped in a quadrupolar electrostatic field $\phi(\rho, z) = \frac{V_0}{2d^2}(z^2 - \rho^2/2)$ plus a homogeneous magnetic field are obtained most easily from the Lorentz force:

$$\vec{F} = q(\vec{E} + \vec{v} \times \vec{B}) \tag{1.1}$$

where q is the charge, $\vec{v}$ is the velocity vector, and $\vec{B}$ is the magnetic field. Since $\vec{B} = B\hat{u}_z$, the magnetic force affects only the motion on the radial plane, and thus the motion in z is governed by

$$\ddot{z} = \frac{q}{m}E_z = -\frac{qV_0}{md^2}z \tag{1.2}$$

which is just the equation for a harmonic oscillator with frequency

$$\omega_z = \sqrt{\frac{qV_0}{md^2}} \tag{1.3}$$

Notice that I didn't define what V_0 and d are. For a standard hyperbolical Penning trap V_0 is the voltage difference between ring and endcap electrodes, and d is a parameter relating the relative positions of the electrodes. But in general they will depend on the geometry given to the electrodes, and because of this we will regard them as just parameters which give the scale for voltages and lengths.

Despite the axial motion being decoupled from $\vec{B}$, the remaining degrees of freedom get coupled through its influence:

$$\ddot{x} = \frac{q}{m}(B\dot{y} - \frac{V_0}{2d^2}x) \tag{1.4}$$

$$\ddot{y} = -\frac{q}{m}(B\dot{x} + \frac{V_0}{2d^2}y) \tag{1.5}$$

, but can be uncoupled through the new variable $u = x + iy$. Defining $\omega_c = qB/m$ we obtain a single equation from the two equations above:

$$\ddot{u} + i\omega_c\dot{u} + \frac{\omega_z^2}{2}u = 0 \tag{1.6}$$

Solving this equation yields two uncoupled harmonic oscillators of frequencies

$$\omega_{\pm} = \frac{\omega_c}{2} \pm \sqrt{\frac{\omega_c}{4} - \frac{\omega_z^2}{2}} \tag{1.7}$$

which we have already mentioned above by the name of "reduced cyclotron" and "magnetron" frequencies.

1.2.2   Motion of a cloud of trapped particles

The situation is however quite different when instead of a single particle, we have a cloud of them. The idealization regarding a perfect quadrupolar potential or a perfect homogeneous magnetic field can be achieved in a real experiment with voltage compensation and shimming coils, respectively. That makes the treatment above almost exactly what happens in a well devised experiment.

However, when a cloud of particles is trapped, electrons interact with each other via Coulomb with a strength related to their spatial density. There's no experimental way we can avoid or compensate this fact. This makes the picture of three independent harmonic oscillators per trapped particle become false. Since the Coulomb interaction will couple all degrees of freedom of all trapped particles, a new description of the situation is needed.

It is clear that we cannot expect solving the equation of motion of , let's say, 1000 particles Coulomb-interacting in an analytic fashion, but still, some information can be gathered. In fact, just by modeling the cloud of particles by a uniformly charged sphere (which is sufficiently true even for non zero temperatures) we obtain a useful insight: the interaction of a single electron with the charged sphere shifts its axial frequency to lower values in proportion to the charge density of the sphere. Since the field seen by a particle due to that sphere depends on its distance to the center of the sphere, each particle sees a different space charge and its axial frequency is shifted differently. That gives a broad resonance which is asymmetric and shifted as a whole to lower frequencies with respect to ω_z (see (Desaintfuscien) for more details).

But not only that, the cloud as a whole can be excited resonantly , as if it where a unique particle, at the frequency ω_z.

So if we sum up both effects, the resonance of a cloud of trapped particles has two different peaks: one broad peak centered near ω_z but shifted to lower frequencies, which we will call "individual" or "non-collective" resonance, and a narrow peak exactly centered at ω_z which represents the cloud moving as a whole, and which we will name as "center-of-mass" (COM) or "collective" resonance (see (Valenzuela) for an experimental example of this double-peak resonance structure).

1.2.3 Quantum computing with traps

The fact that a trapped particle can be stored during long times, as has been experimentally demonstrated, gives the hope that the experimenter can use such physical system to store a qubit. Further it has been also experimentally demonstrated that a trapped particle can be cooled down to the subKelvin regime with dilution refrigerators, and controlled with radiation(Gabrielse)(laser cooling of trapped particles had been already demonstrated in (Wineland; Dehmelt)).

In the case of a Penning trap there are three harmonic oscillators, with an infinity of quantum levels, and a spin. This gives a choice where to store the quantum information, being the most natural that of the spin.

The universality of a quantum computer becomes proven when it is shown that any 1-qubit rotation (remember that a qubit is a 2-level system and can be always represented by a spin) and a CNOT gate on 2-qubit, can be performed (Deutsch2). Therefore, by choosing from our system two different quantum states and naming them $|0>, |1>$, we need to show that we can transform any of them in *any* superposition of both. Further, we need to show that two systems like these can be made to interact in such way that a CNOT (or *XOR*) gate can be performed on them. Of course, any operation which we apply needs to conserve our quantum systems inside the Hilbert space consisting of $|0>, |1>$, and that's why the spin is always the natural choice for a qubit.

Up to now there have been several experimental demonstrations that these two operations can be done with ion traps. The state of the art, however, has been preceded by Paul traps due to their easy access with radiation and the facility to build a linear array of trapped ions. Two examples are to be found

in (Wineland2) and (Blatt), where implementation of two qubit gates has been already performed. Teleportation and other quantum information related topics have also been addressed by these groups, so the reader can refer to them for more information. However, the fact that linear traps use time-dependent fields leads to heating of the trapped particles, thus limiting the coherence time.

In next section I show a proposal worked out by the QUELE network (funded by EU) for quantum computing with several planar Penning traps containing one trapped electron each. Each individual electron's spin can be addressed and have a general rotation performed on it by radiation. Furthermore, an effective interaction between spins can be achieved and used to perform CNOT gates.

1.3   Motivation : QUELE project

As we have said, quantum computing is a field of high interest, not only at the level of quantum information's first principles, but also as an experimental challenge and a possible future tool for mankind.

The basics of quantum computing has been demonstrated in linear Paul traps and is being still enriched, but the fact that those traps work with time-dependent voltages gives the feeling that static fields will probably provide a more coherent control. Our main aim has been thus to provide a realistic scheme for quantum computation with Penning traps and to build a tailored trap fulfilling the requirements.

Working with electrons has the advantage of higher motional frequencies due to their small mass. This way, the inner clock of the quantum computer would be faster[1]. A scheme for quantum computation with a linear array of cylindrical traps was given by Ciaramicoli, Marzoli and Tombesi in (Tombesi2). There, scalability and universal computation were demonstrated. Our main development as compared to this proposal was the idea of having a trap with open geometry. This ensures radiation from a single source reaching every single trap of an array, whether linear or planar, of traps. Because of this reason we designed a planar

---

[1]The logical speed of a quantum computer will not only depend on the intrinsic frequency achieved by its physical constituents, but the latter will for sure impose a lower bound for its speed.

trap, with electrodes printed on an isolating surface. Furthermore, this type of trap can be machined with known techniques in chip fabrication, thus enabling the miniaturization of a planar array of planar traps on the same substrate.

With the planar Penning trap as a tool, we aim at trapping single electrons in these traps at a temperature of $100mK$ or below, with a magnetic field of several Tesla. Such temperature regime is needed in order to have the cyclotron motion at its ground state. The electron looses energy by synchrotron radiation, and gains none from the environment due to the low temperature (black-body photons at this temperature do not have enough energy to excite the cyclotron motion). Since the damping rate for synchrotron emission is $\frac{dE}{dt} \propto B^2$ (Gabrielse), it is important to have a high magnetic field.

A typical resonant tank-circuit of narrow bandwidth will be used for picking up the induced voltage at the resonance frequency of the axial motion of the electrons. The qubit is planned to be stored in the electron's spin, which is a natural two-level system. With a microwave generator we can manipulate rotations on the spin, thus proving the possibility of 1-qubit operations. The addition of a quadratic magnetic gradient (with a Nickel ring for example) shifts the axial frequency of the electron in proportion to the projection of the spin operator, thus enabling the measurement of the qubit information.

For 2-qubit operations, in particular the CNOT gate, we plan to couple the spins of different electrons by mediation of their Coulomb repulsion. When a linear magnetic gradient is applied, the spin and axial motions of an electron get coupled. The Coulomb interaction couples the axial motion of different electrons, and thus at the end their spins are coupled in an effective way, due to the magnetic gradient. We also have an alternative coupling method based on the induced image currents in the trap's electrodes. These currents follow the oscillation of the trapped electron, and by connecting the electrodes of different traps, we couple the axial motions of their hosted electrons.

In Figure 1.3 we see the main setup for our project. The basic idea is to have a 2D array of traps inside a magnetic field. Trap are loaded with electrons coming from a "loader" trap, whose lower endcap electrode has been perforated according to the positions of the planar traps below it. Creation of electrons will be done with a field emission point (FEP). Radiation of microwaves is inserted in

the setup via a wave guide. Under the array of planar traps we see the electronic control system and the resonant tank-circuits.
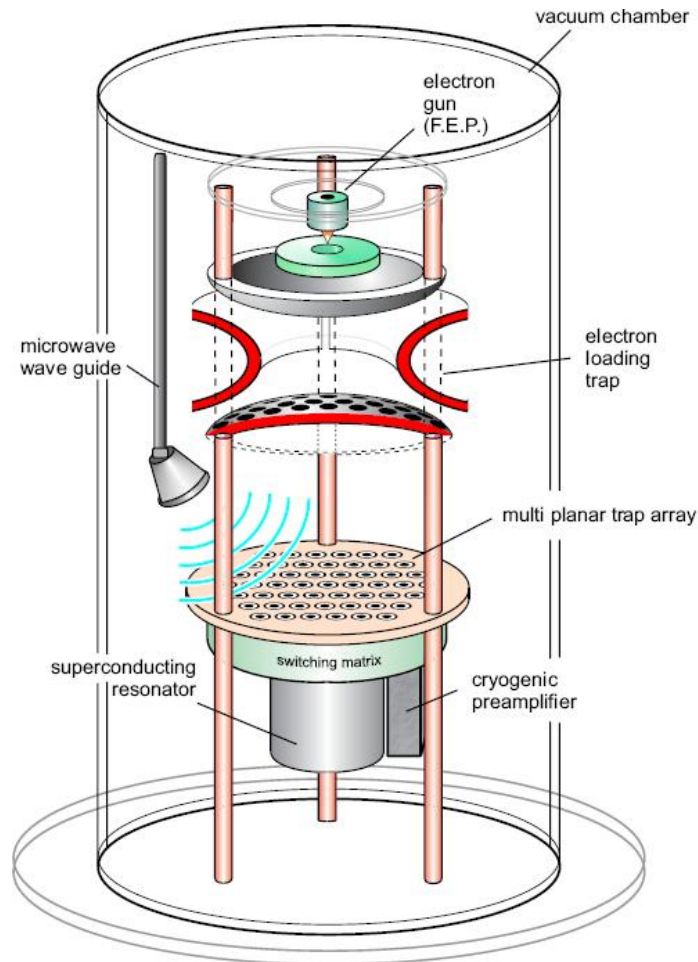
Figure 1.3: Illustration of the setup of the future QUELE experiment. This is the 100mK part of the setup containing the traps and control systems (Courtesy of Stefan Stahl).

Apart from the sketch in fig. 1.3, there will several zones with different temperatures, so as to smoothen the temperature transition for electronic components. Attached to the system, a computer-controlled collection of apparatuses will provide the necessary control.

In order to implement these ideas, it was necessary to study theoretically the

properties of our novel trap, and test it experimentally. The detection system, based on the axial motion's frequency shifting depending on the spin projection, has already been used in g-factor experiments with great success(Werth). However, it very much depends on the trap's electrostatic potential being perfectly quadrupolar, and this had to be investigated too. The CNOT gate operation, which relies on the effective spin-spin interaction, has to be calculated for this type of trap and for realistic parameters.

For all these reasons, I first studied the theoretical properties of the planar trap, the feasibility of the spin detection method and the spin-spin interaction, which will be shown in next chapter.

I also did first experimental test with two planar traps of different sizes, to confirm the theoretical study. This will be shown in chapter 3.

Chapter 2

Planar Penning trap, theory

A planar Penning trap was conceived as the projection of a standard 3D Penning trap into a plane. Its easiest realization is the one shown in Figure 2.1, with a central disk electrode and an outer ring electrode. Another possibility could have been with two ring electrodes, but it's equivalent. The central disc can be thought of as being the endcaps, and the ring as the ring electrode of a Penning trap. The symmetry axis of the trap is perpendicular to the plane and parallel to the magnetic field.
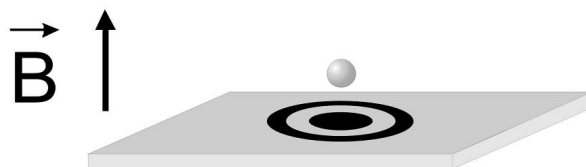

Figure 2.1: Planar Penning trap scheme. Electrodes (black) printed on an isolating substrate(gray).

2.1   Electrostatic Potential

In order to choose a best profile for this trap, both mathematical and experimental issues have to be considered before hand. Experimentally, it's not a good idea to leave blank space between electrodes, since they can get charged up by

collision with electrons leaving the trapping volume. This charges will modify uncontrollably the potential and will remain a long time.

In the mathematical side, leaving blank spaces between electrodes always means solving a *mixed* boundary value problem, i.e. part of the boundaries will be of Dirichlet type and part of Neumann type. This complicates the mathematical problem extremely and will be avoided here for the sake of analyticity.

The same applies for the border of the trap, for either the trap is of finite size (Dirichlet boundary) and the rest of the space is a Neumann boundary, or the trap extends radially to infinity. Since the idea is to finally have an isolating substrate covered with an array of such planar traps, the problem can be decomposed into an individual trap surrounded by a ground electrode extending to infinity, by the principle of superposition of electrostatics. Once we find the solution for the potential of this trap, the solution for the whole array of traps is just the sum of each individual solution placed one next to each other forming a lattice.

Of course, traps work in vacuum and therefore need to be isolated, which is normally done by a metal tube which encloses the trap. This tube could be represented by a cylinder of radius R_c and length L_c having its symmetry axis aligned along the one of the trap. However, the traps with which we are going to work experimentally are small in comparison to this tube, and the trapping region is smaller yet. This means that the electrostatic potential in the region we are interested in, shouldn't change if we change a tube boundary by a boundary placed at infinity. The general expansion for the potential in cylindrical coordinates, with rotation symmetry around z, is:

$$\int_0^\infty dk (A(k)e^{-kz} + B(k)e^{kz})(J_0(k\rho) + C(k)N_0(k\rho)) \qquad (2.1)$$

where $A(k)$, $B(k)$ and $C(k)$ are coefficients which need to be adjusted to the geometry of our problem. Pushing the metal tube to infinity means eliminating the divergent terms above and therefore:

$$\phi(\rho, z) = \int_0^\infty dk A(k)e^{-kz} J_0(k\rho) \qquad (2.2)$$

With all these assumptions the problem has been greatly simplified but the reader must not forget that by simplification we loose realism in the description. In next

section I will review several analytical approaches which can be taken to deal with the complete problem, including blank spaces, finite-sized trap and the inclusion of a cylinder at a given distance R_c. However, considering the whole realistic picture of a planar Penning trap inside a metal grounded cylinder increases far beyond our needs the difficulty of the mathematical problem, and will be exposed only for the sake of completeness and not because it's needed for our purpose.

Summarizing, the trap we will consider consists of several ring electrodes with a disc electrode in the center, plus an outer grounded electrode extending to infinity. An example with only two active electrodes with equal width can be seen in Figure 2.2.
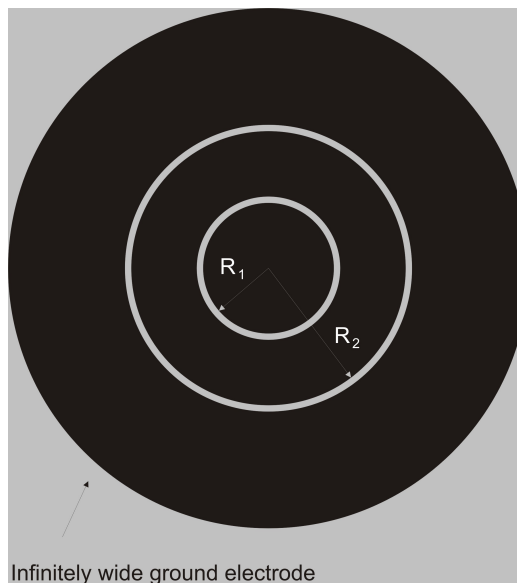
Figure 2.2: Final planar Penning trap scheme with two equally wide active electrodes plus an infinite outer grounded electrode.

The choice of contiguous electrodes plus an outer one extending to infinity reduces the statement of boundaries into a single expression:

$$\phi(\rho, 0) = V(\rho) \tag{2.3}$$

where $V(\rho)$ is the distribution of electrodes on the plane for given applied voltages. So, solving the electrostatic potential in our trap is equivalent to invert this

equation:

$$V(\rho) = \int_0^\infty dk A(k) J_0(k\rho) \tag{2.4}$$

and find the coefficients $A(k)$, which inserted in equation (2.2), give the complete solution for the electrostatic potential.

Equation (2.4) can be easily inverted by a Hankel transform without being further manipulated, and gives:

$$A(k) = k \int_0^\infty d\rho \rho V(\rho) J_0(k\rho) \tag{2.5}$$

As $V(\rho)$ is a piecewise function with value V_i between $\rho = R_{i-1}$ and $\rho = R_i$, equation 2.5 can be integrated to yield

$$A(k) = \sum_i A_i(k) \tag{2.6}$$

with

$$A_i(k) = V_i[R_i J_1(kR_i) - R_{i-1} J_1(kR_{i-1})] \tag{2.7}$$

Now, with equation (2.2) and equation (2.7), the electrostatic potential can be found in any point in space, either by analytical or numerical integration of equation (2.2) and hence the problem is solved.

Integration of the equation (2.2) for all space, to the extent of my knowledge, doesn't yield an analytical expression and needs a numerical treatment. However, an explicit analytical solution for the potential along the z axis can be found:

$$\phi(0, z) \equiv \phi(z) = \int_0^\infty dk \ A(k) e^{-kz} = \sum_i \phi_i(z) \tag{2.8}$$

,$\phi_i(z)$ being the contribution from each electrode whose value is:

$$\phi_i(z) = V_i \left(\frac{1}{\sqrt{1 + \frac{R_{i-1}^2}{z^2}}} - \frac{1}{\sqrt{1 + \frac{R_i^2}{z^2}}} \right) \tag{2.9}$$

This solution along z, plus assuming that the radial part is quadratic i.e. ideal, yields an approximate electrostatic solution for the case of a trapped particle sufficiently close to the z-axis. In general this is not the case, but there are methods with which a trapped particle can get its radial motion reduced to the

minimum (axialization), and thereby put close enough to the z-axis so as not to need to worry about it.

In addition, the proposed scheme for quantum computation requires that we are able to detect a shift in axial frequency given by the projection of the spin, whose frequency depends only in the shape of the potential in z coordinate. In order to demonstrate that that shift is detectable with this trap, we will need to study the z-shape of the potential for $\rho \sim 0$.

If numerical integration is performed, the complete picture of the potential can be obtained as in Figure 2.3.
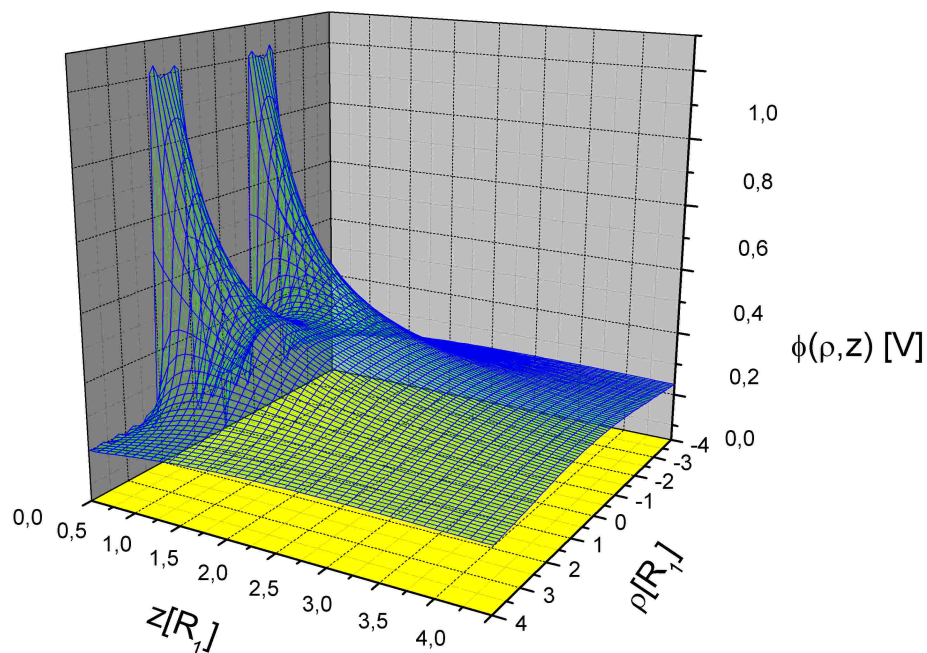

Figure 2.3: 3D plot of the potential for two electrodes configuration with $V_1 = 0V$ and $V_2 = 1V$, and electrode widths equal R_1 (inner disk's radius). The boundary at $z = 0$ has been spuriously softened by the graphics software and can be shown to fulfil exactly the imposed voltage at the trap's surface.

A comparison between the analytical expansion studied above and different

numerical solutions will be given at the end of this chapter.

2.2 A more complete description

The proposed description of our boundary problem can be completed in several ways, but mathematically there seems to be two straightforward ways to proceed: to include a surrounding closed cylinder which encloses the trap, or to consider the spacing between electrodes and finite-size of the trap. It's clear that one can do both at the same time, and not only that, but add realistic objects which might be placed inside the experimental setup in the real experiment, such as a detector, cables, etc. The first of the two mentioned possibilities requires that the boundary we used in last section is not at infinity but at a finite distance; the second one requires changing the type of boundaries, from purely Dirichlet to mixed ones. I will treat both possibilities next.

Of course, there are other combinations such as considering an open-ended cylinder with radius R_c and length $L_c - > \infty$, or a finite-sized trap with no spacing between electrodes inside a cylinder, but they can be obtained from the former two cases and thus will not be described here.

2.2.1 Trap with enclosing cylinder

The geometry that I will assume next consists of a closed cylinder with radius R_c and length L_c oriented along z-axis. Its walls and one of its endcaps have an applied voltage of 0V, and the other endcap will have a voltage distribution $V(\rho)$ (this endcap represents the trap). Since the radial eigenfunctions must vanish at $\rho = R_c$, k will not be now a continuous variable but a discrete one. The z coordinate will not be anymore expressed by e^{-kz}, but by $sinh(kz)$ (hyperbolical sinus) for convenience. Since $sinh(0) = 0$ we will adopt an antiintuitive orientation for the cylinder: we'll place it upside down, with the $V(\rho)$ endcap at L_c and the grounded one at $z = 0$.

The following discussion can be seen in a more general fashion in (Jackson) but I'll repeat the basics here and show a comparison with my own derivation included in former section.

As explained before, the values for k are discrete in this geometry since the limiting walls in ρ direction are at a finite distance from the center, and yield

$$k_n = x_{0n}/L_c \quad , \quad n = 1, 2, 3...$$ (2.10)

with x_{0n} being the zeroes of the zeroth-order Bessel function of the first kind $J_0(x)$. This is natural since the expression for the potential in this geometry must be of the general form:

$$\phi(z, \rho) = \int dk \ A(k) sinh(kz) J_0(k\rho)$$ (2.11)

and it must vanish at $\rho = 0$ for any z included in the inner volume of the disk. Then , finally we have that:

$$\phi(z, \rho) = \sum_{n=1}^{\infty} A_n sinh(k_n z) J_0(k_n \rho)$$ (2.12)

and by imposing the last boundary condition $\phi(L_c, \rho) = V(\rho)$ we see that

$$V(\rho) = \sum_{k=1}^{\infty} A_n sinh(k_n L_c) J_0(k_n \rho)$$ (2.13)

which is a well known Fourier-Bessel series and can be inverted to yield the desired coefficients:

$$A_n = \frac{2}{R_c^2 J_1^2(k_n R_c)} \int_0^{R_c} d\rho \ \rho V(\rho) J_0(k_n \rho)$$ (2.14)

The integral above is the same one as in equation (2.5) and therefore

$$A_n = \frac{2}{R_c^2 J_1^2(k_n R_c)} \frac{1}{k_n} \sum_i V_i [R_i J_1(k_n R_i) - R_{i-1} J_1(k_n R_{i-1})]$$ (2.15)

where index i runs over electrode's number.

At this point ends analyticity. The reader must observe that k_n have been defined as the zeros of the zeroth order Bessel function of first kind $J_0(x)$, which have no general analytic expression. Only asymptotic formulae and numerical methods to obtain them exist, and therefore even $\phi(z, 0)$ cannot be integrated analytically. Figure 2.4 shows a 3-dimensional plot of the potential and Figure 2.5 gives a comparison with this approach and my approach, for the potential
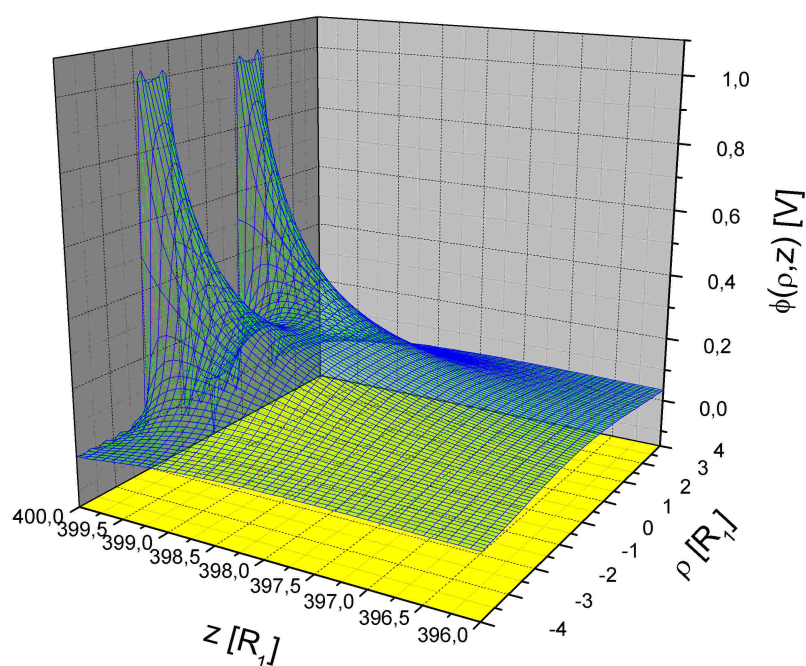
Figure 2.4: 3D plot of the potential for two electrodes configuration with $V_1 = 0V$ and $V_2 = 1V$, and electrode widths equal R_1 (inner disk's radius). $R_c = 20R_1$ and $L_c = 400R_1$

along z-axis. In figure 2.5 we can see that the similarity of the potential for the case with and without cylinder is amazing. There's a slight difference for z near 0, most probably because the numerical calculation of the potential can never include all k up to infinity. A difference would be seen also for big z since now the enclosing boundaries are not at infinity, but this region has been excluded from the plot.

This shows that we have gained no further quality in he knowledge of the potential, but lost a lot of computational power. I conclude from this that including the cylinder in calculations has been a mere curiosity and proceed studying the next possible completion: spacing between electrodes and finiteness of trap's size.
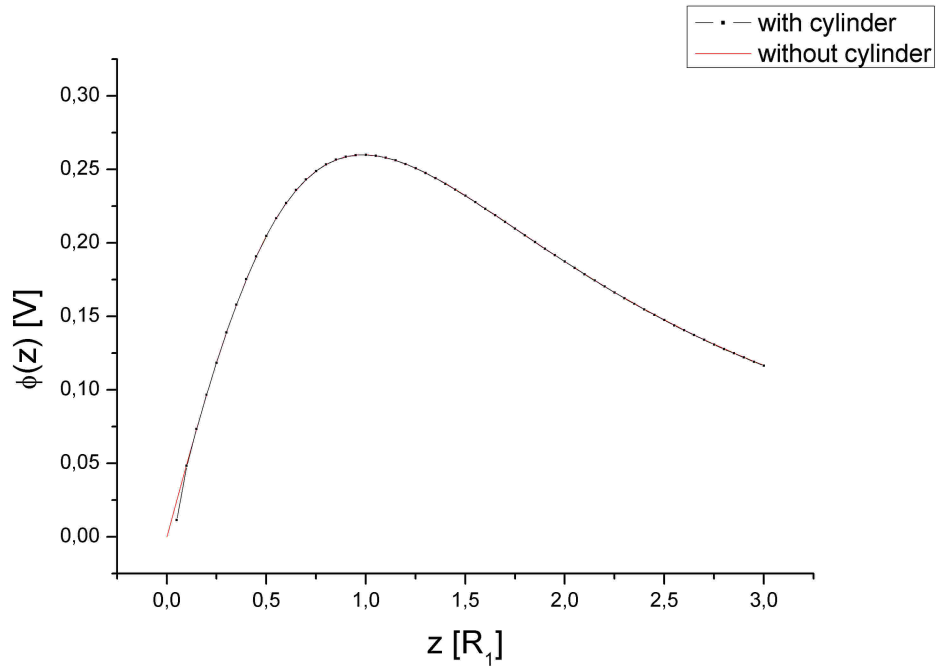

Figure 2.5: Same parameters as in Figure 2.4, plotted for $\rho = 0$. The cylinder's length and radius are experimentally realistic.

2.2.2 Mixed boundary conditions approach

To illustrate the difficulty involved in this approach, I will use the geometry of section 2.1, but this time without the grounded electrode which extends to infinity. I consider here only two electrodes: an inner disk, and a ring, an surrounded by empty space. This problem can be included in the more general one usually called "electrified disk".

Since the boundary conditions for $z \to \infty$ and $\rho \to \infty$ are the same as in section 2.1, I'll keep the polynomial expansion in eq. (2.2). In fact, the only difference with that section is in the boundary plane $z = 0$. Instead of $\phi(\rho, 0) = V(\rho)$, with $V(\rho)$ being the voltage distribution we apply to the different electrodes, the condition now is:

$$\phi(\rho, 0) = V(\rho) \quad , \quad 0 \le \rho < R_{trap} \tag{2.16}$$

$$\left. \frac{\partial}{\partial z} \phi(\rho, z) \right|_{z=0} = 0 \quad , \quad \rho > R_{trap} \tag{2.17}$$

where R_{trap} is the total radius of the trap, and eq. (2.17) expresses our knowledge of the surface charge being zero in the rest of the $z = 0$ plane. These equations, when expressed in terms of the polynomial expansion become:

$$\int_0^\infty dk A(k) J_0(k\rho) = V(\rho) \quad , \quad 0 \le \rho < R_{trap} \tag{2.18}$$

$$\int_0^\infty dk \ k \ A(k) J_0(k\rho) = 0 \quad , \quad \rho > R_{trap} \tag{2.19}$$

The mathematical problem has changed from section 2.1 only in the sense that eq. 2.4 is now split into two equations. In order to find suitable coefficients $A(k)$ these must satisfy both integral relations at the same time. Even if the reader doesn't realize, the mathematical problem has increased hugely in difficulty. Integral equations of this type are usually called "dual integral equations" and constitute a field on its own right in applied mathematics. For a general overview of the subject and a summary of mathematical tools, see (Sneddon). We will use this book as a reference for the remainder of this section.

The problem has been solved in several ways by different authors, but I will only sketch the approach of Sneddon, just for the sake of illustration. In the following section, $R_{trap} = 1$ will be assumed for simplicity.

2.2.2.1 Sneddon's solution

A solution for the "electrified disk" is given by Titchmarsh (1948) by a rather complicated method, and Sneddon(Sneddon2) gets to the same solution using a more elementary one.

The solution is sought by expressing the coefficients $A(k)$ in terms of a generating function, which makes the former coefficients satisfy eq. (2.19) automatically.

In Sneddon's derivation, the generating function of $A(k)$ is given by relation

$$A(k) \;=\; \int_0^1 \psi(t)cos(kt)dt \tag{2.20}$$

$$=\; \psi(1)sin(k) - \int_0^1 \psi'(t)sin(kt)dt \tag{2.21}$$

, and he introduces the function

$$G(\rho) = \int_0^\infty kA(k)J_0(k\rho)dk \tag{2.22}$$

which, inserting equation (2.21) in, shows that $G(\rho) = 0$ for $\rho > 1$ (remember that $R_{total} \equiv 1$), after some integral manipulation. This means that equation (2.19) is directly satisfied, as expected.

In order to find $\psi(t)$, we substitute (2.20) into the function

$$F(\rho) = \int_0^\infty A(k)J_0(k\rho)dk \tag{2.23}$$

and obtain

$$F(\rho) = \begin{cases} \int_0^\rho \frac{\psi(t)dt}{\sqrt{\rho^2-t^2}} & , \quad 0 \le \rho < 1 \\[2ex] \int_0^1 \frac{\psi(t)dt}{\sqrt{\rho^2-t^2}} & , \qquad \rho > 1 \end{cases} \tag{2.24}$$

Since equation (2.18) is equivalent to $F(\rho) = V(\rho)$, $0 \le \rho < 1$, it's clear from the upper equation in (2.24) that ψ is the solution to the integral equation

$$\int_0^\rho \frac{\psi(t)dt}{\sqrt{\rho^2 - t^2}} = V(\rho) \;\; , \;\; 0 \le \rho < 1 \tag{2.25}$$

whose inversion gives us $\psi(t)$:

$$\psi(t) = \frac{2}{\pi}\frac{d}{dt}\int_0^t \frac{\rho V(\rho)d\rho}{\sqrt{t^2 - \rho^2}} \tag{2.26}$$

From this expression for $\psi(t)$ we can find $A(k)$, after integration by parts and a little manipulation:

$$A(k) = \frac{2}{\pi} \left(cos(k) \int_0^1 \frac{uV(u)du}{\sqrt{1-u^2}} + k \int_0^1 \frac{udu}{\sqrt{1-u^2}} \int_0^1 vV(uv)sin(kv)dv \right) \quad (2.27)$$

For our particular case, further simplification is possible. Due to the piecewise nature of our $V(\rho)$, the first integral yields:

$$\int_0^1 \frac{uV(u)du}{\sqrt{1-u^2}} = \sum_i (V_{i+1} - V_i)\sqrt{1-R_i^2} \quad (2.28)$$

with i running over electrode number. In the second integral we first integrate the v part:

$$\int_0^1 vV(uv)sin(kv)dv = \sum_i \frac{V_{i+1} - V_i}{k^2 u} \left[kR_i cos(\frac{kR_i}{u}) - u \left(kcos(k) - sin(k) + sin(\frac{kR_i}{u}) \right) \right] \quad (2.29)$$

Inserting this equation into (2.27) and completing the integration for the variable u is only possible analytically for the part of $-u(kcos(k) - sin(k))$ and not for the $cos(kR_i/u)$ and $sin(kR_i/u)$, so (2.27) becomes further split:

$$\begin{aligned}
A(k) &= \frac{2cos(k)}{\pi} \sum_i (V_{i+1} - V_i)\sqrt{1-R_i^2} \\
&+ \frac{2}{\pi} \frac{kcos(k) - sin(k)}{k} \sum_i (V_{i+1} - V_i) \left(1 - \sqrt{1-R_i^2} \right) \\
&+ \frac{2}{k\pi} \sum_i (V_{i+1} - V_i) \int_{R_i}^1 \frac{1}{\sqrt{1-u^2}} \left(kR_i cos(\frac{kR_i}{u}) - usin(\frac{kR_i}{u}) \right) du
\end{aligned}$$

The first two summands here can be simplified into one giving

$$\begin{aligned}
A(k) &= \frac{2}{\pi} \sum_i (V_{i+1} - V_i) \left\{ \left[cos(k) - \frac{sin(k)}{k} \left(1 - \sqrt{1-R_i^2} \right) \right] \right. \\
&+ \left. \frac{1}{k} \int_{R_i}^1 \frac{1}{\sqrt{1-u^2}} \left(kR_i cos(\frac{kR_i}{u}) - usin(\frac{kR_i}{u}) \right) \right\} du \quad (2.30)
\end{aligned}$$

We leave the u integral so for the moment, and try to integrate for k to get the potential along z axis:

$$\phi(0, z) \equiv \phi(z) = \int_0^\infty A(k)e^{-kz}dk \quad (2.31)$$

After integrating over k a surprise comes, a piece of the u integral becomes solvable analitically, and the potential becomes

$$
\begin{aligned}
\phi(z) \;=\; & \frac{2}{\pi} \sum_i (V_{i+1} - V_i) \left\{ \frac{z}{1+z^2} - atan(\frac{1}{z}) \left(1 - \sqrt{1 - R_i^2} \right) \right. \\
& + \; \frac{R_i}{z\sqrt{z^2 + R_i^2}} \left(\frac{R_i \pi}{2} - R_i \; atan\sqrt{\frac{z^2 + R_i^2}{1 - R_i^2}} - acos(R_i)\sqrt{z^2 + R_i^2} \right) \\
& + \; \left. \int_{R_i}^1 \frac{u}{\sqrt{1-u^2}} \; acot\left(\frac{uz}{R_i} \right) du \right\}
\end{aligned}
\tag{2.32}
$$

A difference between this method and other solutions by other authors is that here only an integral over u remains, with a finite integration domain. In other approaches one has to integrate in a semifinite domain, which can be tougher numerically. The result of this study can be seen in Figure 2.6: We see that Sneddon's method yields the same results as my standard derivation in section 2.1, and furthermore the calculation times are hugely reduced in comparison with other mixed boundary approaches. Hence, this method is preferable , but still its calculation times are much longer than the ones needed by the standard derivation.

2.2.2.2 Complete completeness

Throughout the section I have tried to give a more complete description of the real electrostatic problem by making the boundary conditions more realistic. However, the trial has proved unworthy of the effort, since no bigger understanding of the behaviour of the potential has been achieved with more complete descriptions. Nevertheless, I will try to explain what would be the most complete description which could be given, how that problem would be solved and where its difficulty lies.

As already discussed before, our trap consists of metal electrodes printed on an isolating surface of finite size R_{total}. This trap has to be mounted on a holder and afterwards isolated from atmosphere by an enclosing metal cylinder at ground. What about having more elements inside the vacuum-cylinder? We may say that that is too much for an analytical approach, or we can build a experimental setup
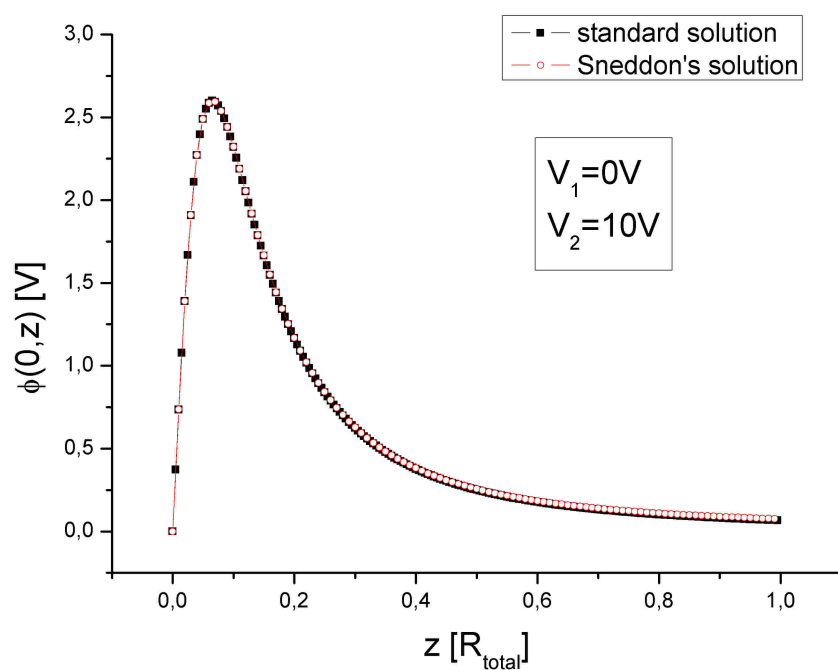
Figure 2.6: Standard versus Sneddon's solutions comparison for the case of a trap with holder. Parameters are the same as in Figure 2.6, which we have used in our experiment.

such that those extra elements are far away from the trap and can be considered negligible with respect to its influence on the trapping region.

In any case a finite-sized trap with gaps between electrodes, inside a finite-sized enclosing cylinder already shows the difficulty of solving such electrostatic problem, which is the goal of this subsection.

We define the electrostatic problem to be that of a voltage distribution in the plane $z = 0$ with gaps ending up at $\rho = R_{cylinder}$. The electrostatic potential needs to be solved only in the region $0 \leq \rho \leq R_{cyl.}, 0 \leq z \leq L_{cyl.}$. The boundary conditions are $\phi(\rho, 0) = V_i$ for $R_{i-1} + d_i \leq \rho \leq R_i$ where V_i is the voltage applied to electrode i, d_i is the gap between electrode $i - 1$ and electrode i and R_i is the radius at which electrode i ends. The trap ends at $R_{tot.}$ and then comes a gap from $R_{tot.}$ to $R_{cyl.}$. Then $\phi(R_{cyl.}, z) = 0$ (walls) and $\phi(r \leq R_{cyl.}, L_{cyl.}) = 0$ (cylinder cap), plus stating that the normal derivative of $\phi(\rho, z)$ is zero for the regions $(\rho, 0)$ with $R_i \leq \rho \leq R_i + d_i$ and for $R_{tot.} \leq \rho \leq R_{cyl.}$, give the complete statement of the boundary conditions.

It comes immediately to our memory that up to now we have been dealing with a maximum of two regions: a region with Dirichlet-type boundary, and a region with Neumann-type. And it becomes evident that now our problem, our trap having N electrodes, has $N + 2$ Dirichlet-type regions and N Neumann-type regions. In total, the number of integral equations which the coefficients $A(k)$ have to satisfy is $2N + 2$.

In previous sections we studied the problem of the electrified disk, which has $N = 1$ and no cylinder, hence having 2 integral equations to solve. Such problems are typically called "dual integral equations" since the goal is to obtain a function $A(k)$ which satisfies both equations. The obvious difficulty of their mathematical treatment wa proven by the fact that a numerical help was always needed at the end. The reader can imagine how huge and challenging can be searching for an analytical approach to a $(2N + 2)$-al integral equations problem. This reason automatically rules out any other possibility than directly solving laplace's equation numerically by different methods.

2.3   Comparison with numerical methods

I do not want to extend much on the point of solving Laplace's equation for our
trap with numerical techniques, for we have seen that by making a more real-
istic analytical approach to the problem no further qualitative nor quantitative
insight has been gained in a substantial amount. Therefore I will expose some
customary comparison between our standard derivation, given in section 2.1, and
purely numerical methods, taking the parameters used to compare with the mixed
boundaries approach in subsection 2.2.2 .

I will first consider a typical relaxation routine and then a finite elements
one. I will briefly summarize what they consist and compare their results to our
standard derivation.

2.3.1   Relaxation method

Relaxation, or "finite differences", method is a well known one. It's normally
used in electrostatic problems given its easy implementation and despite its slow
convergence speed. The method consists in splitting the region where the poten-
tial is to be calculated into an equally spaced grid o points. Laplace's equation
can be thence cast into a finite-difference equation which states that the value of
the potential at the point with labels "i, j, k" is the average of the potential at
its nearest neighbour points.

The method then is implemented by the following steps:

1)making an initial guess at the values of the potential in each point of the
grid ($\phi_{i,j,k}$).

2)stating the boundary conditions on $\phi_{i,j,k}$.

3)substituting $\phi_{i,j,k}$ by its nearest neighbours's averaged values for the rest of
points.

Of course, a halting criterium for the algorithm is needed, and it must be
inserted after 3):

4)if the newly calculated $\phi_{i,j,k}$'s differ from the ones calculated in the iteration
before by less than "dV", halt the iteration process. ("dV" is the goal accuracy

we want to achieve for the function ϕ).

From the structure of this method, it can be seen that it consists in propagating the values of the boundaries by the Laplace equation itself in a discretegrid-way. Therefore, its convergence is slow! Acceleration of the process can be aided by changing the way we average in step 3), i.e. by replacing 3) with 3'):

$$3')\phi_{i,j,k}^{(new)} = \lambda * (neigbour's\ average) + (1 - \lambda) * \phi_{i,j,k}^{(former)}$$

where λ is a parameter between 0 and 1, to be chosen accordingly to the nature of the problem. Despite its convergence slowness, this method is rather easy to implement, and thus suited for easy boundary problems such as electrostatics.

If we use this method to calculate our potential for the geometry described in 2.2.2, Figure 2.7 is obtained. A complete agreement is observed, corroborating the results obtained almost analytically in section 2.2.2.

2.3.2 Finite elements method

Finite element methods divide the problem of interest into a mesh of geometric shapes called finite elements. The potential within an element is described by a function that depends on its values at the cell corners (nodes) and parameters defining the state of the element. Several such cells are assembled to solve the entire problem. A total "energy" associated with the mesh configuration is found as part of the calculation and this is minimized by adjusting the parameters specifying the elements. The solution can be refined by subdividing the regions of the mesh that contribute most to the total "energy" of the solution, or by increasing their complexity (i.e. increasing their number of nodes).

The typical application of this method concerns mechanical stresses, thermal and fluid flow problems, when the complexity of the boundary regions is big, and the need for best efficiency is high.

For our problem, an axisymmetric electrostatic potential, the problem is two dimensional (ρ, z), and can be divided into 2D elements. The easiest choice are simple triangles. In Figure 2.8we see the mesh used to obtain our potential.
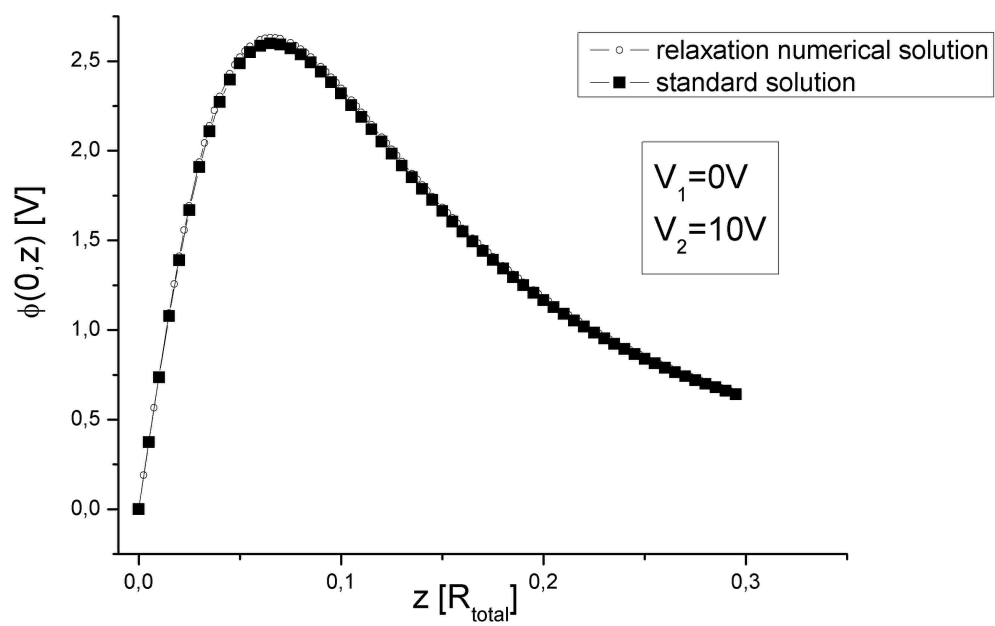
Figure 2.7: Standard versus relaxation's solutions comparison for the case of a trap with holder. Parameters are the same as in Figure 2.6.

Since the trap is centered at $\rho = 0$ and $z = 0$, the tiniest triangles are around it, and they grow in size as their distance to the trap increases. This can be perfectly understood in terms of field gradients and is similar to adaptive size methods for numerical calculation of physical particle trajectories (the bigger the force, the smaller the needed time step, the bigger the field gradient the smaller the triangles). The enclosing boundaries have been chosen to be the same as in the relaxation method. They are 15 times bigger than the trap+holder's radius ($R_{tot.} = 1$) and 15^2 bigger than R_1 ($R_1 = 1/15$, as before). The region of interest lies at $z \sim R_1$, and so the external boundaries are effectively at infinity.
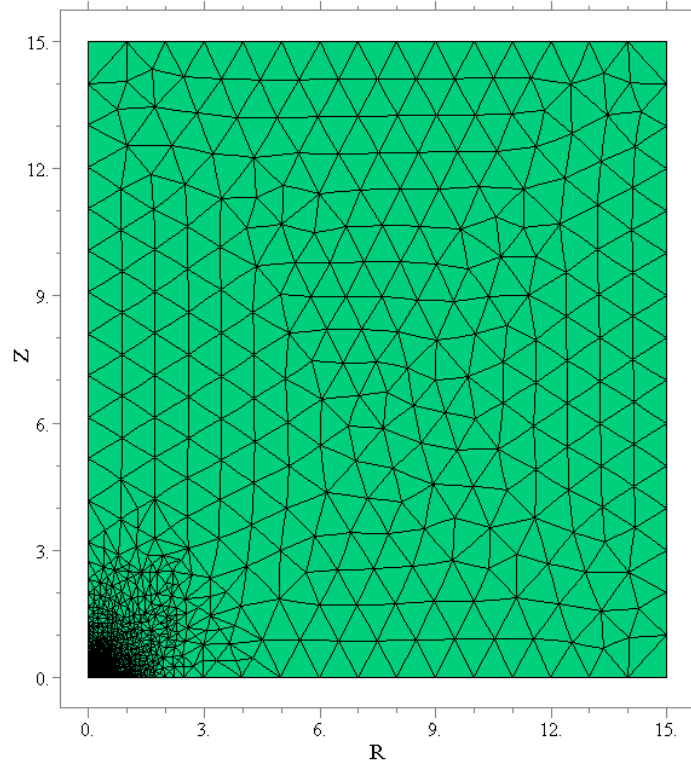

Figure 2.8: Mesh used for our calculation. Triangles's sizes are iteratively reduced until the accuracy criterium is met.

The comparison of the potential calculated via this method, with the standard one yields Figure 2.9, which shows a perfect agreement with our standard derivation. As before, we conclude that our simple analytic formula (2.9), is sufficient to give us both qualitative and quantitative information about the potential shape and properties, which will be the object of interest in next section.
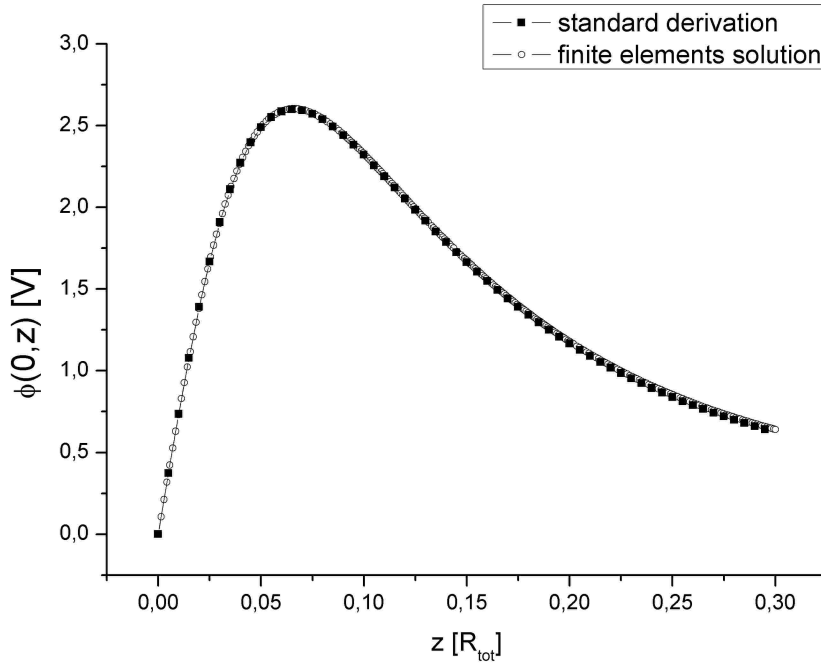
Figure 2.9: Comparison of finite elements method with the standard derivation. Same parameter values as before were used.

2.3.3 Conclusion

The abundance of methods given here, despite the existence of much more methods still, shows that our standard derivation is good enough for describing the shape of the potential. In next sections we will see some of the properties of the potential which can be extracted from this derivation. In the experimental part of the thesis it will be seen that our measurement confirm this, too.

2.4   Trap's Properties

Till now I have only discussed whether the solution equation (2.9) was sufficiently good and which improvements could be tried. I hope to have convinced the reader that, what I have been calling the "standard derivation", is not only sufficient but enormously faster to compute and easier to analyze than any other approach.

Results have been presented for a trap with two electrodes, giving a highly z-nonsymmetric potential. Standard Penning traps are known to have 2 active electrodes (ring and endcaps) plus a third electrode which corrects the shape of the potential so as to make it most quadrupolar, at least in the region of the minimum, i.e. the trapping region. This experimental aid is needed since no real trap is perfect, in many senses, and we aim to have the biggest realizable precision. Our trap is by no means an exception to this fact, and the addition of a third electrode is mandatory for our purposes. In order to state the situation properly and leave no place for misunderstandings, I will specify once again the geometry of our trap:

1) The trap consists in a collection of electrodes, with given applied voltages, lying on the plane $z = 0$ and extending to $\rho \to \infty$.

2) The potential $\phi(\rho, z)$ is studied for the half-space $z \geq 0$ and the enclosing boundaries are at infinity, namely $\phi(\rho \to \infty, z) = 0$ and $\phi(\rho, z \to \infty) = 0$.

3) The voltage distribution on the plane $z = 0$ is piecewise, thus having $\phi(\rho, 0) = V_i$ for $R_{i-1} \leq \rho \leq R_i$, and i being the number labelling electrodes. and in particular:

4) We are going to work with a voltage distribution with values:

$$
\begin{aligned}
V_1 \quad &for \quad 0 \leq \rho \leq R_1 \\
V_2 \quad &for \quad R_1 \leq \rho \leq R_2 \\
V_3 \quad &for \quad R_2 \leq \rho \leq R_3 \\
0 \quad &for \quad R_3 \leq \rho < \infty
\end{aligned}
$$

(2.33)

which is just the same conception as in Figure 2.2 plus a third electrode outside electrode 2.

As seen previously, the potential along z-axis can be cast in the form:

$$\phi(0, z) = \sum_{i=1}^{3} V_i \left(\frac{1}{\sqrt{1 + \frac{R_{i-1}^2}{z^2}}} - \frac{1}{\sqrt{1 + \frac{R_i^2}{z^2}}} \right) \quad (2.34)$$

In Figure 2.5 we saw an example of the potential shape along z with $V_1 = 0V$, $V_2 = 10V$ and electrodes of equal widths ($R_2 = 2\ R_1$). To get a feeling of the influence given by the now added third electrode, I plot the potential for the same voltages, equal widths ($R_2 = 2\ R_1$, $R_3 = 3\ R_1$), and varying V_3. The result is Figure 2.10[1]:

From the image above we deduce several things: *first*, that the position of the minimum can be varied by varying the relationship V_3/V_2; *second*, that the depth of the minimum can be varied not only by scaling all voltages, but by also varying the relationship V_3/V_2; *third*, that the shape of the potential well gets more symmetric for values of V_3 which seem to lie around $V_3 \sim -2V_2$; *fourth*, that by adding electrode 3, we have now two extrema instead of one, and that by adding a fourth electrode we might get three extrema, thus having two independent trapping regions plus an unstable zone in between. All these points will be studied in detail in the following subsections.

2.4.1   Position of the minimum

The position of the "minimum" is defined as the position z_0 on the z axis such that $\left. \frac{\partial \phi(0,z)}{\partial z} \right|_{z_0} = 0$. Despite eq. (2.34) being so simple, if one tries to obtain the position of the minimum as a function of the parameters $z_0 = z_0(\{R_i\}, \{V_i\})$, one finds a "surprise" namely that it cannot be obtained analytically by any means.

The expression defining the minimum is a sum of fractions of powers of roots whose arguments are different. In my opinion this equation cannot be solved

---

[1]Remember that we are always referring to negatively charged particles. Hence, when I say "minimum", a mathematical maximum is seen, etc.
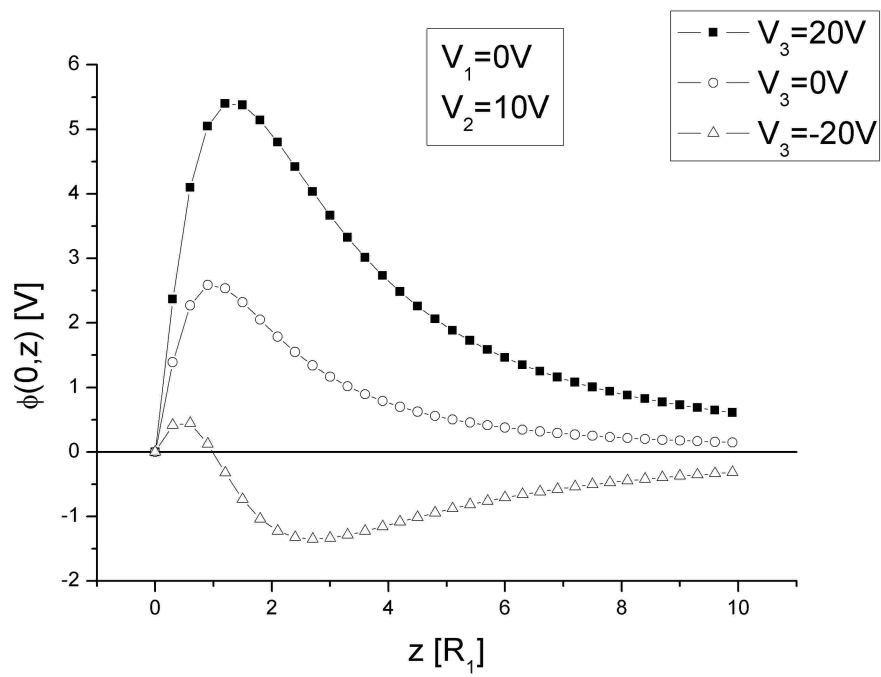
Figure 2.10: Potential shape along z axis for equal electrodes' widths ($R_2 = 2\ R_1$, $R_3 = 3\ R_1$).

except in the case of all V_i being zero except one of them. We will do the job numerically.

We have seen in Fig. 2.10 that by going to more negative V_3, the position of the minimum is moved towards the origin in z. It can be interesting to plot the position of the minimum for fixed parameters and varying V_3. An example can be seen in figure 2.11 for electrodes of equal widths:

Figure 2.11: Position of the minimum changed by changing the ratio V_3/V_2 with fixed geometry and $V_1 = 0V$. A clear threshold value is seen around $V_3/V_2 \sim -3$
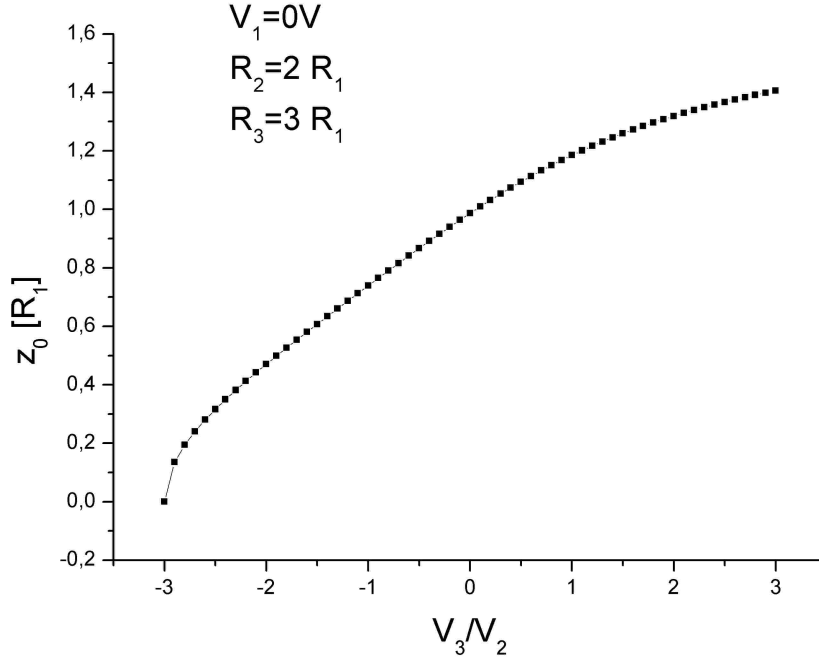
It looks like the minimum can be asymptotically shifted to $z = 0$ if $V_3 \rightarrow -3\, V_2$. It should though be realized that by shifting the minimum to 0 we are also reducing the depth of the well, and for an effective experimental minimum shifting to be feasible we would also need to increase both V_2 and V_3 gradually to compensate such effect.

Such shifting may be of interest in decoherence studies related to interaction with the metal surfaces. Such decoherence would be dependent on the distance between ion and surface, which could be varied by this procedure.

2.4.2 Depth of the potential well

The definition of the well can be defined to be equal to $|\phi(0, z_0)|$. If $V_1 \neq 0$, "depth" is a not so well defined concept, and for the sake of simplicity, and

without loosing too much generality I will use $V_1 = 0V$ from now on. Due to the fact that z_0 has to be found numerically, also does the depth.

In Figure 2.10 we deduced that there are two factors influencing the depth of the potential minimum: the overall scale of applied voltages, and the ratio V_3/V_2. A general scaling of voltages such as $V_i \rightarrow \alpha \ V_i$ will make the depth α times bigger. And the effect of the ratio V_3/V_2 on the depth can be seen in Figure 2.12:
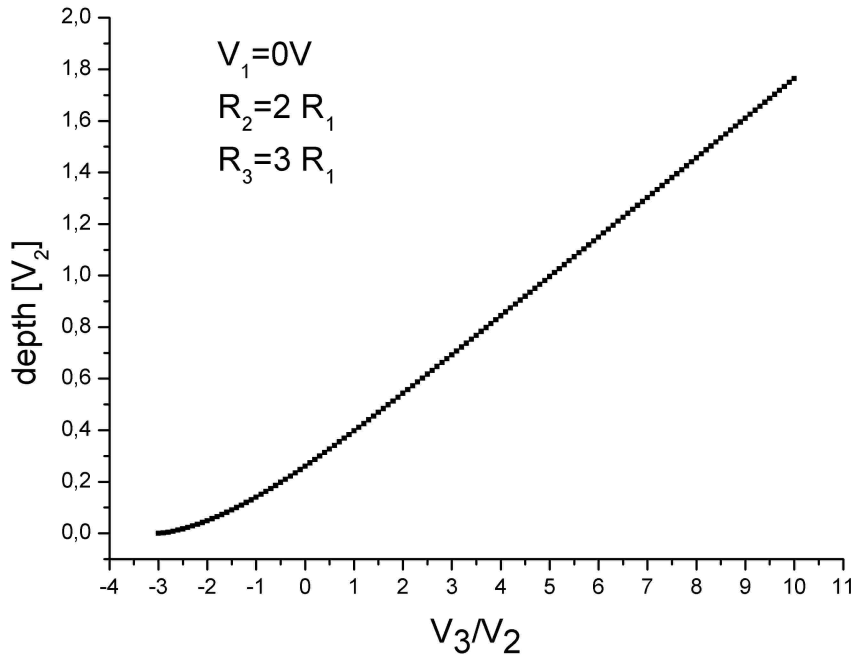
Figure 2.12: Depth of the minimum versus ratio V_3/V_2 with fixed geometry and $V_1 = 0V$.

It's clear that for $V_3/V_2 \gg 1$, electrode 2 can be neglected and the depth is proportional to V_3/V_2. For negative values, there's a delicate balance between V_3 and V_2 which gives again a threshold at around $V_3/V_2 = -3$, which we already mentioned regarding the shifting of the minimum's position.

Another detail which should be pointed out is the case $V_3 = 0$, for which the

depth is about a *fourth* of the total applied voltage (V_2). For $V_3 \leq 0$ the depth is even smaller than a *fourth* of the applied voltage ($V_2 + V_3$). In short, the depth of the potential well is always smaller or equal to around $0.25V$ where V is the scale of voltages applied to the trap.

2.4.3   Curvature of the potential

The curvature of the potential at a given position z is given by its second derivative at that point. Since the potential can be approximated as a parabola around the position of the minimum, thus giving a harmonic trapping potential around it, the curvature at that point gives the eigenfrequency of the motion for a trapped particle. The expression relating curvature ($\phi''(z0)$) and frequency (ω) is:

$$q\phi''(z0) = m\omega^2 \tag{2.35}$$

where q and m are the charge and mass of the trapped particle, respectively.

From a simple dimensional calculation, it can be seen that the frequency scales proportionally to $\frac{\sqrt{V}}{R}$, with V being the scale of voltages and R the typical size scale. This would apply to a scaling of all voltages or all sizes.

Experimentally reasonable parameters for a trap will always have all R_i of the same order, and the same with all V_i, and thence an estimation of the order of magnitude of the frequency can be given. If however we are curious about the details we may have a look again at Figure 2.10, and intuit that the curvature gets changed by the ratio V_3/V_2, too.

Figure 2.13 shows the behaviour of the curvature versus the ratio V_3/V_2. If we were to plot the frequency, the shape would be almost equal.

Going from 0 to more negative values of V_3/V_2 we squeeze the potential shape to a maximum point near $V_3/V_2 = -2$ and after that point the depth of the potential depth decreases too fast and thus the curvature, till it goes to 0.

The expected curvature behaviour for $V_3/V_2 > 0$ is to decrease to zero when increasing V_3/V_2, since we would be broadening the potential well. However a minimum is seen around $V_3/V_2 = 1$. The explanation is that when V_3/V_2 grows too much, the potential is dominated by the third electrode and the whole potential scales with it in voltages. Since the curvature is proportional to the voltage

scale, the curvature will scale linearly with V_3/V_2. This asymptotic behaviour is corroborated in Figure 2.15.
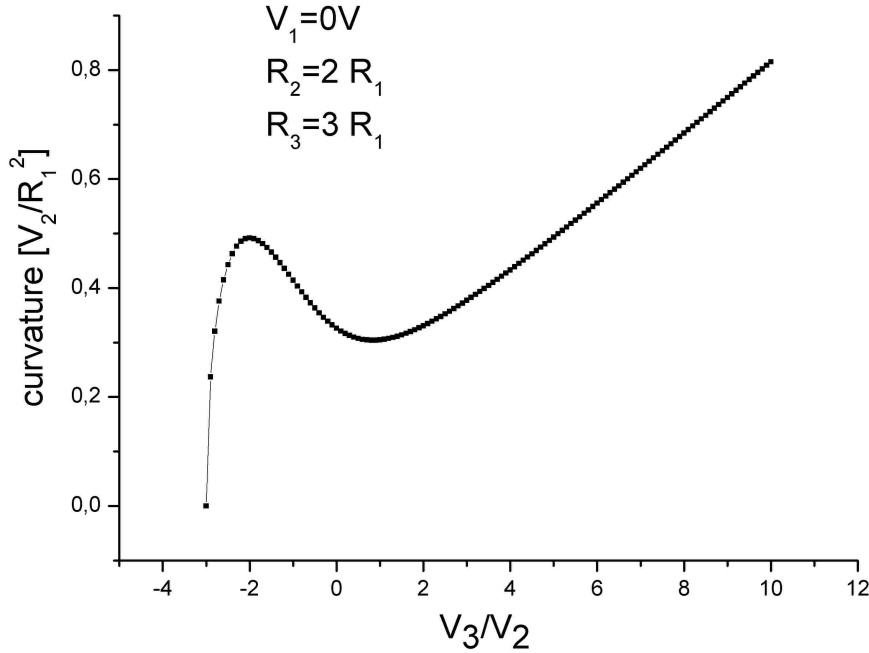
Figure 2.13: Curvature at the minimum versus ratio V_3/V_2 with fixed geometry and $V_1 = 0V$.

Another consequence of Figure 2.15 is that by changing V_3 with the rest of parameters fixed, we can change the curvature by a factor ~ 1.7. This sounds useful for a manipulation of frequencies, however the equivalent factor for frequencies is ~ 1.2, which is not much.

2.4.4 Anharmonicity of the potential

In the preceding sections I enumerated some properties of the electrostatic potential produced by the planar trap. These properties are quite general and are useful when getting a feeling of how the potential behaves.

Now the point is more crucial. Traps are well established among physicists because they have proven to high-quality, high-precision tools, known to the very minutest detail. In our case there is the plan to build an array of planar traps in quantum regime and perform individual and CNOT gates on singly-trapped electrons, and for such a task the spin was chosen as qubit. But I will not enter into details for this will be explained in section 2.5.

For now it suffices to know that when a trapped electron is subject to a quadratically inhomogeneous magnetic field, its axial eigenfrequency depends on its spin projection along z. Whether the projections is "up" or "down" can be monitored if we are able to measure the very small spin-dependence of the axial frequency. For typical experimental parameters and detection techniques, the relative shift of frequency between spin up and down is about 4×10^{-5}. For an axial frequency of around $100 MHz$, that means resolving a 4KHz frequency difference.

Detection of axial frequencies is normally achieved by a resonant tank circuit attached to the electrodes of the trap. The thermal voltage fluctuations across the circuit get shortcut when its frequency coincides with the axial frequency of the electron in the trap. This shortcut for similar electron and circuit frequencies, gives a dip in frequency space whose width can be calculated from the properties of the tank circuit. For typical g-factor high precision measurements (Werth), the circuit consists in a capacitance given by the one between trap's electrodes and the parasitic one of cables, an inductance, and an effective resistance. For typical values of circuit's capacitance $C \sim 7.5pF$ and circuit's quality factor $Q \sim 300$, we expect dip widths of around 1KHz for electrons having an axial frequency around 100MHz.

In principle such a dip width is sufficiently narrow to differentiate between spin up and down. However, the electrostatic potential embedding the electron is not perfect and therefore not parabolic in z. This causes the electron's axial motion to broaden its frequency width. It is most desirable that this width is smaller than the spin frequency shift that we want to measure, so as to have best chances to distinguish *up* and *down* spin projections.

In order to have the narrowest axial width, we need to have a most harmonic electrostatic potential, i.e. almost perfectly parabolic in the trapping region. The

perfectness of the potential can be quantified in a perturbative sense: the axial frequency of the electron is known in the position of the minimum, and small contributions come from the fact that the electron runs over a certain range in z, namely $|z| \leq A$, and the potential has different curvatures along its path. Classically, the distance traveled by an electron with energy E in a parabolic potential is

$$A(E) = \sqrt{\frac{E}{m\omega_z^2}}. \tag{2.36}$$

The anharmonicity (or imperfectness of the potential) can be defined as the relative difference of frequencies of a particle with energy E and one with minimal energy: $E_0 = \frac{1}{2}\hbar\omega_z$:

$$\kappa(E) = \frac{\omega_z(E) - \omega_z(E_0)}{\omega_z(E_0)} \tag{2.37}$$

which, if we express the potential as

$$\phi(z) = \sum_{n=0}^{\infty} \frac{C_n}{n!}(z - z_0)^n \tag{2.38}$$

, can be expressed as:

$$\kappa(E) = \sum_{n=0}^{\infty} \frac{(A(E))^{n+1}}{(n+1)!} \left| \frac{C_{n+3}}{2C_2} \right| \tag{2.39}$$

where we have substituted here the $z - z_0$ for the amplitude of the motion $A(E)$ as a first estimate. It should be noted that, in contrast with normal Penning traps, the potential has non-zero odd terms in the expansion, which comes from its z-reflection asymmetry. Therefore the most important anharmonic term is the C_3 one.

This perturbative approach is best suited for small motional amplitudes, which happens to be the case if trapped particles are sufficiently cooled down. Tank circuits are normally operated under a liquid helium bath at $\sim 4K$ so as to detect a single trapped particle's signal. Since the particle is coupled to this circuit, the latter's resistance will damp the particle's motion till its motion gets thermalised to the ambient temperature, in this case $4K$. From eq. (2.36) and $E \sim k_B T$ the motional amplitude is $\sim 60\mu m$ at $\omega_z \sim 100MHz$ (which is the case

for $R_1 = 2.5mm$, $V_1 = 0V$, $V_2 = 1V$ and $V_3 = -2.25V$, with equal electrodes' widths) and the anharmonicity , from eq. (2.39), is $\sim 6 \times 10^{-4}$. This means that for typical trap's parameters and optimum V_3/V_2, the amplitude is too big and the electron "sees" too much anharmonicity. Luckily, dilution refrigerators are nowadays at our disposal, being able to reach temperatures of about $100mK$ (and lower). An electron thermalised to such bath, with the same parameters as above, will have an axial amplitude of $\sim 10\mu m$ (~ 250 times smaller than R_1) and an anharmonicity of $\sim 1.7 \times 10^{-5}$. That's already sufficient for differentiating spin projections.

It should be noted that the reasoning above has been done for the case of equally wide electrodes and by tuning V_3/V_2 for optimum harmonicity. Variation of all trap's parameters could in fact lead to an even more harmonic trap, and this will be the subject next.

2.4.4.1   Most harmonic trap

I will study next which trap's parameters minimize completely the anharmonicity. As before we state $V_1 = 0V$ for convenience. Nevertheless the problem of minimizing the anharmonicity is a complex one, since *first*: the anharmonicity is calculated from the derivatives of $\phi(z)$ at z_0 (minimum's position) and needs a numerical treatment; *second*, the space of parameters is bigger than 2, and thus any function (such as κ) of it doesn't lend itself to graphical representation. Parameter space consists in $\{R_i, V_i\}$, in total 5 parameters (having already stated that $V_1 = 0V$), and then the anharmonicity is a function of 5 variables which cannot be graphically represented in standard ways.

A circumvention of this problem can be done if we are to represent relative parameters, i.e. V_3/V_2, R_2/R_1, R_3/R_1, meaning by this that R_1 gives the size scale and that V_2 gives the voltage scale. The space of parameters then reduces to three dimensions, and still the anharmonicity $\kappa(V_3/V_2, R_2/R_1, R_3/R_1)$ cannot be easily represented. A good idea is to take one of those dependences as a parameter and the other two as variables. Then we could represent $\kappa(R_2/R_1, R_3/R_1; V_3/V_2)$, that is, a 3D plot of κ for each discrete value of V_3/V_2. Any combination like that would do.

2. PLANAR PENNING TRAP, THEORY

I choose an arbitrary motional amplitude of $R_1/100$ for the rest of the subsection. Notice that this doesn't affect our goal, since a most harmonic trap's parameters will be so for any amplitude. I've chosen it sufficiently small so that our perturbative expression (eq. (2.39)) is good enough.

Regarding the representation of κ, it might well be a natural choice to choose R_2/R_1 as discrete parameter and then plot $\kappa(R_3/R_1, V_3/V_2)$, since the natural question is "given a certain fixed configuration of the first two electrodes, which produce the trapping themselves, what would the optimum size and voltage of a corrector electrode be?". The best weapon a scientist can hold in his/her hand when attacking problems with many parameters is his/her intuition, and choosing a representation of the parameters which fits well to our own perception is not only more than justified, it is advisable.

To get the reader to intuit the nature of the anharmonicity for this trap, I first present an example with fixed geometrical parameters $R_2 = 2R_1$, $R_3 = 3R_1$ and $V_1 = 0V$, so that only one free parameter remains: V_3/V_2. Moreover, we know that the potential is most harmonic when the second and third electrodes have opposite signs. Thus we restrict the range of V_3/V_2 to negative values. Figure 2.14 shows the result. We can see the same threshold at V_3/V_2 as before, which flags the disappearance of the trapping region beyond that point. We also see an absolute minimum of the anharmonicity at around $V_3 = -2.25V_2$ which is the goal of our efforts.

With this picture in mind we extend the idea to a space with one more dimension, i.e. now we make R_3/R_1 free too. Still, we keep the fixed parameter $R_2 = 2R_1$. Figure 2.15 is the result:
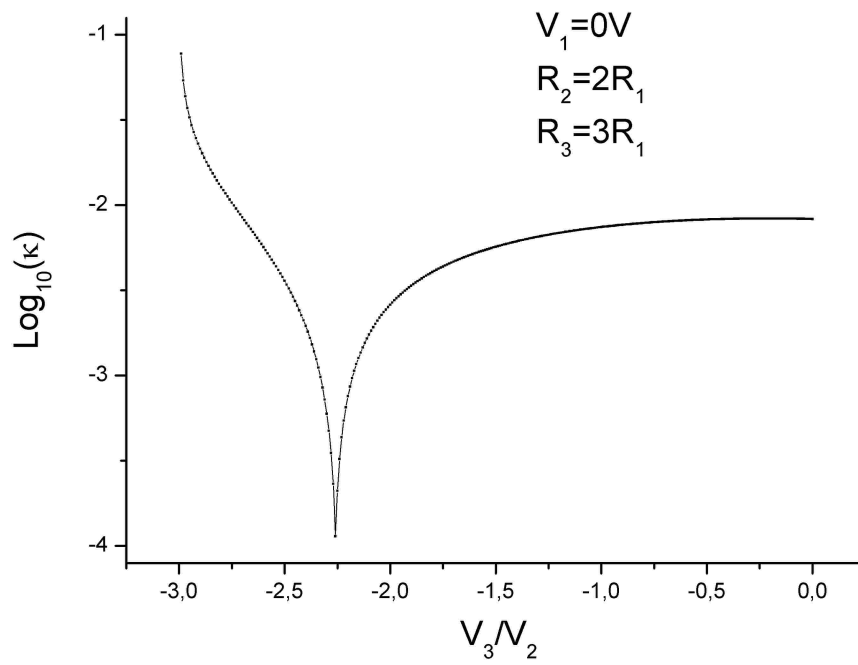
Figure 2.14: Order of magnitude of the anharmonicity with fixed geometry and $V_1 = 0V$, as a function of V_3/V_2. A well determined minimum is seen.
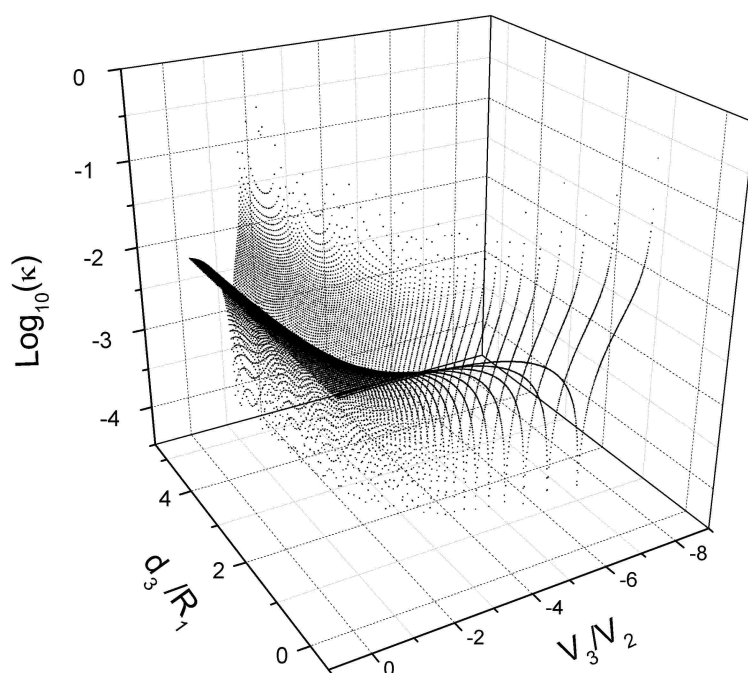
Figure 2.15: Order of magnitude of the anharmonicity with fixed $R_2/R1$ and $V_1 = 0V$, as a function of V_3/V_2 ad d_3/R_1. A valley can be seen with equal depth all over. The parameter d_3 is the width of electrode 3, and is equal to $R_3 - R_2$.

In Figure 2.14 we can see the same as in Figure 2.15 but extended along d_3/R_1, where d_i is defined as the width of electrode i. What we see is a *valley* centered at "position" $\frac{d_3}{R_1} = f(\frac{V_3}{V_2})$, and most important, whose *depth* is equal all along. This means that it doesn't matter how wide the corrector electrode is, we will always find a voltage which will make the trap most harmonic. In other words, there's no improvement by playing with the width of the third electrode.

However, if we want to be absolutely sure of the non-importance of electrode widths, we also have to make R_2/R_1 free. In order to plot everything at the same time, I will minimize $\kappa(R_2/R_1, R_3/R_1, V_3/V_2)$ with respect to the parameter V_3/V_2 for every pair of $\{R_2/R_1, R_3/R_1\}$. The result is Figure 2.18:
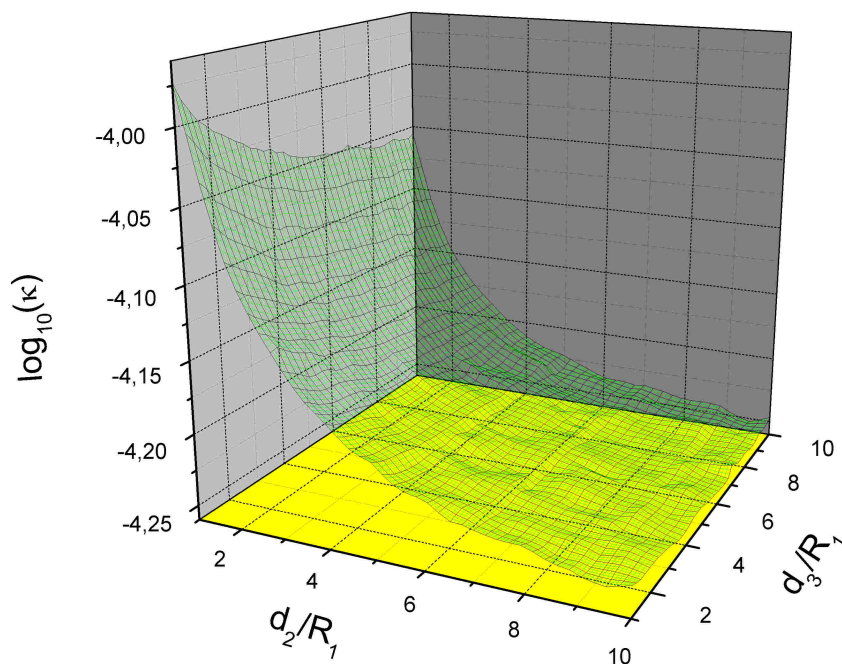

Figure 2.16: Order of magnitude of the anharmonicity, minimized for V_3/V_2, with fixed $V_1 = 0V$. Little bumps in the surface come from numerical errors.

In Figure 2.16 we see the geometrical dependence of κ. It decreases exponentially for increasing d_2 or d_3, but much faster for d_2. We would conclude that the best

option is making $d_3 = d_1$ and $d_2 = 10d_1$ or bigger. But if we compare when both d_2 and d_3 are ten times bigger than $d_1 (\equiv R_1)$, and when both are equal to d_1, we see that κ only changes by a factor $\simeq 2$. That's not much, and the situation wouldn't be better if we go for bigger d_2 and d_3.

To sum up we can say that by playing around with the widths of electrodes we can just gain a factor ~ 2 in the anharmonicity κ. This occurs for $d_3 = d_1$ and $d_2 \geq 10d_1$.

It is therefore more advisable to have a good precision in voltages rather than adjusting geometrical parameters. As can be seen in Figure 2.14, $log_{10}(\kappa) < -3$ only if our precision is less than $\sim 0.5 V_3/V_2$, $log_{10}(\kappa) < -3.5$ only if our precision is less than $\sim 0.1 V_3/V_2$, etc.

NOTE: It should be noted that all this analysis has been done to third order in the amplitude, i.e. taking up to C_5 in the expansion of the potential around the minimum. This has been done so because our purpose is to distinguish between spin projections. Were we to use this trap for high precision measurements such as mass spectrometry or g-factor experiments, higher order terms would have to be considered.

2.4.4.2 Orthogonalization

The treatment considered up to here is based in the treatment of the anharmonicity as one piece, defined by equation (2.39), and not even that because we used the truncated series up to $n = 2$. This truncation was enough for the precision we established we needed in order to assure operability of the trap in future quantum computing experimental situations. A more detailed study of the trap as a general purpose tool would have to take into account the independent analysis of individual terms in eq. (2.39), distinguishing first between odd and even terms, and later analyzing every single term, up to the precision needed in each experiment.

A typical condition which should be satisfied by standard Penning traps, either hyperbolical, cylindrical, cylindrical without endcaps, etc., is being *orthogonalized*. Not only must they be compensated, i.e. their anharmonicity corrected by an extra electrode, but they must be orthogonalized. What does that mean? It

is well-known that an axisymmetric trap with mirror symmetry about the axis can be constructed such that its *trapping axial frequency doesn't depend on the compensation (or correction) voltage*. This means that whatever the "width" of the corrector electrode is, we can always find a "width" for the other electrodes such that the frequency will be independent of the tuning of the corrector electrode's voltage. I put "width" in quotation marks because that's what the case is with our trap; every electrode is defined by its width (or equivalently its radial position) and its voltage, however should we be talking about a cylindrical trap the word would be "height", should we be talking about a hyperbolical trap the word would be "distance from the center of the trap".

This conditions is highly desired by experimentalists, since the frequency window where they have to look for an axial signal is narrow, they do high precision experiments, and finding the axial signal's peak every time the compensation voltage is changed is not an option. In any case, the study of a trap's properties is not really finished unless we have defined in which conditions it is orthogonal.

Let's state the problem in our case: can one find a combination of geometrical parameters $d_2/R_1, d_3/R_1$ such that the frequency doesn't depend on V_3?

As a fast approach we can plot the frequency vs. $\{V_3/V_2, d_3/R_1\}$ for different d_2/R_1 and try locate a parameter region where orthogonality holds, that is the frequency doesn't change along V_3/V_2. The result can be seen in Figure 2.17, no "flat" region -along V_3/V_2- exists. We can begin here to doubt whether this trap is at all orthogonalizable.

A further insight to the problem comes when we compare our trap with a standard one, with z-reflection symmetry. In such traps, the potential can be decomposed, as in our case, in two summands:

$$\phi(z) = V_0 \phi_0(z) + V_c \phi_c(z) \tag{2.40}$$

where the first term is the potential of the trap with its corrections electrode at 0V, and the second is the potential of the trap with all electrodes at 0V except the corrector one. The thing is that "orthogonality" can be stated so:

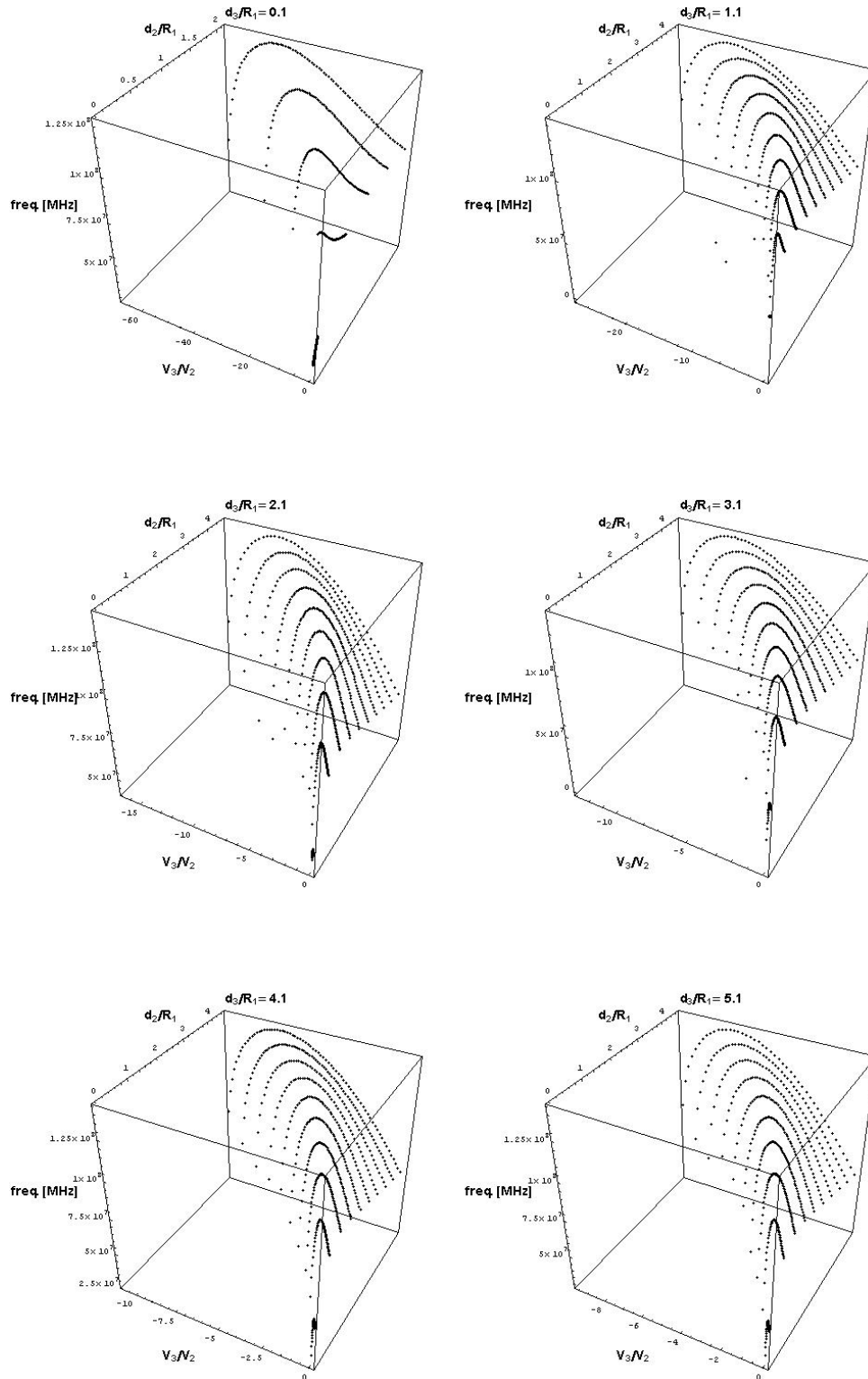$$\left[\partial_z^2 \phi(z)\right]_{z=z_0} \equiv \phi''(z_0) \neq f(V_c) \tag{2.41}$$

Figure 2.17: Array plot of $\omega_z(\frac{V_3}{V_2}, \frac{d_3}{R_1}; \frac{d_2}{R_1})$. No region of orthogonality seems to exist.

or

$$\frac{\partial}{\partial V_c}\phi''(z_0) = 0 \tag{2.42}$$

and thence,

$$\frac{\partial}{\partial V_c}(V_c\phi_c''(z_0)) = 0 \tag{2.43}$$

The crucial point comes to sight now, when the real difference between standard Penning trap and a planar Penning trap is perceived. Equation 2.43, for standard Pennning traps means:

$$\phi_c''(z_0) = 0 \tag{2.44}$$

since neither z_0 nor $\phi_c''(z)$ depend on V_c, but for a planar Penning trap the same equation reads:

$$\frac{\partial}{\partial V_c}(V_c\phi_c''(z_0(V_c))) = \phi_c''(z_0(V_c)) + V_c\frac{\partial z_0(V_c)}{\partial V_c}\frac{\partial \phi_c''(z_0)}{\partial z_0} = 0 \tag{2.45}$$

where it should be noticed that $\frac{\partial \phi_c''(z_0)}{\partial z_0}$ is a function of V_c too. It can also be written

$$\phi_c''(z_0(V_c)) + V_c\frac{\partial z_0(V_c)}{\partial V_c}\phi_c'''(z_0(V_c)) = 0 \tag{2.46}$$

It's not surprising that in the case of standard Penning traps we can find a combination of geometrical parameters which make an orthogonal trap, for (2.44) doesn't depend on V_c. Instead, equation (2.45) <u>does</u> depend on V_c and needs to be fulfilled for every V_c, which is a much more restricted situation. Nevertheless, a solution could exist. How is it that there is none?

If we reconsider (2.45) we can write

$$\frac{\partial}{\partial V_c}(V_c\phi_c''(z_0(V_c))) = 0 \quad \Rightarrow \quad V_c\phi_c''(z_0(V_c)) = const. \tag{2.47}$$

where "constant" means with respect to V_c. Now we must remind the reader that $z_0(V_c)$ cannot be expressed analytically and therefore we must suspect that (2.47) might not be satisfied for all V_c.

The proof that this trap is not orthogonalizable has to be performed again numerically. In Figure 2.18 I have plot the function $V_c\phi_c''(z_0(V_c))$ running along V_3/V_2 for several pairs of $d_2/R_1, d_3/R_1$ (in our trap $V_c \equiv V_3$).
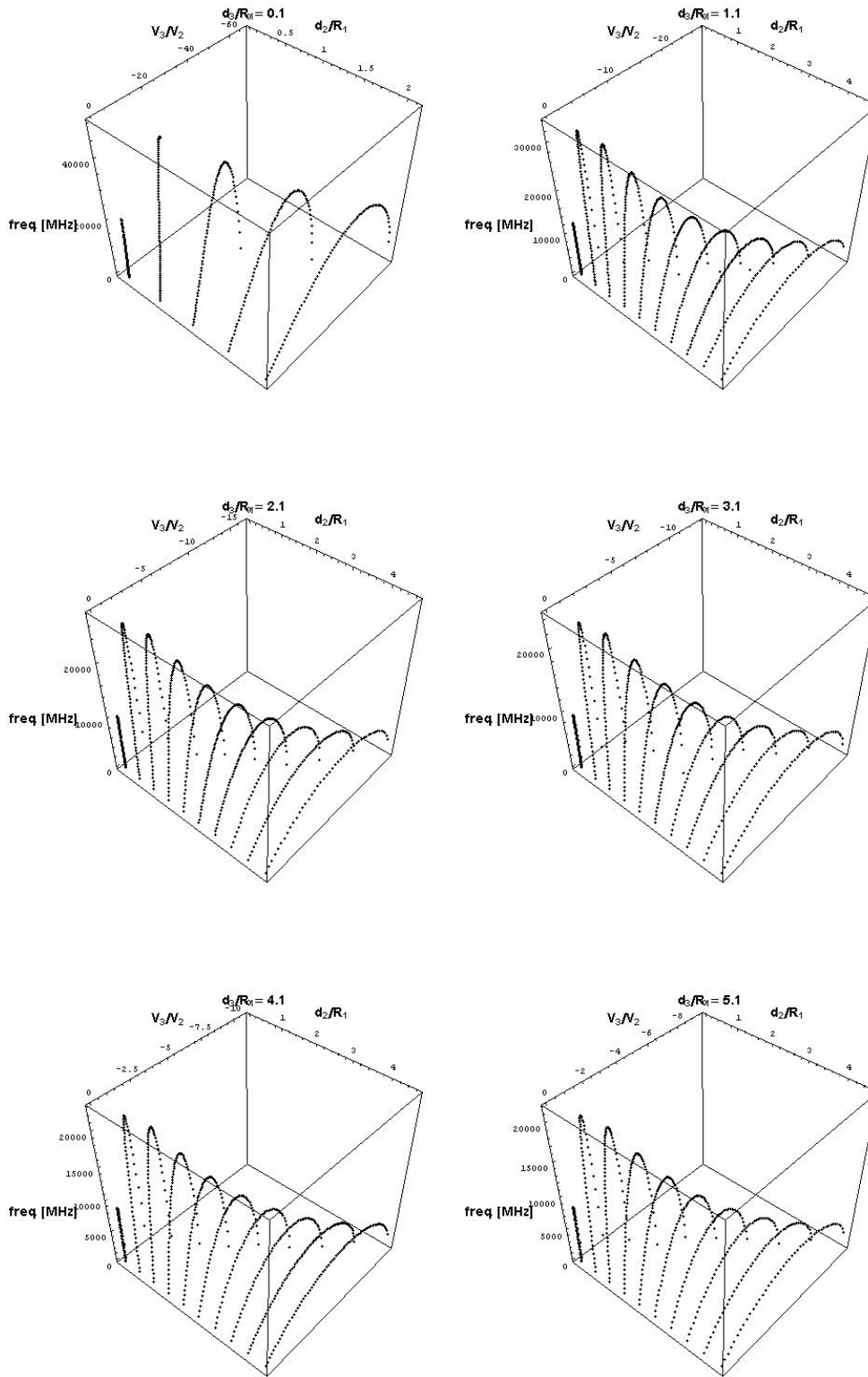
Figure 2.18: Array plot of $V_c \phi_c''(z_0(V_3))$.

What is shown there is qualitatively the same as seen in Figure 2.17, that there's no hope for orthogonality in this trap. Despite our complete lack of knowledge of the analytical expression of $\phi_c''(z_0(V_c))$, since z_0 has no analytical expression, we could have hoped that it would be proportional to $1/V_c$, and thus that (2.47) would be satisfied. The conclusion is that this is not the case for a planar Penning trap.

A deeper insight might be gained with further studies of the properties of the function $\phi_c''(z_0(V_c))$ itself, but the major difficulty is the non analyticity of $z_0(V_c)$. This makes this analysis rather hard and out of the scope of my thesis, perhaps better suited for a mathematician.

A compromise between our hopes and the facts we have shown comes by changing the sentence: we expect $V_c\phi_c''(z_0(V_c))$ "not to change with V_c", by the sentence:we expect $V_c\phi_c''(z_0(V_c))$ "not to change *much* with V_c". Looking again at Figure 2.18 we notice that this functions has an extremum along V_3 for every pair of d_2, d_3. This point is where minimal variation of $V_c\phi_c''(z_0(V_c))$ is found, and by restricting the correcting voltage V_3 to this range we make the most orthogonal trap possible for a planar one. It should be added that this region coincides with the region where anharmonicity is minimized, and so the pains of an experimentalist working with a planar trap are minimized also. Whenever we know that our trap has a V_3 such that it is most harmonic, we know that its axial frequency will not change much if we fine-tune V_3. It's not a perfect solution but it's a solution.

2.4.4.3   Other possible definitions of anharmonicity

Anharmonicity has been studied here in a perturbative way, which is appropriate when dealing with small motion amplitudes. However, the trap maybe operated at room temperature for other purposes, and without cooling the trapped particles. In such case, particles are thermalised to a temperature $T > 273K$ (a standard laboratory is normally never colder than $0°C$, even in Germany), and their amplitudes are not small.

In that situation different definitions of anharmonicity can be produced by:
1) Extending the perturbative scheme to more orders

2) Evaluating the curvature in different points of the potential and comparing with its value at the minimum

3) Doing 2) but with a "weight" factor for every point evaluated. The weight factor can be defined following different criteria: time spent by a trapped particle in that point, probability of a trapped particle to be at that point,etc.

Several of these possibilities will be investigated when I talk of the experimental results concerning anharmonicity, since I used a trap at room temperature with no particle cooling. Comparison with experimental results will be given. Please refer to section 3.2.5.2.

2.4.5 Double well configuration

A planar trap with two electrodes creates a trapping region, which we defined as the "minimum" (even if it was plot as a maximum). By adding a third electrode we saw that a "maximum" was created (recall Fig. 2.10). If we add a fourth electrode, a new extremum is produced, and this time it is a new "minimum". This new minimum is capable of trapping and is effectively isolated because of the existence of the "maximum" between both "minima".

Figure 2.19 shows an example of a double-well (or double-minimum) configuration. As can be seen, each minimum has different shape and curvature and therefore eigenfrequencies. With this configuration we can trap particles with different frequencies. In fact we could trap two different clouds of negatively charged particles and a cloud of positively charged ones in between.
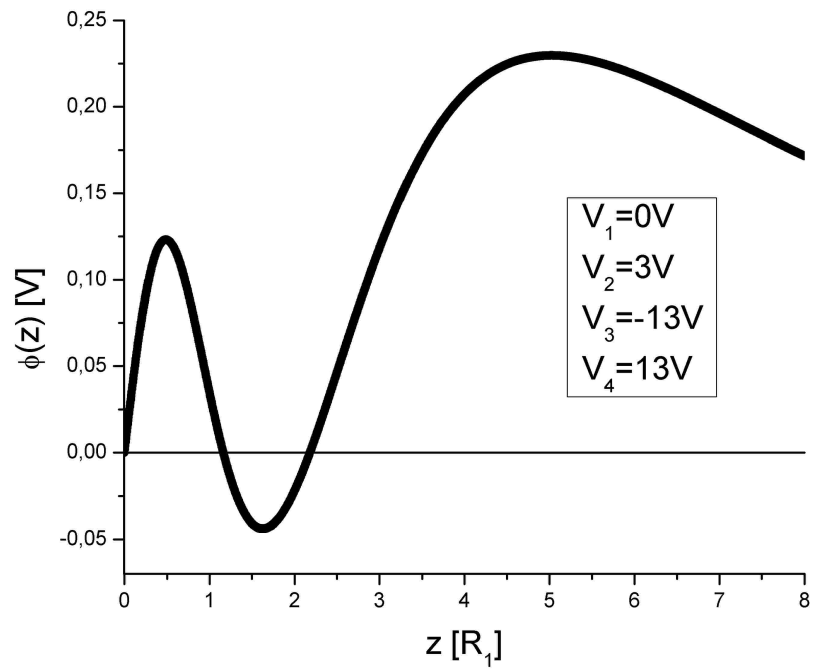
Figure 2.19: Double well configuration for negatively charged particles.

2.5 Quantum communication between different traps

Planar traps have the disadvantage of not having z-reflection symmetry, in contrast with other Penning traps. However they have several features which make them good candidates for the implementation of quantum computing: *first*,due to their open geometry they can be easily accessed with radiation; *second*, it can be fabricated massively with the same technology used to print circuit boards; *third*, it can be minituarised to μm level with thin-layer technology, the one used for fabricating chips, which is a typical requirement for any candidate to quantum computation.

Because of this, it is necessary to study the possibility of communicating two singly trapped particles (in two independent traps) in order to perform two qubit operations. It is known that a universal quantum computer has two basic operational requirements: it should perform arbitrary rotations in individual qubits, and it must be able to perform a CNOT gate over every pair of qubits.

A basic way of storing a qubit in a trapped particle is to use one of its quantised degrees of freedom, preferably its spin because it is a two-level system. The natural extension for N qubits is to have N traps with one trapped particle in each, and a communication method between each pair of particles.

Since the normal detection scheme for a trapped particle is to pick up the electric signal it induces in the electrodes of the trap with a resonant tank circuit, it is most natural to use the same principle for communicating qubits. The idea is to connect two traps with a wire and let the induced image charges of each interact. This gives an effective interaction between the particles(Galve).

Another possibility comes from the fact that, being the trap's geometry open, two singly trapped particles in different adjacent traps feel a Coulomb interaction between each other, and could be used to exchange information between the spatial degrees of freedom. A slight modification of this method yields an effective spin-spin interaction between particles, mediated by the Coulomb interaction(Ciaramicoli).

Another possibility is to store several qubits in different degrees of freedom of the same particle(Tombesi), for example spin and cyclotron. To exchange

information between them we need them to be coupled, which is directly implemented by inhomogeneities (anharmonicities) in the electrostatic potential and relativistic corrections. Else, we can introduce radiation coupling both degrees of freedom.

I will study here the first two possibilities.

2.5.1 Method of induced image charges

A particle confined in a trap induces, because of its oscillation, an oscillating current in the electrodes of the trap confining it. This effect is caused by the coulomb interaction of the particle with the free charges in the electrode's metal. This oscillation, representative of the trapped particle itself, can be "transported" to another trap if we connect them via a wire. In this way, two particles confined in different traps can interact effectively.

In a planar Penning trap the idea is implemented as seen in figure 2.20. Since the axial motion of a trapped particle is perpendicular to the surface of the trap it yields the biggest contribution to the induced image charges. Therefore I will study the communication channel for this degree of freedom.
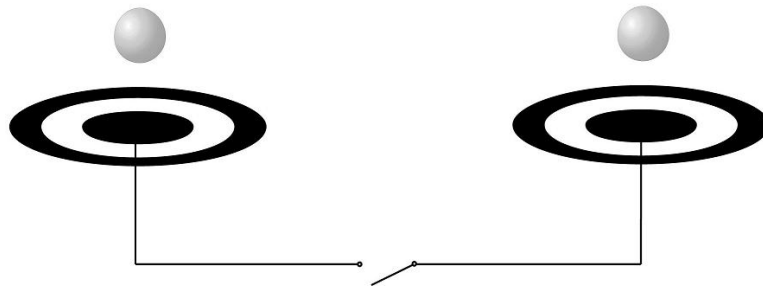

Figure 2.20: Communication exchange scheme. An electronic fast switch could turn on and off the connection through the wire.

The idea is to connect a wire to the central electrode of both traps, since this electrode is the one closest to the trapped particle and its contribution is the biggest. This is similar to a proposal by A.S Sørensen et al. (Sorensen), in which they consider trapped particles with dipolar charge.

2. PLANAR PENNING TRAP, THEORY

Due to the principle of superposition of electromagnetism, the problem of the trap in figure 2.20 with voltages V_1, V_2 plus a little fluctuation of V_1 is equivalent to the same problem with $V_1 = V_2 = 0V$. This means that we can restrict our attention to the central disk electrode at $0V$ plus a fluctuation induced by the oscillation of the trapped particle. We will consider here very thin disks.

Let the upper surfaces of the central electrodes have a common radius R and carry charges Q_1 and Q_2, respectively, while the remaining system, i.e. the two lower surfaces and the connecting wire, carries a common charge $Q_3 = -(Q_1+Q_2)$. The latter equation means that because $V_1 = 0V$ the neat charge in the system is 0.

The classical Hamiltonian of this system is

$$
\begin{aligned}
H \;=\;& H_1 + H_2 + q\frac{Q_1}{2\epsilon_0 R^2}(\sqrt{R^2 + z_1^2} - z_1) \\
&+ q\frac{Q_2}{2\epsilon_0 R^2}(\sqrt{R^2 + z_2^2} - z_2) \\
&+ \frac{Q_1^2}{2C_1} + \frac{Q_2^2}{2C_2} + \frac{Q_3^2}{2C_3},
\end{aligned}
\tag{2.48}
$$

where q is the charge of a trapped particle, H_i are the particle Hamiltonians (which are effectively harmonic oscillators), C_i are the capacitances of the surfaces, and z_i are the height of particles above the surfaces.

Here it has been assumed that the inductance is negligible, i.e. that the dynamics of the system is much slower than the resonance frequency of the wire.

We further assume that the reordering of free charges inside the electrodes and wire is much faster than the oscillation transmitted by this method, and therefore that the charges follow adiabatically the oscillation of the trapped particle. In such case, we can write:

$$
\frac{dH}{dQ_i} = 0 \qquad \forall i
\tag{2.49}
$$

which gives us a dynamical relation between the Q_i and the z_i:

$$
\begin{aligned}
Q_1 \;=\;& \frac{Cq}{8R^2\epsilon_0}\left(3z_1 - 3\sqrt{R^2 + z_1^2} - z_2 + \sqrt{R^2 + z_2^2}\right) \\
Q_2 \;=\;& \frac{Cq}{8R^2\epsilon_0}\left(-z_1 + \sqrt{R^2 + z_1^2} + 3z_2 - 3\sqrt{R^2 + z_2^2}\right)
\end{aligned}
\tag{2.50}
$$

We have taken equal disk electrodes, so $C_1 = C_2 \equiv C$, and a wire with negligible capacitance, so $C_3 = C_1 + C_2 + C_{wire} \approx 2C$.

Equations (2.50) can be used to eliminate the dependence of the hamiltonian H on the Q_i. We have then a Hamiltonian which depends only on z_1 and z_2. This Hamiltonian consists of a constant term $\frac{-3C}{16R^2\epsilon_0^2}q^2$, a term which modifies the natural eigenfrequencies of each individual electron $\frac{3Cq^2z_i}{16R^4\epsilon^2}\left(\sqrt{R^2 + z_i^2} - z_i\right)$, and an interaction term which we name by H_{int}:

$$H_{int} = \frac{Cq^2}{16R^4\epsilon^2}\left(\sqrt{R^2 + z_1^2} - z_1\right)\left(\sqrt{R^2 + z_2^2} - z_2\right) \qquad (2.51)$$

This is an effective interaction mediated by the free charges in the wire and lower surfaces.

Equation 2.51 can be rewritten quantum mechanically in terms of ladder operators for each particle, since they are supposed to be axial harmonic oscillators. In a harmonic oscillator the displacement with respect to the equilibrium position is written:

$$\hat{z} = \sqrt{\frac{\hbar}{2m\omega}}(\hat{a} + \hat{a}^\dagger) \qquad (2.52)$$

, which in our case would be $\hat{z}_i = z_i - z_0$. Considering that $z - z_0$ is much smaller than R, we can expand the interaction part of the Hamiltonian in powers of $z - z_0$:

$$\hat{H}_{int} \approx \frac{q^2}{2R^3\epsilon}\xi(z_0/R)\hat{z}_1\hat{z}_2 \qquad (2.53)$$

where the relations

$$\begin{aligned} C_{disk} &= 8\epsilon_0 R \\ \xi(x) &= 1 + \frac{x^2}{1 + x^2} - \frac{2x}{\sqrt{1 + x^2}} \end{aligned} \qquad (2.54)$$

were used.

If we express $\hat{z}_i$ with ladder operators and use the rotating wave approximation, we have finally:

$$\hat{H}_{int} = \hbar\omega_{int}(\hat{a}_1^\dagger\hat{a}_2 + \hat{a}_1\hat{a}_2^\dagger) \qquad (2.55)$$

with

$$\omega_{int} = \frac{q^2}{2R^3\epsilon}\frac{1}{2m\omega_z}\xi(z_0/R) \qquad (2.56)$$

The rotating wave approximation (RWA) consists of neglecting operators which oscillate too fast in interaction picture. In our case the interaction hamiltonian operator is proportional to

$$(\hat{a}_1 + \hat{a}_1^\dagger)(\hat{a}_2 + \hat{a}_2^\dagger) = \hat{a}_1\hat{a}_2 + \hat{a}_1\hat{a}_2^\dagger + \hat{a}_1^\dagger\hat{a}_2 + \hat{a}_1^\dagger\hat{a}_2^\dagger \tag{2.57}$$

The first and fourth terms oscillate with frequencies $\pm|\omega_{z,1} + \omega_{z,2}|$ while the remaining oscillate with $\pm|\omega_{z,1} - \omega_{z,2}|$. The RWA states that the former terms can be averaged out in a time average since they oscillate much faster than the latter.

From (2.55) we see that trapped particles are exchanging a quantum of information at a rate ω_{int}. How fast is this? If we assume two trapped electrons in traps of $R \sim 1mm$, then $\omega_z \sim 100MHz$. A most harmonic planar trap has been shown to have typically $z_0 \sim R/2$, and with these numbers $\omega_{int} \sim 10Hz$. If we go to the submillimeter range, $R \sim 0.1mm$, then $\omega_z \sim 1GHz$ and $\omega_{int} \sim 1KHz$.

A further speed up of this frequency comes from manipulating the distance of the electron to the surface z_0/R. The function $\xi(x)$ can vary the order of magnitude of ω_{int}. For example $\xi(0.1) \approx 0.8$, $\xi(1) \approx 0.1$ and $\xi(3) \approx 0.003$. This means that we can improve an order of magnitude in ω_{int} by decreasing z_0/R to 0.1 . It was shown in previous sections that the distance z_0 could be manipulated to a certain extent, at the expense of increase the scale of voltages. Increasing the voltages (V) augments the axial frequency thus reducing ω_{int} proportionally to $\sqrt{V}$. So at the end it is more effective to reduce the scale of R since ω_{int} scales with $R^{-3}\omega_z^{-1}$ and ω_z only scales with R^{-1}.

2.5.2 Spin-spin effective interaction

In a proposal by Wunderlich (Wunderlich) the idea of using field gradients to couple internal degrees of freedom and consequently effectively coupling the spin of different trapped particles was given. The extension of this idea to the case of an array of trapped electrons, calculated by Dr. Ciaramicoli and me, was given in (Ciaramicoli).

The scheme is simple, let two independently trapped electrons couple their axial motion to their spin dynamics. The coulomb interaction between the electrons couples their axial motions, and indirectly their spin dynamics.

The treatment given in (Ciaramicoli) refers to a two dimensional array of planar traps with the addition of a linear magnetic gradient. There, the full three dimensional equations of motions are given and the spin-spin effective coupling calculated, considering all degrees of freedom. It is shown that the contribution of non-axial motional degrees of freedom can be neglected. Therefore I will present here a less detailed approach, considering only two electrons and only their axial motion and spin.

Let's consider two planar traps lying on the same plane but separated by a distance L, with an inhomogeneous magnetic field whose z component is $B_z = B_0 + bz$. The non-Coulomb part of the Hamiltonian of these electrons is:

$$\hat{H}_i = (\hat{N}_i + \frac{1}{2})\hbar\omega_z + \frac{1}{2}\hbar\omega_s\hat{\sigma}_{z,i} + \frac{1}{2}\hbar\omega_s\frac{b}{B_0}\hat{z}_i\hat{\sigma}_{z,i} \tag{2.58}$$

if we consider that the electrons are near the ground state and the trap has been compensated for best harmonicity. It consists of an axial oscillator with eigenfrequency ω_z, a spin motion with eigenfrequency ω_s and a term which obviously couples both motions. Here we use the conventional definitions $\hat{N} = \hat{a}^\dagger\hat{a}$ and $\hat{z} = \sqrt{\frac{\hbar}{2m\omega}}(\hat{a} + \hat{a}^\dagger)$, in terms of the harmonic oscillator's ladder operators[1].

The coulomb interaction between each other, if both electrons' motion are centered at $z_{0,1} = z_{0,2} \equiv z_0$ is:

$$\hat{H}_C = \frac{e^2}{4\pi\epsilon_0}\frac{1}{\sqrt{L^2 + (\hat{z}_1 - \hat{z}_2)^2}} \tag{2.59}$$

which for small z_0, i.e. low electron temperature, becomes:

$$\hat{H}_C \approx \frac{e^2}{4\pi\epsilon_0 L^3}\hat{z}_1\hat{z}_2 \tag{2.60}$$

plus a constant that we obviate.

In (2.58) the hamiltonian is that of an electron trapped in a perfectly quadrupolar and with an exaclty homogeneous magnetic field, plus a term coupling axial and spin motions. We can perform a unitary transformation $\hat{H}' = e^{\hat{S}}\hat{H}e^{-\hat{S}}$ to the total hamiltonian so that this term disappears. The adequate operator is:

$$\hat{S} = \sum_{i=1}^{2}\lambda(\hat{a}_i^\dagger - \hat{a}_i)\hat{\sigma}_{z,i} \tag{2.61}$$

---

[1] the z_i coordinate is $z_i = z_0 + \hat{z}_i$, because the equilibrium position of the oscillator is z_0, and I've dropped the term $\frac{1}{2}\hbar\omega_s\frac{bz_0}{B_0}\hat{\sigma}_{z,i}$ from $\hat{H}_i$ because it only shifts slightly the frequency ω_s

so that the axial ladder operators transform as:

$$\hat{a}_i \rightarrow \hat{a}_i - \lambda \hat{\sigma}_{z,i} \qquad (2.62)$$

By substituting (2.62) in (2.58) we find that the value we need is

$$\lambda = \frac{1}{2} \frac{b}{B_0} \sqrt{\frac{\hbar}{2m\omega_z}} \frac{\omega_s}{\omega_z} \qquad (2.63)$$

and the Hamiltonian of both electrons is:

$$\hat{H} = (\hat{a}_1^{\dagger}\hat{a}_1 + \frac{1}{2})\hbar\omega_z + (\hat{a}_2^{\dagger}\hat{a}_2 + \frac{1}{2})\hbar\omega_z + \frac{1}{2}\hbar\omega_s\hat{\sigma}_{z,1} + \frac{1}{2}\hbar\omega_s\hat{\sigma}_{z,2} + \hat{H}_C \qquad (2.64)$$

so the axial-spin self coupling has been hidden into the Coulomb part by this unitary transformation. All the interesting information is now in $\hat{H}_C$. Let's have a look at it:

$$\hat{H}_C = \gamma \left[(\hat{a}_1 + \hat{a}_1^{\dagger})(\hat{a}_2 + \hat{a}_2^{\dagger}) - 2\lambda\hat{\sigma}_z(\hat{a}_1 + \hat{a}_1^{\dagger} + \hat{a}_2 + \hat{a}_2^{\dagger}) + 4\lambda^2\hat{\sigma}_{z,1}\hat{\sigma}_{z,2} \right] \qquad (2.65)$$

where $\gamma = \frac{e^2}{4\pi\epsilon_0}\frac{1}{L^3}\frac{\hbar}{2m\omega_z}$. We see a spin-spin coupling term, the last one, and several other terms which can be investigated under the light of the RWA.

Let's define $\hat{H}_0 = \hat{H} - \hat{H}_C$, and change to interaction picture. I remind the reader that in interaction picture $\hat{a}$ has a phase oscillating at rate ω_z, and then we can approximate $\hat{H}_C$ by the terms which do not oscillate:

$$\hat{H}_C \approx \gamma \left(\hat{a}_1\hat{a}_2^{\dagger} + \hat{a}_1^{\dagger}\hat{a}_2 + 4\lambda^2\hat{\sigma}_{z,1}\hat{\sigma}_{z,2} \right) \qquad (2.66)$$

So the basic interaction between electrons is by exchange of quanta in the axial degree of freedom and a spin-spin coupling. If a quantum processor be made up of an array of planar traps in such a way, and by storing information only in the spins, the Hamiltonian is Ising type $H \approx h_0 \sum_i \sigma_{z,i} + J \sum_{i \neq j} \sigma_{z,i}\sigma_{z,j}$, and lends itself to the same treatment as an NMR molecule for quantum computing.

For the case of an array with inter-trap distance of $1mm$, magnetic field of several tesla, $b \sim 50 T/m$, and an axial frequency of $100 MHz$, the spin-spin coupling has a frequency of around $20 Hz$. These feasible numbers demonstrate that an array of planar trap can well be treated as an NMR molecule for quantum computation, but under control and without the necessity of considering ensembles of molecules.

Chapter 3

Planar Penning trap, experiment

After having studied the properties of the planar Penning trap, the natural following step is to confirm experimentally every single property we have theoretically predicted.

The objective is to demonstrate that:

1) The planar trap can store charged particles in a stable way.

2) The harmonic properties of the trap are as studied theoretically.

3) A double-well configuration exists with different eigenfrequencies.

4) This trap can be miniaturized without loss of control or change in its main properties (apart from the scaling laws which apply to any trap's observable dependent on size).

Next, I give a sketch of the setup I used to test the properties of the trap.

3.1   Setup

A typical setup for Penning traps consists of a vacuum chamber where the trap dwells, which is inserted into the bore of a superconducting magnet of several Tesla. Inside the chamber there is the trap with its voltage connections, the

mechanism for creation of particles, and a detection system which collects information on the particles' observables. If in addition the system needs low temperatures, the vacuum chamber gets divided into a low-temperature zone, where the trap (and typically a resonant LC tank-circuit attached to it) dwells, and a room-temperature zone connected to the exterior of the vacuum chamber, to the control system (whether it be a PC or just an oscilloscope).

The setup that I used, is to be seen as a preliminary test on the general properties of this new kind of trap, and particularly on its anharmonicity. For this, a room temperature situation and an easy detection scheme are most valuable for their simplicity. The fact that our setup is at room temperature means that the detection system is too, and thus we have no means to detect one singly trapped electron in our trap. Instead, a cloud of them will be detected, with as less electrons as permitted by the sensitivity of the detection system. For detection, a resonant circuit could be used, but a destructive method is easier to implement and requires less elements, accelerating thus the whole experimental construction.

The next step, in a quantum computing context, would be to test the trap at very low temperatures with a much more developed detection system, with an specifically designed control system (including radiating sources for coherent control of individual qubits). In this case, the aim would be to demonstrate arbitrary rotations in singly trapped electrons, plus the possibility of quantum information exchange between two different traps. Let's not forget that after this operations, a well designed quantum state detection scheme would be needed to extract the resulting information.

I specify next the detailed properties of the setup. A sketch of the whole setup can be seen in fig. 3.11.

3.1.1 Vacuum

This section is quite trivial and is intended only as a guide for PhD students and similar, which are just beginning to build their own first vacuum system. For any other reader I just want to state that we used a typical vacuum combination of prepump+turbopump for initialization, and an ion getter pump for maintenance

of a vacuum level of $10^{-8}mbar$. This level is good enough for our purposes, and going below that would require other techniques (UHV pump system, or cryogenic pumping).

A good vacuum condition is a must when considering trap physics. The molecules of gas remaining insider the vacuum chamber will collide with trapped particles, giving them an impulse kick, and releasing them thus from their trapping condition.

In order to avoid such particle loss, the vacuum should be as good as possible. Experiments at room temperature with a background gas pressure of about $10^{-8}mbar$ have shown that particles could be stored at least several minutes, so it will suffice. Going below $10^{-9}mbar$ requires a complete new approach to vacuum techniques since there begins the ultra high vacuum level (UHV), and thus we avoid this complication.

A vacuum chamber is typically a metal cylinder with flanges on both ends. This flanges are just an special ending of the cylinder which allows vacuum connection to another metal conduct which also has a flange. In this way, several pieces can be mounted next to each other so as to form a close conduct region where vacuum is properly maintained. Of course the last elements in this vacuum row is a series of pumps.

To achieve a vacuum level of $10^{-8}mbar$ we can use the habitual setup: a prepump, a turbopump, and an ion getter pump. A prepump is a pump which provides the initial power. It is the first to be turned on when vacuum is to be prepared, and is the one which produces the first stage of vacuum. The level thus achieved is between 10^{-3} and $10^{-4}mbar$, depending on how many minutes it is left working. After its work, the turbopump will be turned on. After a time of about one day, depending on the volume of the vacuum chamber and the degassing elements, the pressure is around $10^{-6}mbar$. At this point we can activate the ion pump and let it stabilize. Once stabilized, we can close the vacuum chamber so that only the ion pump has access to it.The ion pump will then work at least one day to achieve $10^{-8}mbar$.

3.1.2 Magnet

The highly homogeneous magnetic field which we usually write in our simplistic hamiltonians is much easier to write than to produce, and cheaper too. In order to have a magnetic field of several Tesla, and homogeneous at least in the trapping volume, needs the use of superconducting coils, capable of embedding high currents without being immediately vaporized. Such coils, whose material is rather expensive, are typically submerged in a liquid Helium bath ($\sim 4K$ temperature). The latter is submerged in a liquid Nitrogen bath ($\sim 77K$ temperature) because of its smaller evaporation rate.

The magnetic field produced by our magnet has been measured along its symmetry axis in its most homogeneous range, i.e. in its center; but also the fringe field was measured so as to have the complete map of the field. In figure 3.1 we see the homogeneous part of the magnetic field. It is homogeneous up to a part in several thousands. This high homogeneity was carefully tuned for future high precision trap experiments which will use this magnet in the near future.
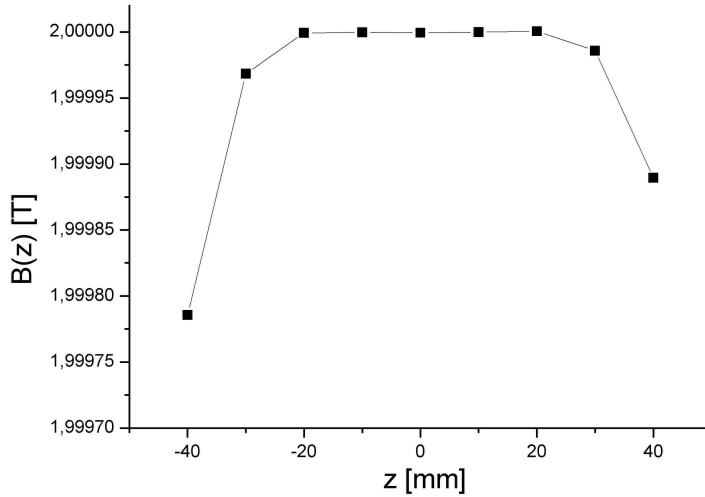

Figure 3.1: Magnetic field on the axis of the magnet's bore. It is highly homogeneous, changing $2 \times 10^{-4}T$ in a range of $4cm$.

The magnetic field outside the bore of the magnet was measured, and fitted

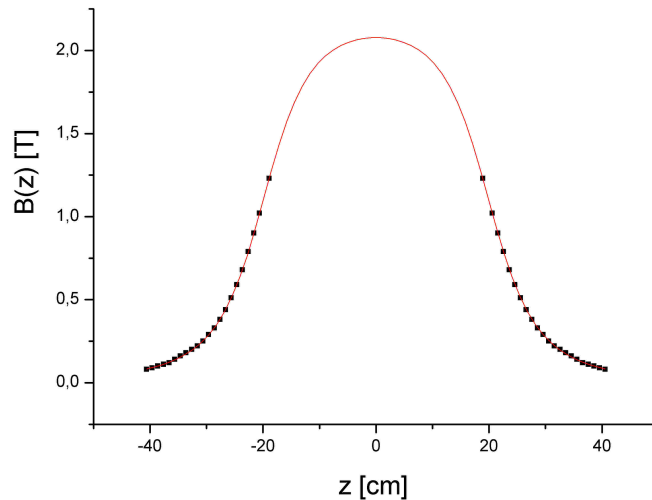by Stefan Ulmer with an expression for a single coil. The result is figure 3.2.

Figure 3.2: Magnetic field outside the magnet's bore. The fit has been done considering the magnetic field produced by a single coil of adjusted length and radius parameters.

The rapid variation of the magnetic field in this region allows us to change the value of the magnetic field that we impose on our trap. By just sliding the whole setup outwards, we can reduce the magnetic field felt by trapped particles. Of course, a rail has to be mounted for the whole setup to be movable.

3.1.3 Trap

The traps for this experiment were designed to have some metal electrodes printed on an Al_2O_3 isolating surface. The sketch is seen in figure 3.3
The technique used is thick-layer. In fig.3.3 we see two traps, which in fact are related by a scaling factor of 2 (this is only exactly true for their respective R_is).

The big one has 5 electrodes plus an outer grounded one. Its third electrode is split so as to have the possibility of applying quadrupolar radiation on the electrons. The isolator border has no metal on it since we want to clamp the whole trap from it. The trap has a small hole in the center through which
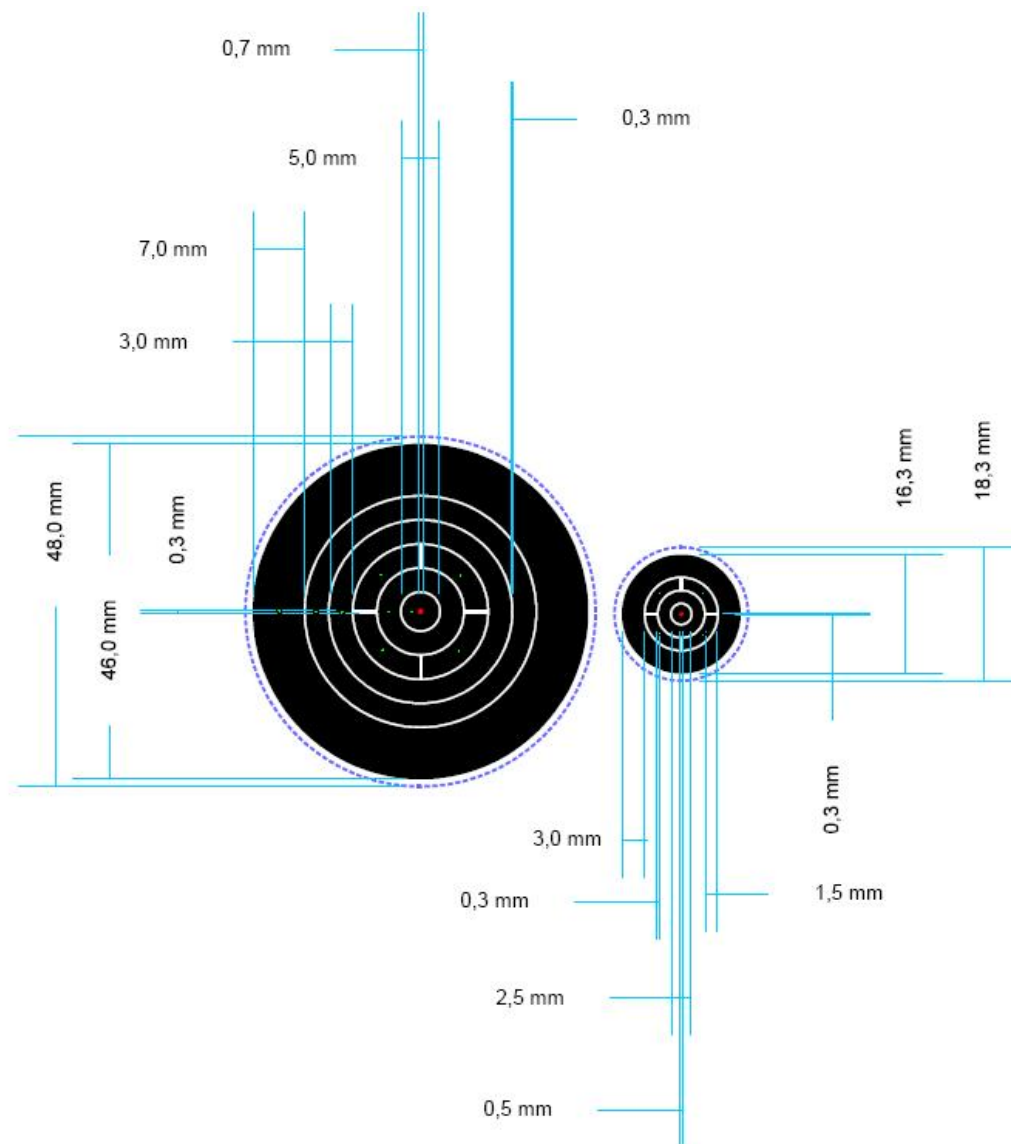
Figure 3.3: Design of front part of the planar trap. The red circle in the center represents a bore. The green circles represent metal contacts going to the rear part through the isolating material. Black represents metal and white, the isolator. The violet dashed line is a "cut here" line.

electrons will be injected. The green points represent contacts which connect each electrode to the rear part of the trap.

The small one has only three electrodes plus the ground. Its total diameter is therefore less than half of the big trap, despite its R_1 being exactly half of the big trap's one.

The real traps can be seen in fig.3.4 and in fig. 3.5.

Figure 3.4: Real trap's front side. The light-gray surface is metal and the dark-gray lines and white border is isolating material.

In our designs we haven't tried to minimize the gap between electrodes since we didn't want any residues to shortcircuit any pair of electrodes. Since the potential shape has been seen not to vary too much when having gaps, the only disadvantage to this decision if the possible charging up of this isolator space, due to collision of electrons which leave the trapping region. A countermeasure we thought of is to cover these gaps with a semiconductor layer so as to slowly

Figure 3.5: Real trap's rear side. The contact feedthroughs connect the electrodes on the front with the lines in the rear. The contact lines end up in the border of the trap, so as to clamp them to individual channels which go the exterior of the vacuum chamber.

discharge the isolator, while producing no shortcircuit. Finally, some problems of logistics avoided that we could apply such layer and the experiment was performed without it. However, no too important charging effects were observed; and the ones we saw got discharged after less than half an hour.

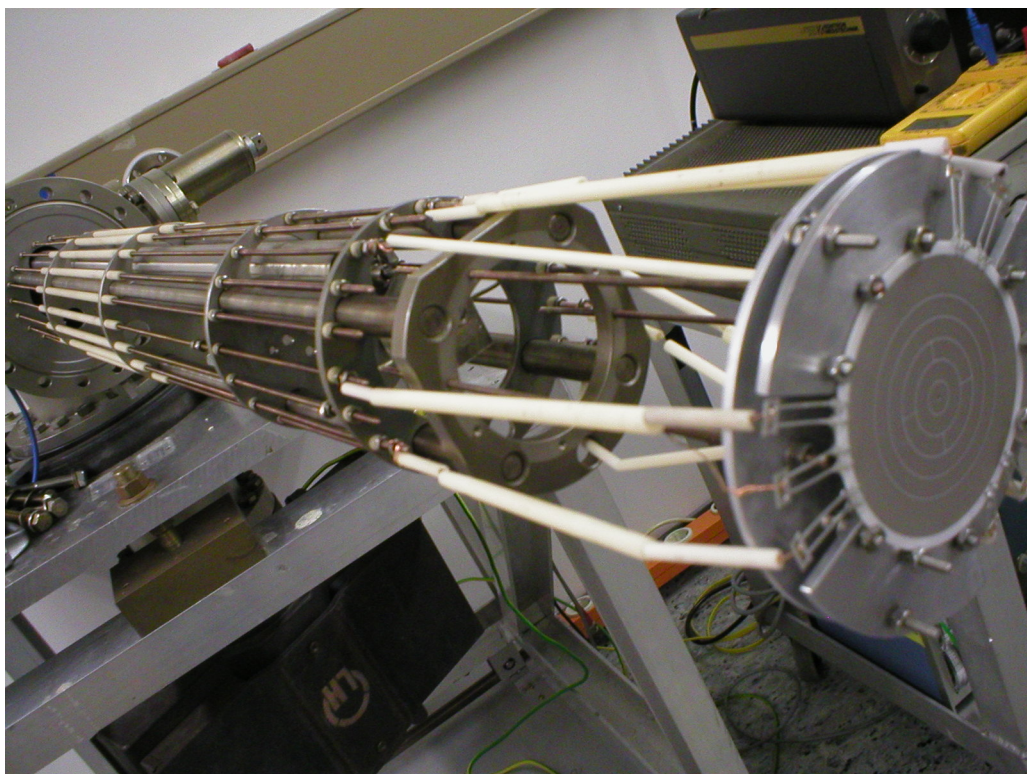The whole picture of trap installed on a holder and with all connections already prepared can be seen in fig.3.6.

Figure 3.6: Real trap's complete picture. The trap is held with several pieces of metal which are connected to a metal plate holder. The voltage connections of the traps are taken by some clamps to the setup rails which go to the outside world.

In the picture we see that our setup is made of a column of rods plus a holding structure. This rods are connections to outside of the vacuum chamber. The flange at the left of fig.3.6 is to be connected to the cylinder which closes the vacuum volume. There is a holder plate attached to the structure, which holds

mechanically the trap by touching only its border. The rear contacts we saw in fig.3.5 are pressed by clamps which are connected to the rods of the structure.

The first observation I would do if I would see this picture for the first time is: how are you going to align the trap's surface with the magnetic field? Obviously, this is a source of future problems since misalignments of this kind produce coupling between all three degrees of freedom of trapped particles and result in a reduction of their storage lifetime. In our case, since we were not to do an experiment of high precision, this alignment was done by my eye. The reader may now be abhorring of such a procedure, but it should be said in my favor that the human eye has a precision normally far underestimated. I would rather affirm that my eye can align the trap with a precision of less than 2 or 3 degrees, in both angles. Such a tilt is sure to produce coupling and to enhance trapping instabilities, but it's not big.

In next section I explain the creation procedure.

3.1.4   Electron creation mechanism

Electron creation is achieved by thermoionic emission from a hot wire made of thorium and tungsten. Imposing a current of several amperes to the wire dissipates power in terms of light and emitted electrons. The wire is set as a whole on negative voltage so as to accelerate the produced electrons to the trapping region.

Once in the trapping region, those electrons collide with the residual gas thus ionizing it and producing secondary electrons. Secondary electrons which are produced inside the trapping volume and have less kinetic energy than the depth of the potential where they were born, will remain inside the trapping volume. Since we will mostly ionize hydrogen -with an ionization energy of $13.6eV$-, the threshold acceleration needed for primary electrons is above $\sim 14V$. This accelerator voltage can be fine tuned every time, but a voltage between $14V$ and $25V$ was seen to be the best working range in our experiment.

The wire is connected to an independent holder made of isolating material (makor). This can be seen in fig.3.7.
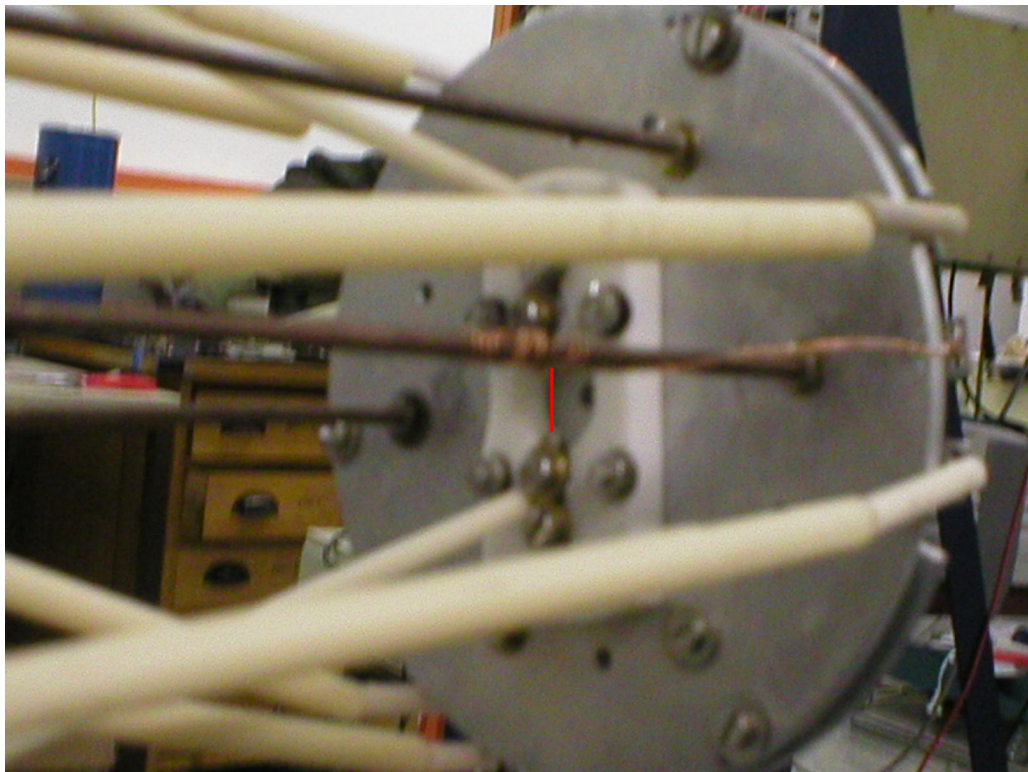The red thick line represents the wire of thickness $\sim 0.1mm$, which is hard to see

Figure 3.7: Sight of the creation filament in the rear part of the trap. It is also connected to the rods of the main structure, so as to provide the necessary current. I have plotted the filament as a red thick line since it could not be seen in the original photo. Its real thickness is $\sim 0.1mm$.

in the original picture. It is held by two screws mounted on a piece of makor, and connected to two independent rods for current provision. The primary electrons are created and accelerated towards the central hole in the trap, through which they reach the trapping region. Since this hole has a radius of $0.7mm$ (see fig.3.3), secondary electrons are created within a cylindrical volume of the same radius. Considering that the length of that cylinder is $L \sim z_0/2$. That gives an initial trapped cloud's volume of $\sim 0.8mm^3$ (for the most harmonic configuration). This number will help determine the number of trapped electrons in a later section.

3.1.5 Detection mechanism

A simple and straightforward detection scheme is to use an electron multiplier. The goal is to measure the eigenfrequencies of the electrons, which is done by dipolar excitation. Such radiation is varied in frequencies to scan the whole shape of eigenfrequency resonances. When the frequency of the radiation coincides with an eigenfrequency, electrons will absorb energy and oscillate in an every time wider orbit, finally leaving the trap if the radiated power is enough. So detection of resonances can be measured by exciting the electrons and then detecting how many of them have left the trap.

Detection of the number of trapped electrons could also be done with an attached resonant tank circuit. The number of electrons remaining after radiation, can be calculated from the height or width of the resonance dip. Such detection doesn't require emptying the trap.

In the case of a destructive detection scheme, for example with an electron multiplier, trapped electrons would be radiated and then ejected from the trap after radiation, and collide with the detector producing a current cascade. The amount of current produced by that collision gives the relative number of electrons which have remained in the trap after excitation.

Our creation method gives an abundant jet of electrons every time we like, and we can afford emptying the trap every measurement cycle and filling it up again. Hence, an electron multiplier will do.

Because we want to detect all the flux of electrons, we want to place the detector in the homogeneous region of the magnetic field. Otherwise the electron

flux tube would expand when coming to regions of lower magnetic field, and electrons might escape the collision area of the detector. Therefore, electron multipliers which can work in high magnetic fields are required.

An example commonly used is the multi-channel-plate electron multiplier (MCP). It consists of a 2D lattice of adjacent small tubes made of resistive material. In addition to the resistive material there is an emissive layer, responsible for the production of secondary electrons. The resistive layer serves to distribute the high voltage which is applied in each end of the tubes.

For detection of electrons we would set a positive high voltage at the exit of the tubes and ground at the entrance. The incoming electrons hit the walls and produce secondary electrons which are accelerated. This secondary electrons collide again with the walls and produce more electrons. This process is repeated several times till a multiplication factor of 10^6 is commonly achieved.The tubes are usually manufactured with certain tilt, so as to maximize the initial electron impact. The main idea is shown in fig.3.8.

After the flux of electrons coming from the trap has passed through the multiplier tubes, it collides with a metal plate which is connected to, let's say, an oscilloscope. The result is that every incoming electron cloud produces a sudden pulse of negative voltage in the plate. This becomes a negative signal dip in the oscilloscope.

In fig.3.9 we see the working setup used for our MCP. The MCP has a double stage, i.e. it is like two MCP one after the other. A positive high voltage of around $2KV$ is applied to electrode 3, and it is distributed to electrodes 2 and 1. With the resistors in between we produce a voltage ladder. The plate receiving electron impact is connected capacitively to an electronic amplifier. The signal is afterwards processed in the oscilloscope.

Because the MCP channels are so thin (radius $\sim 10\mu m$) and are tilted with respect to $\vec{B}$, cyclotron orbiting of electrons (with a radius of $\gtrsim 30nm$ for a field of several tesla) will not avoid them from hitting the channels' inner walls. So this is the correct choice.

In order to characterize our MCP, we shot pulses of electrons from our creation filament repeated times, and measured the resulting amplified signal for different MCP voltages and differente magnetic fields. The variation of magnetic field on
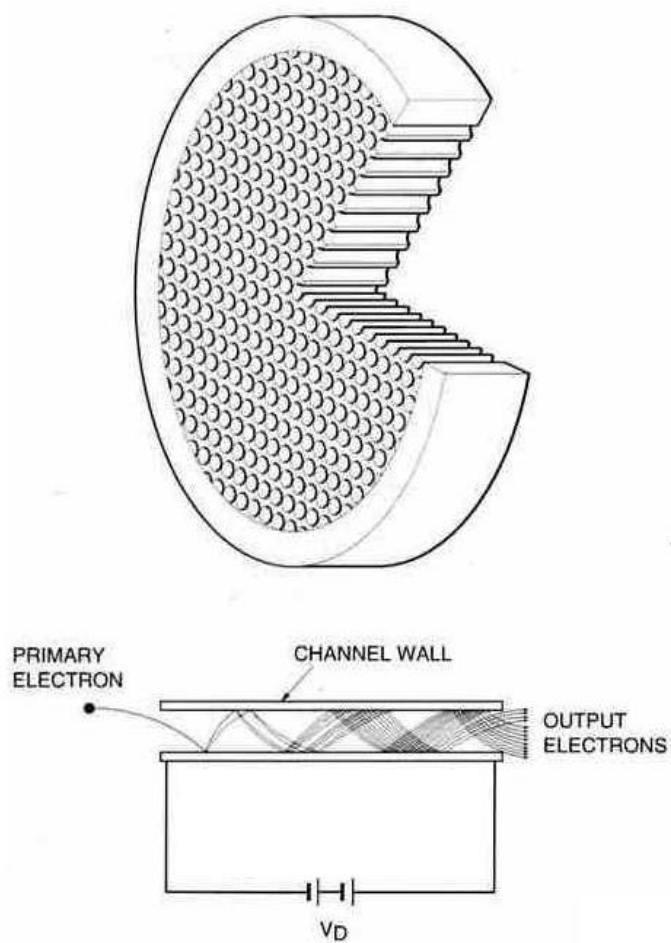
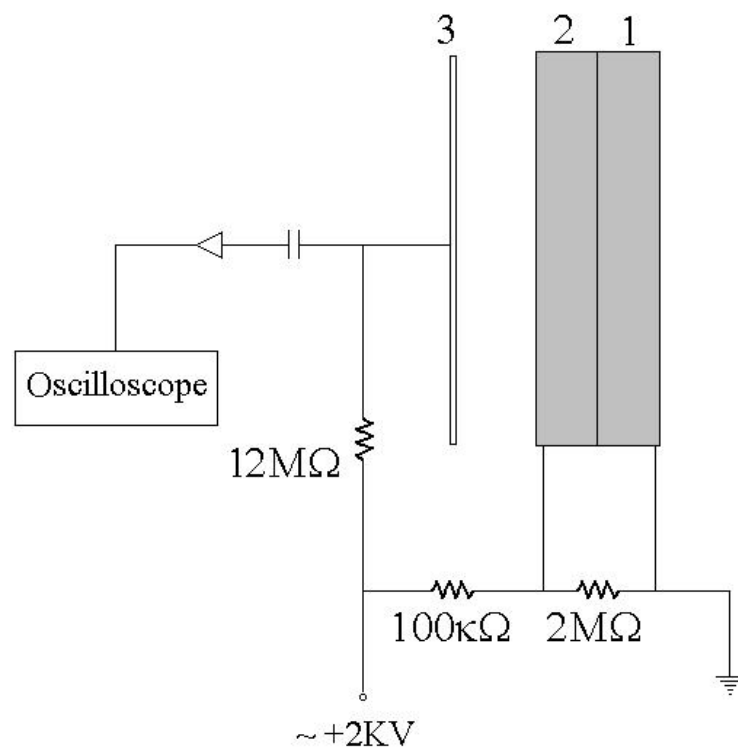Figure 3.8: MCP scheme. Electron multiplication by cascade is illustrated below.

Figure 3.9: MCP circuit setup for detection of negative particles(particles arrive from the right. After multiplication the signal is electronically amplified and registered in the oscilloscope.

the MCP was done by moving the whole setup along the magnetic symmetry axis.

The main results are shown in fig.3.10. There we see the amplification depending on the magnetic field and the voltage applied in the MCP. The picture below was measured by Paula Fernández for her diploma thesis, and the one above was measured by Paula and me. The fitted curve in the picture below was obtained by use of the theoretical curve from Hamamatsu$^{\text{TM}}$.

Considering that our MCP is placed in a region where the magnetic field is around $1T$, the amplification is still good. It is seen, too, that the best operating voltage is around $2kV$. Both experimental curves fit quite well with previous characterizations of this MCP, in particular the one by Hamamatsu which is the manufacturing company.
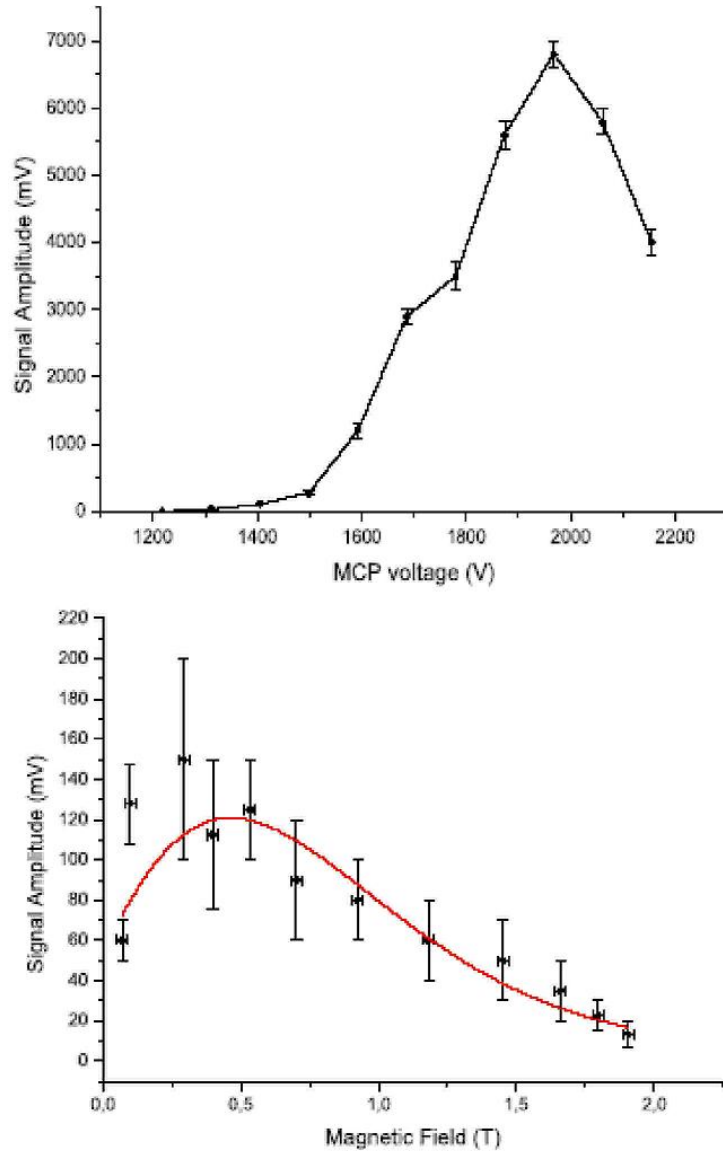
Figure 3.10: Electron multiplication depending on applied MCP voltage and magnetic field. The amplification saturates for voltage differences bigger than $\sim 2kV$. The solid line in the magnetic dependence part is the curve given by the manufacturer; the experimental data was extracted from the Diplomarbeit of Paula Fernández. Best operation is performed at $\sim 0.5T$, however enough amplification exists for $\sim 1T$, which is the actual field that our MCP "suffers".

3.1.6 Complete setup

A complete scheme of the setup used for our experiment can be seen in fig.3.11: It consists of the vacuum chamber which allocates the creation filament, planar
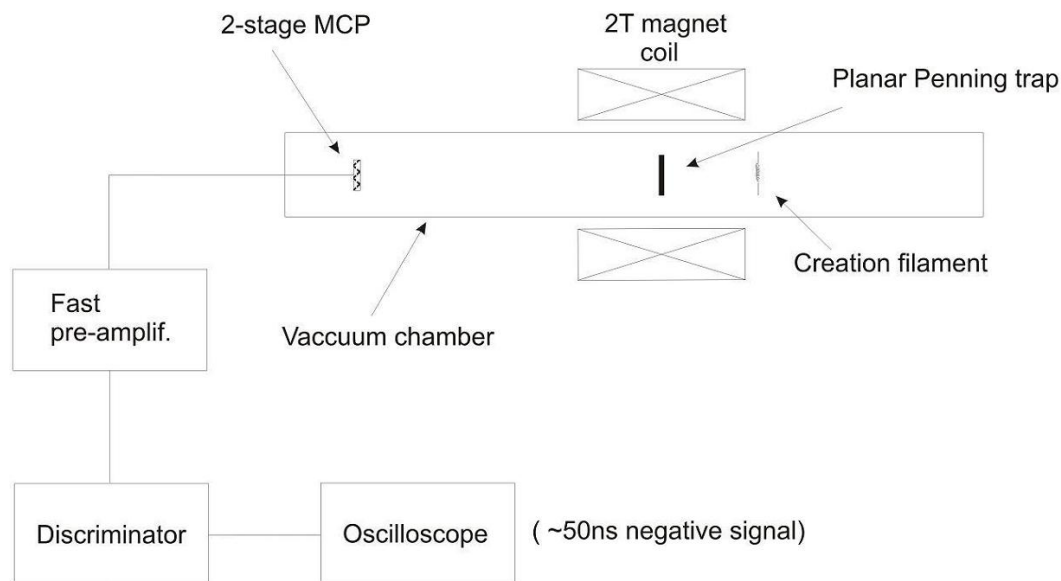

Figure 3.11: Scheme of the experiment. Vacuum chamber with trap, creation filament and MCP detector is positioned in the bore of our magnet. The electronic setup consists of an amplification stage plus visualization in the oscilloscope.

trap, and MCP detector. This vacuum chamber is inserted into the bore of our superconducting coil magnet of $2T$. The power provision for the filament and MCP, and the voltage control for the planar trap comes from outside. The signal produced in the MCP goes to a fast electronic preamplifier (from Ortec$^{\text{TM}}$) and is afterwards filtered for low-amplitude noise reduction through an electronic discriminator. The remaining signal is then processed by an oscilloscope. The oscilloscope gives basically the height of the signal, since its width in time is almost constant independently on the amount of electrons hitting the MCP; this is so because of the characteristic time of the MCP.

The height of the signal is proportional to the number of electrons hitting the MCP, unless the MCP becomes saturated which is not the case since our trapping volume cannot embed so many electrons. Of course this height gives

only information on the <u>relative</u> amount of electrons. The information on exactly how many electrons we detect could be extracted if we would calibrate the MCP with a known electron source, thus extracting the exact amplification factor of the MCP. However, such calibration is not needed in this experiment since we'll always work with relative number of electrons, for example when we scan for eigenfrequencies.

We see in fig.3.12 a picture of the whole setup. Here the vacuum chamber is closed and trap+filament connections can be seen in its rear part. The setup is mounted on a rail which allows for easy extraction of the setup. This rail allowed us to measure the MCP's multiplication versus magnetic field; it also permitted to scan for the cyclotron eigenfrequency, since our wave generator could not reach the needed value at full magnetic field strength.

The vacuum chamber table has an attached ion getter pump under it, which cannot be seen. All ground connections were attached to this table which acted as a common ground, in order to avoid parasitic signals.
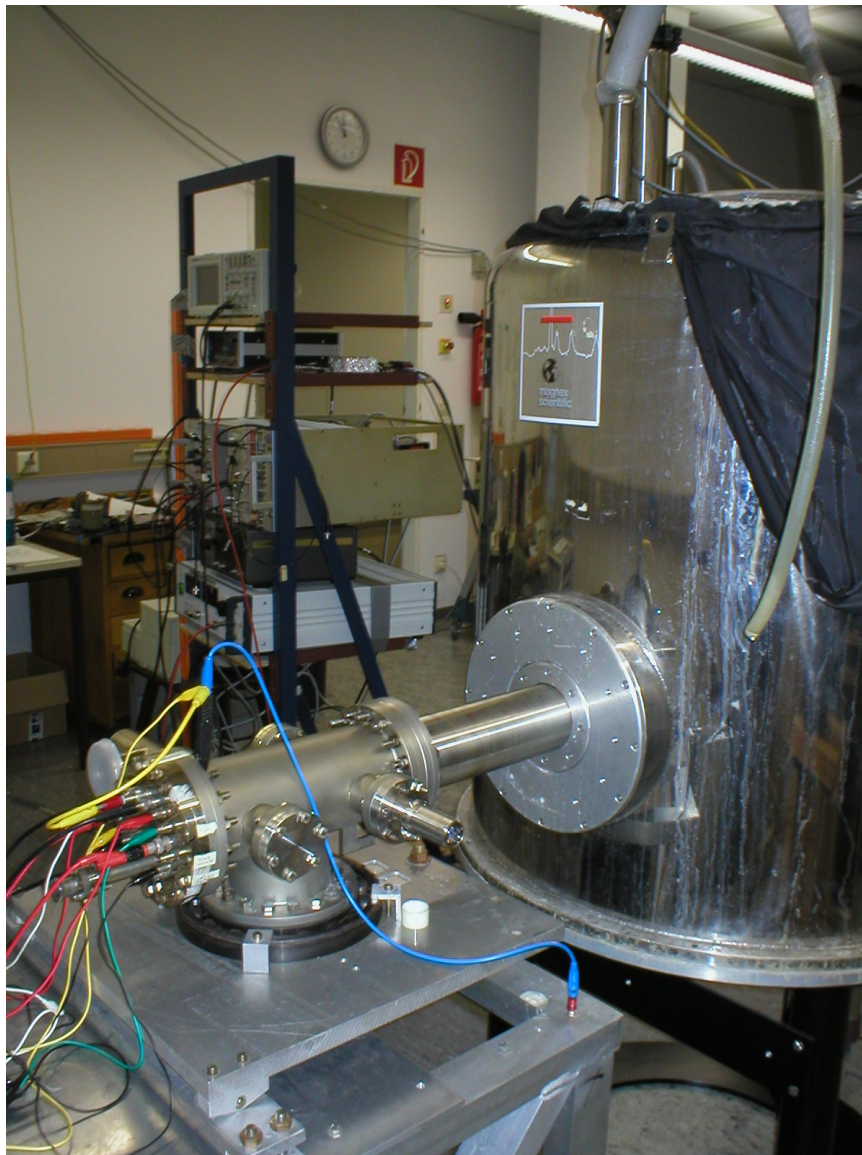
Figure 3.12: Picture of our experimental setup. The vacuum chamber, mounted on a rail, is inserted into the magnet. Control lines feeding the trap and filament are seen in the rear part. The connections for the MCP cannot be seen since they are behind the magnet, at the other end of the vacuum chamber.

3.1.7   Measurement cycle

The measurement cycle in this experiment is rather similar to those used in Penning trap experiments at room temperature. There is first a *creation time*(t_1) where the filament creates electrons and ejects them towards the trapping region. At this stage the filament has a negative voltage so that electrons are repulsed and go to the trap. The storage potential (V_2, with $V_1 = 0V$, and V_3 fixed) is positive so that trapping is possible.

Then a *storing time* (t_2) where the filament stops sending electrons to the trap. This is done by turning the filament's voltage to positive, attracting this way all electrons that it creates. During the storing time the electrons are trapped, and we perform on them any operation we need to do, for example exciting them with radiation.
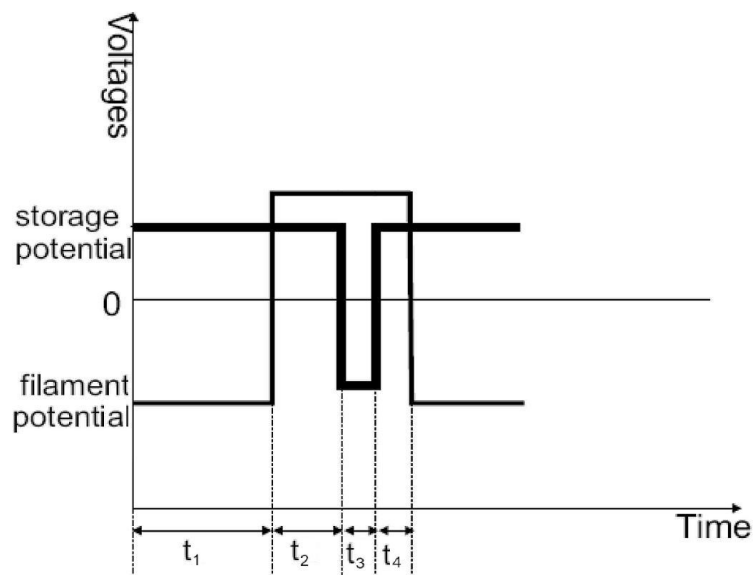

Figure 3.13: Measure cycle composed of: electron creation time (t_1), storage time (t_2), ejection time (t_3) and waiting time (t_4). Storage potential represents V_2, while V_1 and V_3 are kept fixed. The filament, creating electrons continuously, ejects them to the trap or reabsorbs them depending on the sign of its voltage.

3. PLANAR PENNING TRAP, EXPERIMENT

After that comes ejection of the electrons. This is achieved by pulsing the storing voltage (V_2) to negative values during a time t_3, thus forcing the electrons out of the trapping region. Ejected electrons fly towards the detector.

After this has been done there's a *waiting time* (t_4), where the storage potential is restored to the trapping state, but the filament still remains in inactivity. After that time, the cycle of creation, storage and ejection is renewed.

In fig.3.13 we can see the scheme of the cycle, which is rather simple. Typical numbers for these times are: $t_1 = 50ms$, $t_2 = 35ms$, $t_3 = 5ms$ and $t_4 = 10ms$. They were nonetheless fine tuned every time the vacuum conditions or the trap parameters where changed, so as to obtain the best signal to noise ratio.

The potential on the filament, as stated previously was about $\leq -14V$. The positive part was at $\sim\ +1V$.The filament is creating electrons all the time, since it is a bad practice to turn on and off repeatedly the high current in it. Therefore we switch its voltage sign so that these electrons are either sent to the trapping region or reabsorbed by the filament.

The storage potential used was V_2 for the positive part, and around $-7V$ for the ejecting part.

All these values were also fined tuned every time the conditions were changed.

3.2   Results

Well, of course, as in any other experiment with a new trap, the first thing is to check whether our trap works or not. If it works, the experimenter is filled with joy for the first time since the beginning of the whole process of trap design, setup construction, etc. I still conserve the picture in the oscilloscope when we first saw the electron signal confirming that our planar trap worked. It is shown in figure 3.14. The square shape is the storage potential, positive for trapping,
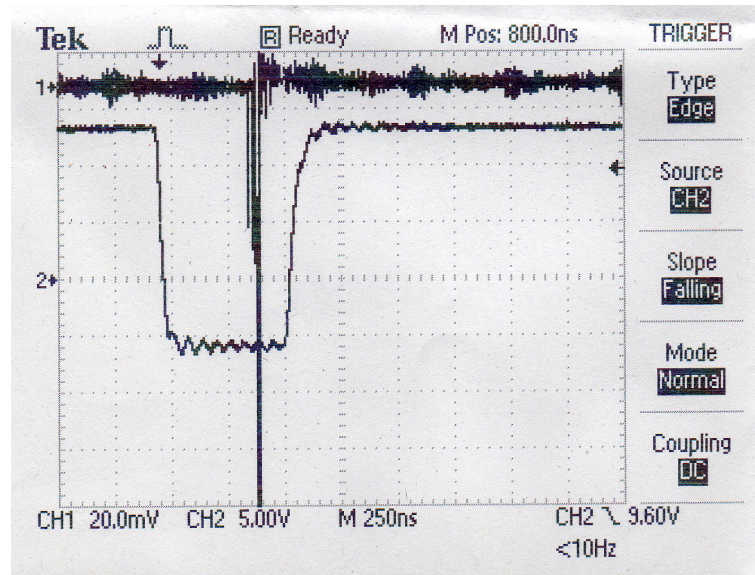

Figure 3.14: First signal detection in our experiment. The narrow dip indicates the cloud of previously trapped electrons arriving to the MCP detector. The square signal is the storage potential. It goes to negative values for ejecting electrons from the trap.

negative for electron ejection. The narrow dip signal shows the cloud of electrons arriving to the MCP detector. The delay time between ejection and detection is around $0.4 \mu s$.

Picture 3.14 shows that our setup works, electrons are trapped and detected as expected. In order to check whether this signal was real or an artifact, we raised the MCP to a potential higher than the cloud's kinetic energy, so that

electrons coming from the trap could not surmount it. In this situation no electrons were detected. That confirms that our signal is really coming from the trapped electrons. Now we can begin measuring the properties of the planar trap[1].

3.2.1 Storage time

The first I measured was the storage time. Storage time is defined as the average time that an electron stays inside the trapping volume. The main factors inducing electron loss are collision with rest gas molecules and internal mode coupling of the electron itself. The first effect can be reduced by improving the vacuum conditions. The second, by making the electric and magnetic fields more homogeneous. Since we store more than one electron each time, the Coulomb coupling of the electrons cloud also translates into an energy transfer, which can only be reduced by working with a less dense cloud.

The storage time thus gives an idea on how stable are electron orbits in our trapping conditions. For standard Penning traps at similar pressures and magnetic field, storage times of the order of minutes or seconds are found (Paasche). I measured the storage time with the planar trap place at highest and most homogeneous field ($B \approx 1.99T$). The resulting storage time is $\tau = 22 \pm 2s$.
Another measurement of the storage time at the region of $B \approx 0.3T$ gave a storage time of $\tau \sim 17 \pm 8ms$. A quick look at fig. 3.2 shows that in that region the magnetic field is highly inhomogeneous, which couples the spatial degrees of freedom of the electrons. In that situation, the magnetron motion can receive and give energy, so it can expand its orbit till the electron comes out of the trapping volume.

It is a known fact that the storage time effectively scales as B^2, so the two different storage times I measured are obviously not following this scaling law. The explanation might well come from the fact that the measurements were not at all done in the same vacuum conditions, not even in the same month! In the lap between both measurements, the setup had to be opened several times and therefore we can neither assure that the vacuum conditions were equal nor that the

---

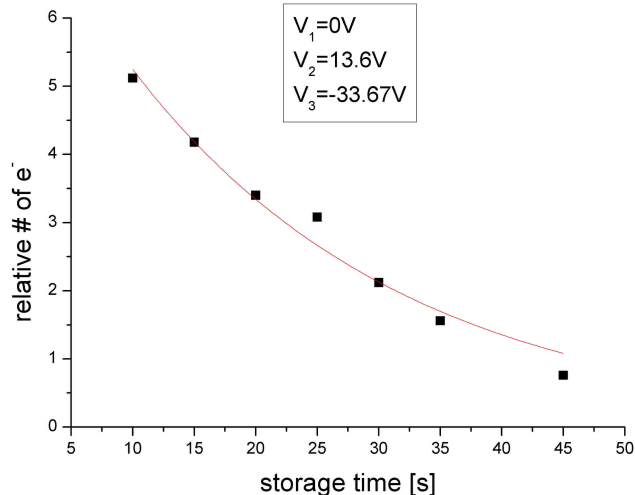[1]Part of the results in next sections has been already published in (Galve2).

Figure 3.15: Storage time at a field of $B = 1.99T$ and best homogeneity conditions. Rest gas pressure was several times $10^{-8}mbar$.

alignment of the trap along the magnetic field was the same. Such misalignments produce important reductions in storage times since they also lead to undesired mode couplings.

3.2.2   Eigenfrequencies

I also measured the motional eigenfrequencies of the trapped cloud of electrons. This was performed by dipolar excitation of their motion with an oscillating voltage in one of the electrodes, which we previously split into four pieces(It was split into four in order to have the possibility of applying quadrupolar excitation too, but this feature wasn't used at the end). This oscillating voltage forces the harmonic oscillator which is the cloud, and when its frequency coincides with any of the cloud's eigenfrequencies the cloud absorbs energy till it escapes the trapping volume.

Due to the anharmonicity of the electrostatic potential and inhomogeneities of the magnetic field, the three eigenmotions are coupled to each other. If we furthermore consider that the trap electronics is coupled to the cloud of electrons

through induced image charges, the complete picture dictates that the electrons's cloud has an effective damping. This causes the cloud not to have strictly unique frequencies of infinitely narrow shape, but resonance curves.

In order to plot those resonance curves, we apply an oscillating voltage in the split electrode with a frequency which runs over a given range. For every single step in frequencies we will measure how many electrons have been excited by this radiation. Since the MCP signal's height is proportional to the number of electrons impacting against it, we can call this "height" "relative number of electrons". For every frequency we trap electrons, excite them and eject them, and note down how many survived the excitation. If this is done for every value of the changing excitation frequency, we end up with a plot of the resonance but inverted (meaning by this that 1 represents that no electron was excited sufficiently, and 0 represents that all electrons were forced out of the trap because of the excitation).

Next figures show the plots obtained for the radial eigenmotions: cyclotron and magnetron. Figure 3.16 shows the scan in frequencies around the magnetron
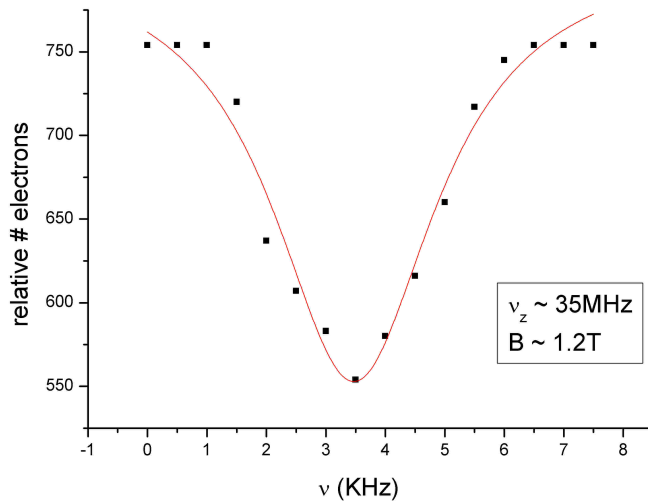

Figure 3.16: Magnetron resonance of a cloud of electrons in the fringe field, with $B \approx 1.2T$ and axial frequency $\approx 35MHz$.

eigenfrequency. The measured resonance is centered at $\nu_- \approx 3.5KHz$ and has

a width of $\Delta\nu_- \approx 2\text{KHz}$. The reason for such a big width is found in the fact that we measured this frequency with our trap sitting in the fringe magnetic field, which is very inhomogeneous. This inhomogeneity broadens the magnetron signal. Figure 3.17 shows the scan for cyclotron motion. This measurement was
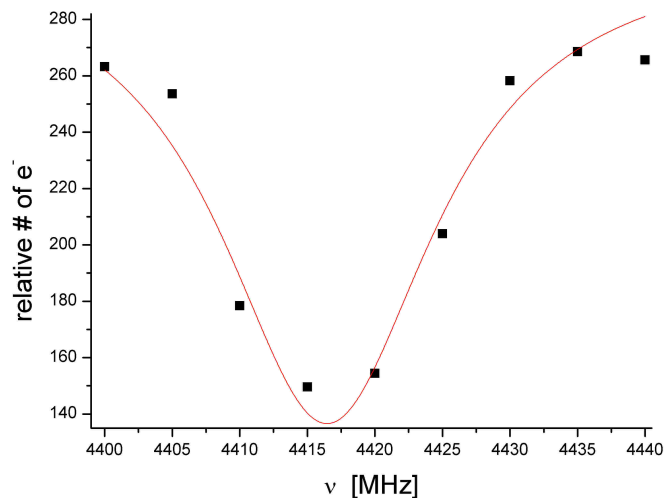

Figure 3.17: Cyclotron resonance of a cloud of electrons in the fringe field, with $B \approx 0.16T$

done in an even less homogeneous magnetic field than the magnetron one. Our wave generator could not provide frequencies high enough to excite the cyclotron motion with the trap in the highest field region, so we worked in its fringe part. The resonance is centered around $\nu_+ = 4.416\text{GHz}$ and has a width of $\Delta\nu_+ \approx 18\text{MHz}$. The magnetic field in this measurement was about $0.16T$. A simple calculation for this magnetic field shows that this frequency is what is expected from the formula $\omega_+ \approx \frac{eB}{2m}$.

This two scans show that the cloud of electrons behaves as expected for any Penning trap, at least in its radial motion, having nearly Lorentzian shapes centered at the expected values.

Next we scanned the axial frequency, and the results can be seen in figure 3.18. The scan was done with $V_1 = 0V$, $V_2 = 13.6V$ and $V_3 = -33V$. This con-

figuration is most harmonic, something which is desired so that peaks are narrow enough, and so that we are able to separate the individual and COM (center of mass) resonances which we expected to see. These two resonances are related to the individual motion of electrons and to the motion of the whole cloud, respectively. The left peak corresponds to the individual motion of electrons. It is wider because every electrons sees a different anharmonicity in the potential and feels a different average Coulomb force coming from the rest of the cloud. The resonance in the right corresponds to the COM motion, that is, the cloud acting as one unique body. This resonance is only broadened by the inhomogeneity of the electrostatic potential. Normally, these separation into two peaks can be most easily seen in the $2\omega_z$ resonance, but we saw it in ω_z too.
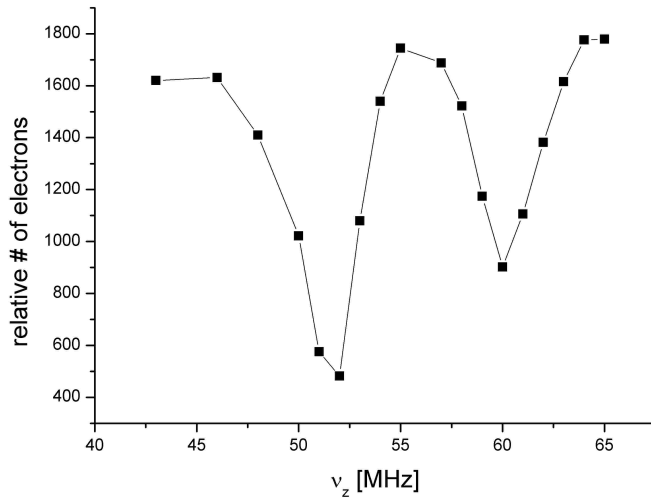

Figure 3.18: Axial resonance's double-peak structure with $V_1 = 0V$, $V_2 = 13.6V$ and $V_3 = -33V$. COM and individual motions are excited at different frequencies due to Coulomb repulsion, being the individual resonance always centered at lower frequencies than the COM one.

The real axial frequency associated to the trap in fig.3.18 is just the COM frequency, that is $\nu_z \approx 60$MHz. Substituting the applied trap parameters into our standard derivation of the potential, we expect an axial frequency of $\nu_z =$

$61.3 MHz$ and a width of $\Delta\nu_z = 3\text{MHz}$, which is what we see in this picture. This demonstrates that our theoretical calculations were right.

Later on I will speak a little bit more about this double resonance and its shape.

3.2.3 e^- number estimation

The number of trapped electrons cam be estimated by two procedures: either we calibrate the efficiency of our detector with a well known electron source, or we study the shift in the individual peak of ω_z. This shift is caused by the fact that the cloud, as a whole, only sees the potential of the trap, but each individual electron feels the Coulomb repulsion of its neighbours. This difference in the total effective potential shifts the individual resonance with the respect to the COM one, in proportion to the amount of electrons which are trapped. They simplest expression for the center of the individual resonance is obtained by considering the cloud as an uniformly charged sphere (Desaintfuscien):

$$\omega_z' = \omega_z\sqrt{1 - \frac{\omega_p^2}{3\omega_z^2}} \quad , \quad \omega_p^2 = \frac{q^2 n}{\epsilon_0 m} \tag{3.1}$$

where n is the number density of electrons, m, q their mass and charge, ϵ_0 is the dielectric constant of vacuum and ω_p is the plasma resonance frequency. This shift was measured for different electron densities under similar conditions to our experiment, but with a hyperbolical Penning trap, in (Valenzuela).

I've reproduced here their graphic (fig.7 in their paper) for illustration, in fig.3.19:

If we have a look at fig.3.18 we see a shift of about 8MHZ@60MHz. Introducing this into eq.(3.1) we obtain an electron density:

$$n = 1.1 \times 10^4 \frac{electrons}{mm^3} \tag{3.2}$$

In order to know how many electrons we really have, and not the density, we need to know the trapping volume. This volume was estimated in section 3.14 to be $\approx 0.8 mm^3$, thus the number of electrons in fig.3.18 is around 8.9×10^3. The difference from our number of electrons and the number in fig.3.19 is due to
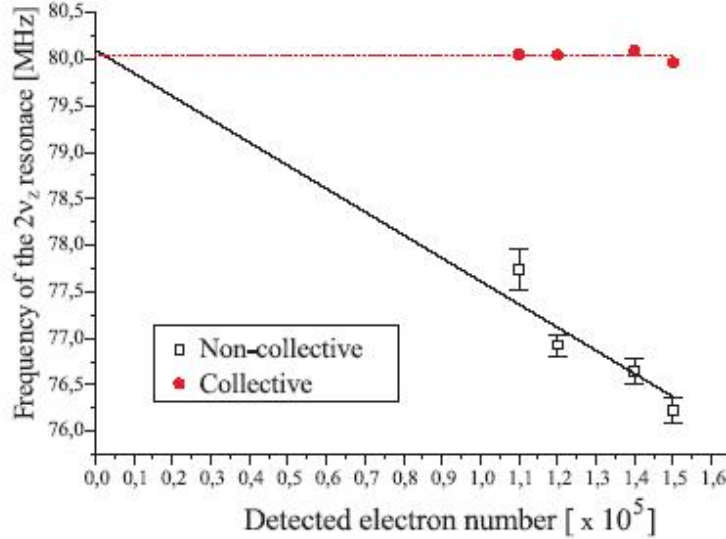
Figure 3.19: Shift in individual(non-collective) axial resonance due to cloud's space charge, with respect to COM (collective) frequency. Figure obtained in previous Penning trap experiments with electrons in Mainz(Valenzuela).

the different trapping volumes; in fact their trapping volume seems to be around $20mm^3$. This difference in volumes makes us have bigger shifts with less electrons in our trap.

3.2.4 Double well configuration

I explained in section 2.4.5 that with 4 electrodes a double well configuration of the potential could be obtained. In such situation we would have two different electron clouds with different frequencies.

I tuned the voltages of our trap to $V_1 = 0V$, $V_2 = 3V$, $V_3 = -13V$ and $V_4 = 14V$, so as to have a similar shape as in fig.2.19. The expected axial frequencies for these voltages are $\omega_z^{(1)} = 4.3$MHz and $\omega_z^{(2)} = 24.6$MHz. The result of the scan in frequency can be seen in fig.3.20:

When I did this measurement, the stability of the signal was very bad and nothing I tried made it any better. Finally I could measure two obvious peaks, which apparently coincide with the harmonics $4\omega_z^{(1)}$ and $3\omega_z^{(2)}$ of the expected frequen-
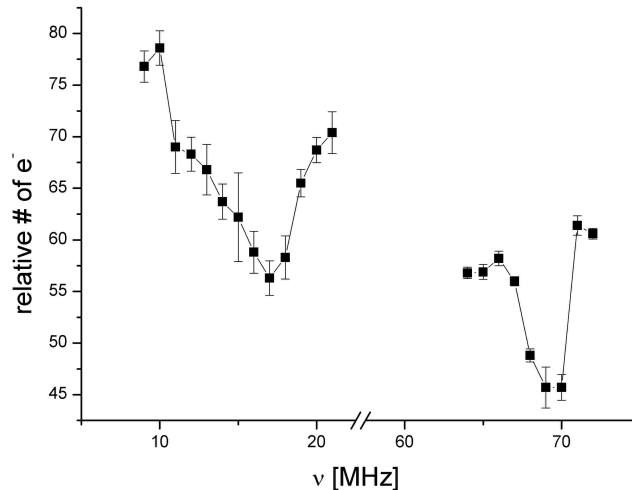
Figure 3.20: Resonance peaks in double-well configuration. Measured frequencies are 17.5MHz and 69MHz.

cies. I do not have an explanation why it was so difficult to have a stable signal for double-well configuration, or why I measured those particular harmonics.

In fact we could think that we have no double-well configuration at all and therefore I have measured different harmonics of the same unique frequency. This can be discarded if we try to match the two experimentally obtained frequencies, since $\omega_z^{(2)}/2 = 12.3$MHz doesn't coincide with 17.5MHz and $16\omega_z^{(1)} = 68.8$MHz is too high a harmonic to be easily measured (every higher harmonic needs more power to get excited).

Some collective effects might be happening, such as repulsion of the different clouds, or a combined motion. We haven't calculated which situation (within double-well configuration) might lead to unstable orbits of the clouds, or how the original frequencies are shifted and broadened. Some nonlinear behaviour could in princple explain the instability of this configuration, and maybe also the measurement of particular harmonics. This is left as a possible study for the future.

I would stress, before finishing over this topic, that I repeated this experiment

more than 10 different times and was successful only once; such is the instability of this configuration, or I was doing something wrong, the future shall judge.

3.2.5 Anharmonicity

Anharmonicity is an abstract concept which has no real observable equivalent. However, it is tightly related to the width of the axial resonance. It is well known that a damped forced harmonic oscillator has a Lorentzian-shaped frequency resonance whose width has to do both with the amount of damping and with the anharmonicities of the potential. This two effects, within my knowledge, cannot be disentangled but numerically. If we perform a numerical simulation we can adjust the damping (the anharmonicites are included by simulating the exact potential) till it matches the experimental resonance widths. It is also possible to make a simulation without damping, in which case the width of the resonance would be fully produced by anharmonicities and we could compare them with those obtained theoretically in previous sections.

In this section, however, I will consider the anharmonicities to be predominant, and therefore the resonance widths being proportional to κ, the theoretical value.

In figure 3.21 we see the first test. For that measurement I used four electrodes, so as to have more electrons inside the trap and a better measurable signal. There we see the measured width of the axial resonance (squares+line) and the theoretical value $\kappa\omega_z$ obtained with an amplitude $A = z_0/5$. The parameters used for the theoretical curve are the real sizes of the trap: $R_1 = 2.5mm, d_i = 3mm$. At first sight we observe that both curves are rather similar in shape and height, but there's a slight shift in V_3 of about $5V$. This shift is quite not a surprise, since our idealization of the trap has neglected the gaps between electrodes. It may mean that, being the gaps non-negligible, the third electrode is further apart in reality than in our idealization, and hence we need a more negative V_3 to make the potential harmonic. I will insist on this point in later graphics.

Another interesting point is the fact that the heights of both minima in the curves coincide. This is due to me fitting the ratio A/z_0, and so it is no big surprise. In fact, this fit can give valuable information on the amplitude, which in a room temperature experiment with a lot of electrons is not really related to
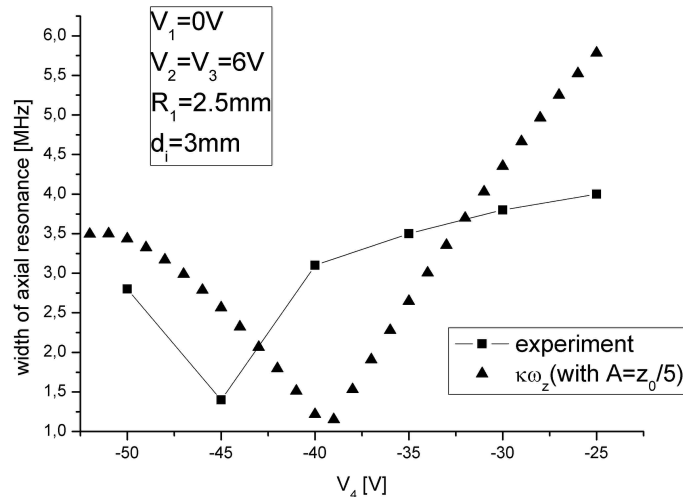
Figure 3.21: Width of the axial resonance, theoretical and experimental. A quite good qualitative and quantitative agreement is achieved, helped by fitting the ratio A/z_0.

the temperature of the setup (due to thermalization), but has more to do with creation conditions, vacuum level, etc.

It is concluded from figure 3.21 that a careful analysis of the effective sizes of electrodes has to be performed. It becomes logical if we think that the gaps between electrodes contribute to sizes but not to voltages. For example, the gap between electrode 1 and 2 makes the position of electrode 2 further apart from $\rho = 0$ than in the idealization, but doesn't contribute the potential since it has no applied voltage at all. Putting an electrode further from $\rho = 0$ makes its voltage contribute less to the potential, and therefore we can understand that there's a complicated balance of sizes and voltages when regarding anharmonicity and other trap observables. In figure 3.22 I have plotted the same curves, but changing the widths of all electrodes except the first. Instead of $d_i = 3mm$(the real sizes), I have used $d_i = 3.5mm$. Now we see that the V_3 for minimum anharmonicity coincides for theory and experiment. This demonstrates that the former explanation is on the right track. Therefore, in an effective way, our trap
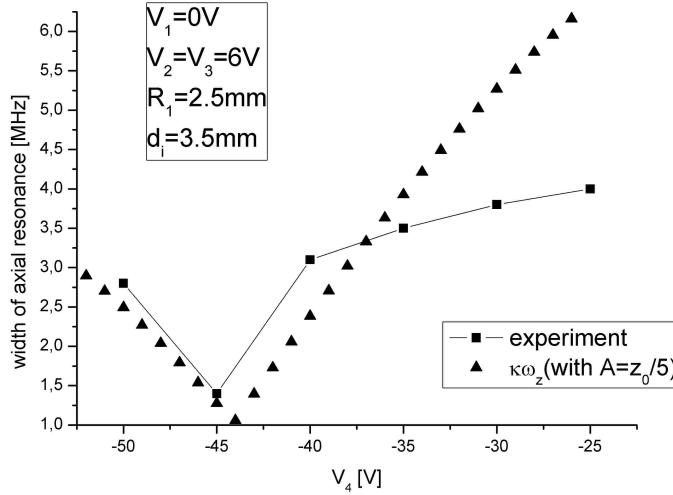
Figure 3.22: Width of the axial resonance, theoretical and experimental. For the theoretical curve we have adjusted A/z_0 and the electrodes's widths d_i.

has dimensions $R_1 = 2.5mm$ and $d_i = 3.5mm$, instead of the real dimensions $R_1 = 2.5mm$ and $d_i = 3mm$. Considering that the gaps are of $\approx 0.3mm$ each, this slight modification in d_i is justified.

We can conclude that the theoretical analysis of the anharmonicity is quite correct, except for the fact that we lack knowledge on the actual axial motion amplitude, and that effective trap dimensions have to be used which are slightly different to the real ones. These facts confirm that we can readily rely on our extrapolations to low temperatures and smaller traps when building a quantum computer made of planar traps.

3.2.5.1 More measurements on the anharmonicity

In order to show how unstable was this measurement I plot next different measurements under similar electron creation conditions with the same trap parameters: $V_1 = 0V$, $V_2 = 13.6V$. Figure 3.23 shows the huge variation seen in the anharmonicity curve. This has to do mainly with filling the trap with different amount of electrons each time. The more electrons we have, the more electrons contribut-

ing to this curve have a bigger A than considered previously. This affects not only the height at which the curve is positioned but also its shape as can be seen. In figure 3.23 we see that the experimental curves with triangles and stars have
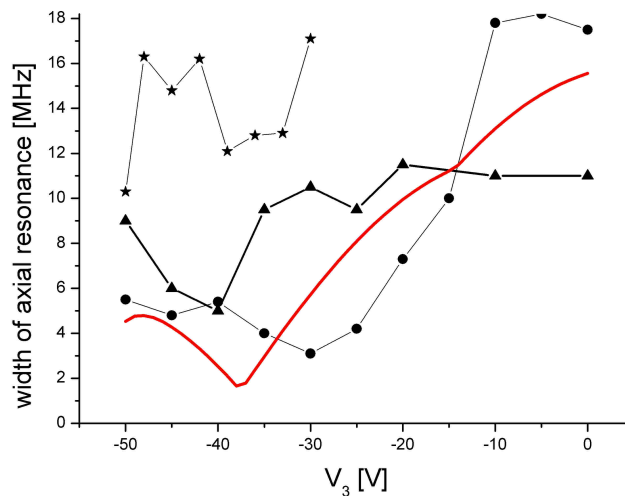

Figure 3.23: Width of the axial resonance, theoretical and experimental. For the theoretical curve(solid line) we have chosen $A = z_0/5$ and the artificial widths $d_i = 3.5mm$. The applied voltages are $V_1 = 0V$, $V_2 = 13.6V$. Error bars (of about 10%) have not been drawn for clarity.

a minimum coinciding with the theoretical one. Of course, we had to previously adjust d_i as done in the previous section. It is rather peculiar that the experimental curve with circles has the shape which is most similar to the theoretical one, but at the same time their minima don't coincide. This points in the direction of considering other definitions of anharmonicity which are more realistic when motional amplitudes are big enough to break the perturbative approach given in our theory.

3.2.5.2 Other definitions of anharmonicity

The easiest redefinition of anharmonicity for big amplitudes seems to be

$$\kappa = \frac{\Delta\omega_z}{\omega_z} = \frac{|\omega(z_0 + A) - \omega_z| + |\omega(z_0 - A) - \omega_z|}{2\omega_z} \tag{3.3}$$

where $\omega(x) = \sqrt{\frac{q\phi''(x)}{m}}$ is the "frequency" in position x. This expression is obviously the average of deviations from ω_z at the extrema of the axial motion of electrons. This simple definition is however rather powerful, as can be seen in figure 3.24. Figure 3.24 is exactly like fig.3.23 but with the theoretical curve substituted by the new definition, which is represented here with a dashed line. The new definition presents a shape similar to precisely the experimental curve which didn't fit with the standard theoretical curve, which means that in that experimental case the motional amplitudes were so big that a perturbative scheme would not fit anymore.
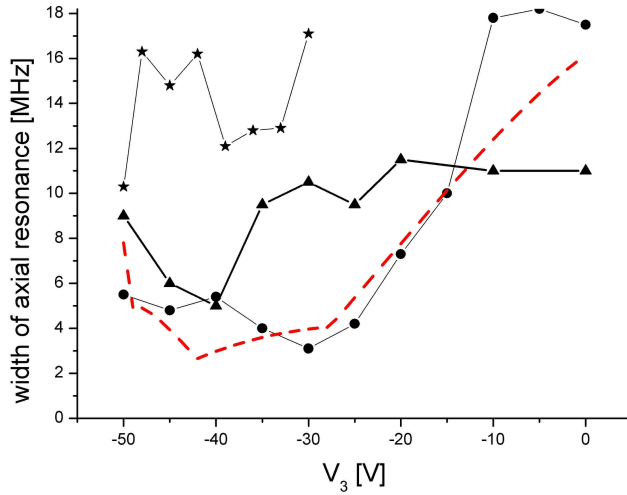

Figure 3.24: Width of the axial resonance, theoretical and experimental. For the theoretical curve(dashed) we have chosen $A = z_0/5$ and the real widths $d_i = 3mm$. The applied voltages are $V_1 = 0V$, $V_2 = 13.6V$.

We could make further definitions with a higher level of complexity, such as averaging in more points, rather than only in $z_0 - A$ and $z_0 + A$, or averaging with

some weight factor related to the amount of time that an electron spends near that points. However, these other definitions don't give any further insight in the problem and yield a rather similar shape. Therefore they will not be presented here.

I would like to stress the fact that these definitions are an important point only if our cloud of particles has not been cooled down either by thermalization to a cold environment, resistive cooling due to coupling with a tank-circuit, or by active methods such as Doppler cooling.

The shape of the anharmonicity versus V_3 should, in any case, be considered as a qualitative description of the system's behaviour. In order to study the problem in a realistic way, we would need to reproduce the experiment numerically in a computer. That means that we would have to emulate numerically the trapping, excitation and ejection of trapped electrons for every step in frequencies, and then note down the width of the resonance curve; and this for every single step in V_3. This procedure is implemented in next chapter.

3.2.5.3 Anharmonicity in V_2, V_3 space

The last measurement on the harmonic properties of our planar Penning trap was done more for scientific curiosity than anything else. The good agreement between theory and experiment is further confirmed if we plot the width of the axial resonance for varying V_2 and V_3. In figure 3.21 we saw that the theoretical analysis agreed with experiment for varying V_3 and with an equivalent width $d_1 = 2d_2$, thus confirming the theoretical behaviour for different electrode sizes. So it is a matter of completeness that I checked the behaviour for varying V_2 and V_3.

The result is figure 3.25 and figure 3.26, where we see that a good agreement is also achieved when varying parameter V_2 too. In figure 3.25 I've pointed out the places where the anharmonic terms C_3 and C_4 are minimized [1]. In figure 3.26 it can be seen that those lines coincide with the theoretical lines. The red points are the theoretical curves plotted for every V_2 used in the experimental curves.

---

[1] in fig.3.23 we saw the C_3 minimization which gives the minimum annharmonicity and the C_4 minimization which was a slight "bump" at around $V_3 = -13V$, in the theoretical curve
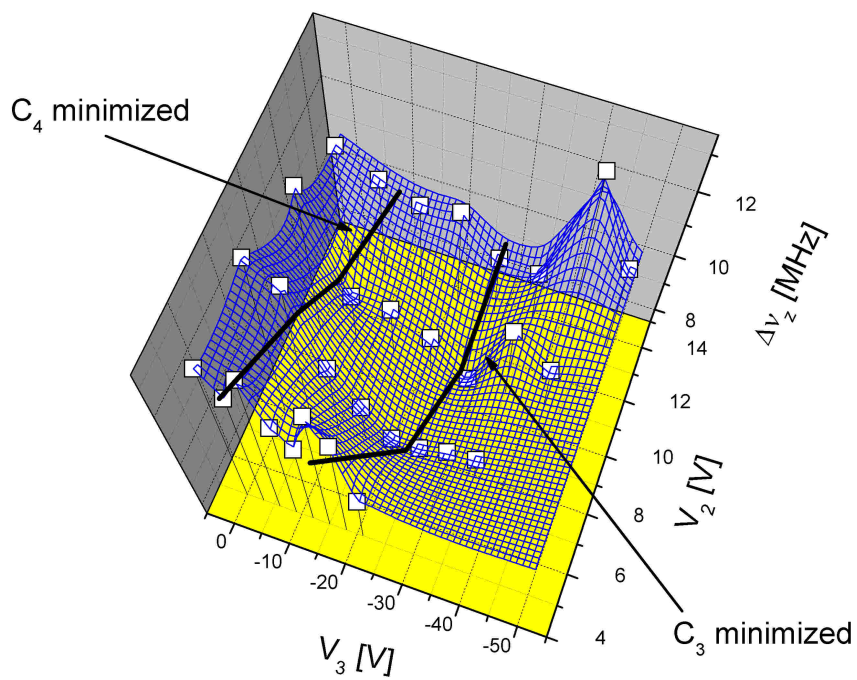
Figure 3.25: Width of the axial resonance measured for varied V_2 and V_3. As usual we have chosen $V_1 = 0V$. The white points are experimental values, and the blue grid is a surface fit to guide the eye.
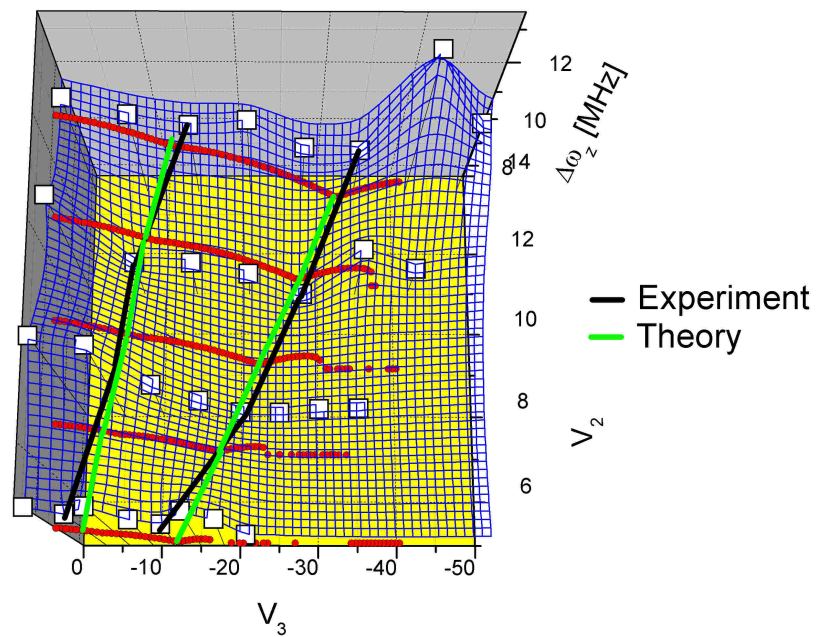
Figure 3.26: Comparison of the measurement in figure 3.25 with the theoretical curves (red points). The C_3 and C_4 minimization lines in green (theory) and black (experiment) show good agreement.

Finally we can conclude that, despite of the little shift due to the size of electrodes being effectively bigger than their real size (remember this was due to the gaps between them), the theoretical prediction for the width of the resonance is quite accurate, and most important of all, it is quite trustable when searching for the corrector voltage needed for optimum harmonicity. This ensures our success in the manipulation of the planar trap by just using our simple theoretical approach, without the need for further and more complex studies.

3.2.6 $2\omega_z$ resonance shape

The subject of this section is not related to the QUELE project, but is interesting enough in itself so as to deserve our attention. The fact that our trap is intrinsically asymmetric leads to an electrostatic potential whose deviation from quadrupolar ideality is dominated by its C_3 term (hexapolar contribution) rather by its C_4 term (octupole). In contrast, the rest of Penning traps, having reflection symmetry along z-axis at the position of electrostatic minimum, have a negligible C_3.

Since we are used to seeing axial resonances at $2\omega_z$ which show COM and individual peaks, as measured in traps with a dominating C_4 I felt quite curious to check whether any major difference could be seen in such plots. Therefore, I performed several frequency scans not only of $2\omega_z$ but also of ω_Z.

A numerical comparison with experiment was done in (Valenzuela) showing that the expected shape for the individual resonance was that of a trapezoid, as can be seen in fig.3.27 (fig.6 in their paper):

From all frequency scans I did, most of them resembled the shape in fig.3.27 but were never exactly equal, and always had a particular feature which made them singular. The first results I present here were all done for conditions of maximum harmonicity, that is, choosing V_3 so that the potential would be most harmonic, even if the voltage configurations vary from one graphics to another[1]. Three of those plots are shown in figure 3.28.

In figure 3.28 we see the individual resonance tend to a trapezoidal shape, but with a protuberance in its right edge. In addition the third plot shows a steep peak in the middle of the individual resonance; this third plot is not exactly the most harmonic configuration since, if the reader remembers, for $V_1 = 0V$ and $V_2 = 13.6V$ the best harmonicity is obtained for $V_3 = 33.67$ and not $V_3 = 30V$.

This discrepancy may have to do with the fact that C_3 dominates our trap, and not C_4, but could also be an artifact of the frequency scan. This can only be

---

[1]The reader may wonder why, if the three plots have been made for most harmonic configurations, the shapes are not similar. It should be noted that prescription of the harmonic properties C_3 and C_4, only implies a characteristic of the potential shape at z_0. Therefore these three shapes have nearly equal C_3 and C_4 at the minimum, but their shapes need not be equal along the trajectory of electrons. This accounts for the different individual resonance shapes.
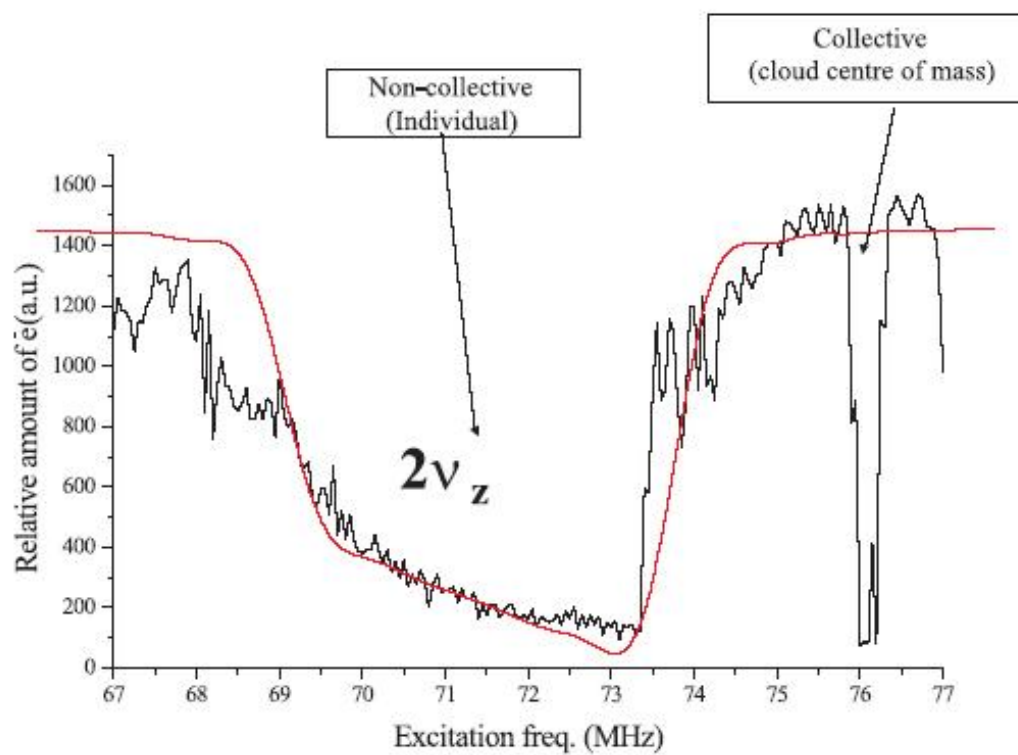
Figure 3.27: Frequency scan at $2\omega_z$, experimental and numerical in (Valenzuela). The expected individual resonance has a trapezoidal shape.
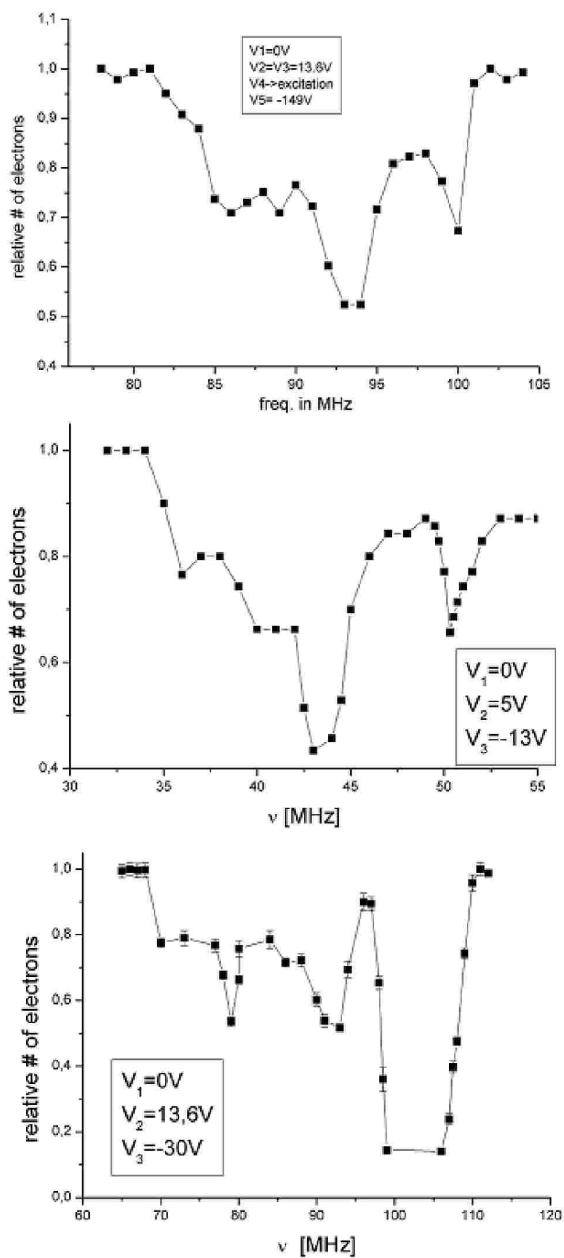
Figure 3.28: Individual and COM axial resonances (at $2\omega_z$) for different voltage configurations, optimized for best harmonicity.

analyzed if we perform a numerical simulation of the electrons trajectories.

It should be noted, however, that minimizing the anharmonicity is equivalent to minimizing the C_3 term, since it is dominant, in whose case C_4 is not minimized.

An example of frequency scan with minimized C_4 can be seen in figure 3.29, which shows that the shape is more similar to a trapezoid than in fig.3.28. Furthermore, a dip or cut can be seen in the middle of the individual resonance, which claims for an explanation[1].

I would like to add the fact, that I found this "cut" or dip in several frequency scans done for the same condition of C_4 minimized.
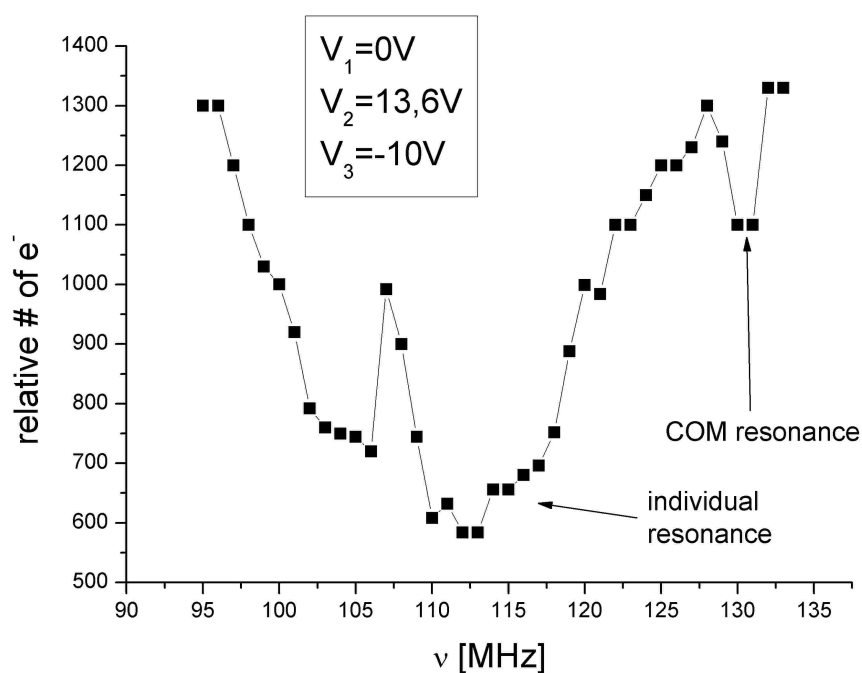
Figure 3.29: Individual and COM axial resonances with minimum C_4. The individual resonance has a trapezoid-like shape, but with a dip in its middle.

---

[1]The asymmetric C_3 term, effectively tilts the potential around z_0, in such a way that its left and right parts have effectively different curvatures. This might lead to a slight bifurcation of the axial eigenfrequency. If this is true, the same effect should be observable in the COM peak, if we were to scan it with more detail.

We can conclude that the individual and COM resonances in the case of a planar Penning trap are similar to those already found in different experiments with standard Penning traps. However, a dip in the individual resonance was found which lacks for an explanation.

3.3 Small Trap

One of the standard criteria for a device to be a candidate for quantum computing is scalability. A device is considered scalable if we can reduce its size without compromising computability, but also if we can use an arbitrary number of them to increase the computational power of the computer. In the case of classical computers, which use classical electronic elements, it is said that it is scalable because its constituents can be made smaller and more abundant in number without reaching any limit in principle. After some decades of computer development, the CPUs have been every time more powerful and smaller, but a future limit is foreseen due to the inherent quantum limits of their elemental constituents. It is clear thus that no device is infinitely scalable, but classical CPUs are scalable enough to be usable.

The situation is exactly the same for quantum computers: we want them to be usable, that's our main concern. And given the current status (a quantum computer occupies a whole laboratory and is only able to factorize the number 15) scalability is a must.

In order to test the properties of the planar trap under miniaturization, we built a trap which had a characteristic size half of the one used in the former measurements. It would have been much better to build a trap an order of magnitude smaller, but it would have been much harder to manipulate. In any case, the QUELE project will build a trap much smaller than the one used in this thesis for the first really quantum measurements. We can consider hence our "small trap" as a preliminary study of the scaling behaviour of a planar trap.

3.3.1 Description

In figure 3.3 we saw the design of our small planar trap, which was built with the same proportions as the big one but with half its characteristic size. It must be noted that the fabrication of both traps was done with gaps between electrodes of the same width, that is $0.3mm$. Therefore, the experimental results for the small trap are expected to differ more from the theory than for the big trap.

Apart from that, no big difference was expected, and no difference was seen, as will be shown next.

3.3.2   Results

The first thing I measured was the axial resonance. Its shape and positioning can be seen in figure 3.30:
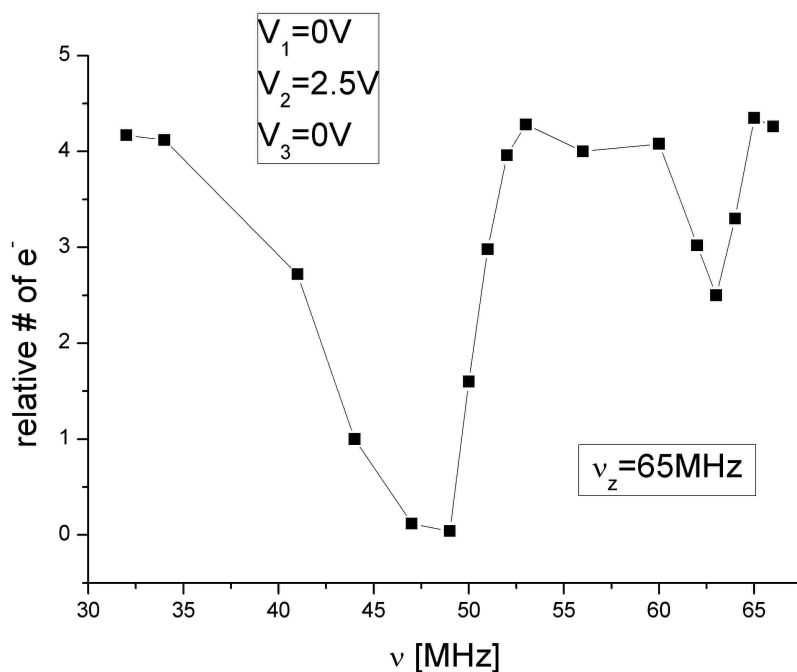

Figure 3.30: Individual and COM axial resonances in the small planar trap, measured at the subharmonic $\nu_z/2$.

The frequency scan was done with the same parameters as before, I mean creation times, filament current, ejection time, trapping time, etc. The voltage were $V_1 = 0V$, $V_2 = 2.5V$ and $V_3 = 0V$. It is seen in figure 3.30 the COM and individual peaks, as expected. No big difference with respect to the big trap is seen apart from the fact that both peaks are further from each other. That's not at all a surprise since we have used the same loading parameters, being the storage volume smaller (as the trap itself). A similar number of electrons is thus stored in a smaller volume thus producing a higher charge density. The higher the charge density, the further apart the peaks appear, as expected.

119

I next measured the storage time to check the stability of electrons in the small trap. The result is seen in figure 3.31. Recall that for the big trap the storage time was of $\tau = 22s$, and here the storage time is about $\tau = 2.5s$. There is an order of magnitude between both storage times, however we cannot associate it to the size-scaling of the traps since storage times are only shortened by higher rest gas pressures or bigger coupling of the spatial modes(field inhomogeneities). I do not believe that this trap produces a less homogeneous electrostatic field thus achieving axial-magnetron coupling, but rather that the alignment of the trap parallel with the magnetic field was harder to achieve "by eye" (or "by hand" if you like it more). Recall that misalignment was the responsible for motional couplings to the magnetron motion, and thus broadening of the electron's orbit until the electron gets out of the trapping volume.
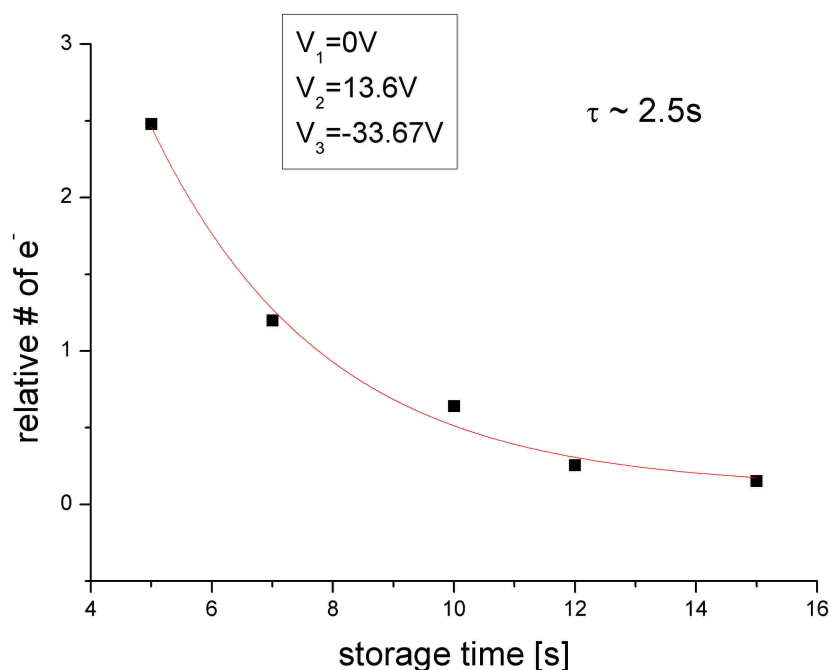
Figure 3.31: Storage time in the small trap for best harmonicity conditions.

To finish with our studies, I checked the anharmonicity curve, which gives surprisingly good results. In figure 3.32 we see that the shape is similar to the theoretically expected one. The main differences are that the width at best harmonicity is bigger than expected from theory, and that the points of C_3 and C_4 minimization are shifted leftwards in experiment. The latter fact is similar to what we saw for the big trap, since the gap between electrodes makes the electrodes effectively bigger.
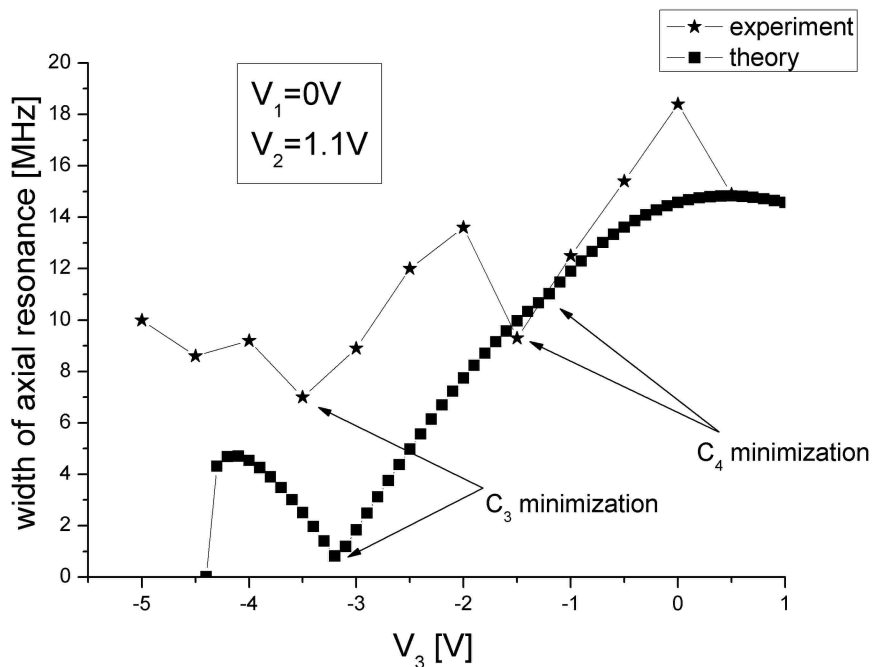

Figure 3.32: Width of the axial resonance for small trap. Axial frequency for these voltages is $\nu_z \approx 54\text{MHz}$.

3.3.3 Discussion

The main features we have presented for the small trap seem to be predictable from our theoretical model and present no lack of scalability. In fact the only

point where a bad scaling could have been seen is the storage time. A short storage time always indicates low stability of the trapped electrons, which is not the case here. I have argued that the storage time of the small planar trap is an order of magnitude worse than in the case of the big trap because of trap misalignment with respect to the magnetic field. This subject could be extended and studied in more detail but I don't see any reason why the storage time would have to be worse for smaller traps (if we are to align those traps with better techniques than just by eye).

Furthermore, a magnetic field of at least 7 Tesla will be used for the future QUELE experiment, thus improving the storage time by a factor of ~ 12.

I conclude hence the experimental studies with a positive feeling of success. The experiment agrees quite well with the theory and supports the idea of using the planar Penning trap as a tool for quantum computation.

Chapter 4

Numerical simulation

The fact that experimentally searching for the eigenfrequency of an harmonic oscillator needs the introduction of an oscillatory force, transform the system from a simple harmonic oscillator to a forced harmonic oscillator. This is just an example of the abstract fact that any knowledge we acquire in this material world comes from interaction; a fact which we tend to forget. An harmonic oscillator has naturally a unique eigenfrequency, but in the very moment that an experimentalist wants to know what this frequency is, he/she needs to transform the studied system in a forced harmonic oscillator system. The result of this want for information transforms the unique eigenfrequency, a Dirac delta function in frequency space, into a broad resonance curve of Lorentz type. This simple fact poses no problem, since that resonance curve is centered at the original unique eigenfrequency, and thus the wanted information can be extracted from the system.

The case is completely different when the system under study is not any more an harmonic oscillator, which is the case when the electrostatic trapping potential is not perfectly quadrupolar (a parabola in the spatial direction of interest). In that situation the inherent frequency characteristics of the system is a curve with a certain width, given by the amount of anharmonicity of the potential. That width is normally obtained by numerical simulation of the trajectory, which is afterwards Fourier analyzed. The problem is that our experimental method introduces a width in the resonance because we are transforming the original system into a forced one. The width coming from this transformation adds to the

intrinsic width of the original anharmonic oscillator. This fact obliges us to study the forced anharmonic oscillator if we want to make a comparison between the experimental results and the theoretical one. In other words, we can't just take the anharmonicity as defined in the theory section, κ, and compare it to what we obtain in the experiment.

This fact alone already justifies a numerical simulation of our system, but there is a further reason. The resonance curves obtained experimentally showed an individual and COM peaks, whose existence must be traced to the fact that our system is not that of a collection of harmonic oscillators, but has a Coulomb interaction between oscillators. This repulsive Coulomb force separates the individual and COM resonances, and gives the characteristic shape of the individual peak. Furthermore we saw that the individual resonances we obtained had not a shape similar to those in Penning traps with reflection symmetry along z axis, making us suspect the possible influence of the asymmetry in the potential provided by our planar trap in this discrepancy.

For all this reasons I decided to implement a simple numerical simulation. The objective is to serve as a link between the theory and the experiment, both regarding the behaviour of the anharmonicity and the shape of the individual resonance.

4.1 Description of the simulation

The numerical simulation was performed by a typical implementation of the Runge-Kutta algorithm of fourth order for solving the trajectories of an ensemble of N trapped electrons embedded in the potential of our actual planar trap and a magnetic field of 2 Tesla. The potential used was the one of our standard derivation, uniformly extended in ρ since the simulation cycles were much shorter than the characteristic period for magnetron motion, and thus this motion could be neglected. The creation process was simulated by an initial random positioning of electrons inside the trapping volume. The initial velocity of the electrons was zero, since an initial velocity is equivalent to having the same particle place at a position with higher potential. Real parameters for the Coulomb interaction were used.

The measurement cycle can be summarized as follows: electrons are created randomly inside the trapping volume with zero velocity, then the system is let evolve with a global force acting on it of the type $F_0 cos(\omega t)$ for a given time τ. After that time, the amount of electrons having left the trapping volume are recorded. This measurement is done $N_{stats.}$ times for a particular ω, and we run over ω from ω_{min} to ω_{max}.

Since the evolving algorithm for the trajectories is a fourth order Runge-Kutta integration method, the time step has to be three to four orders of magnitude smaller than the characteristic period of the fastest motion, in this case the cyclotron. So I decided to use a time step of $h = 10^{-12}s$, which was the biggest time step which allowed for a realistic trajectory. The measurement cycle was characterized by $\tau = 10^{-7}s$ which for an axial frequency of $\nu_z \approx 50$MHz is about 4 axial periods. This proved to be a time reasonably long enough for the forcing term $F_0 cos(\omega t)$ to act.

The artificial introduction of a damping term in the motion was avoided since it tends to broaden the resonance curve, and I wanted to study the pure effect of the anharmonicity.

The relative slowness of computers nowadays (3.06GHz clock speed in this case) obliged me not to simulate the actual number of trapped particles, which as shown in the experiment section was about 9000 electrons, but rather an amount of 10-20 electrons. This number of electrons has been seen to be enough to describe perfectly well the separation in individual and COM resonances in previous simulations(Blumel).

4.2 Results

I reproduced the measurement cycle described above in order to obtain the resonance curve of the axial motion, in which we are now interested. I did several scans, varying the strength of F_0, but also varying the length of the trapping volume A_z. The trapping volume is characterized by the length along z, A_z and the length along ρ, A_ρ. The radial length I chose was the actual one $A_\rho = R_1/5$ and for axial I chose $A_z = 0.3z_0$. With those numbers I obtained the resonance curves for a potential configuration of $V_1 = 0V$ and $V_2 = 13.6V$, with varying V_3. The

results is seen in figure 4.1. There we see that the behaviour coincides extremely well with the theoretically predicted one. The error bars are big because I didn't do much statistics ($N_{stats.} \sim 20$), since I used my personal computer and I didn't want to burn it up in a few weeks. The curve obtained by simulation shows both a coincidence in the minimum anharmonicity and also in the minimization of C_4 at $V_3 \approx -10V$. It shows that a minimum anharmonicity of $\approx 18\text{MHz}@\approx 55\text{MHz}$, is obtained whereas the theoretical value is smaller.

To sum up I can say that the simulated aharmonicity is in the way between the experimental and the theoretical results.
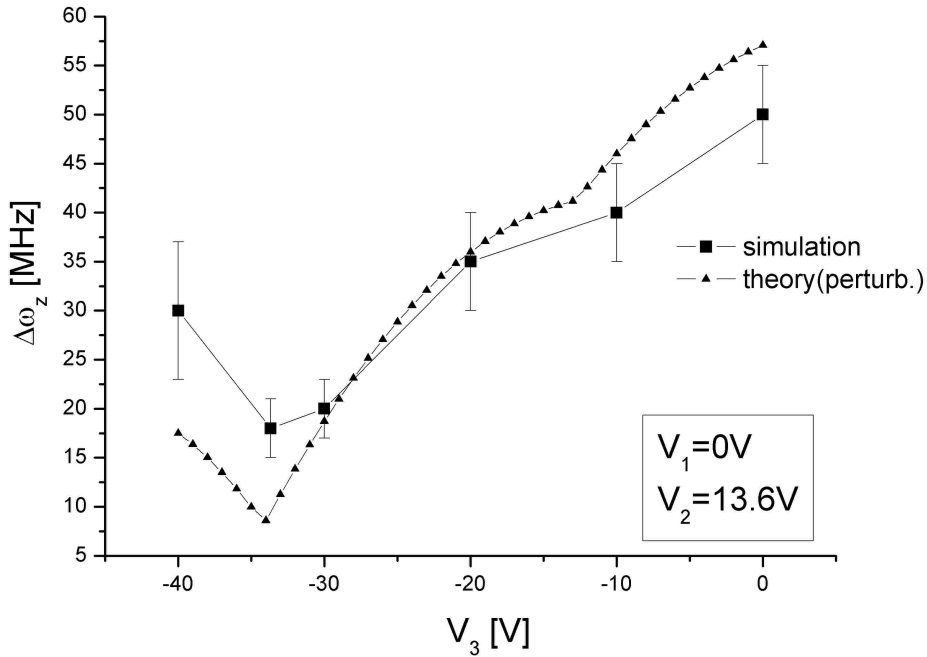

Figure 4.1: Anharmonicity curves from theory and simulation.

4.2.1   Shape of the resonance

In order to resolve the individual (non-collective) and the COM (collective) peaks of the axial resonance, best seen at $2\omega_z$, the electron density has to be high enough, since the distance between them is proportional (for low densities) to that density. A simulation with 10 electrons might have been good for studying the harmonic properties of the potential, but not for resolving these two peaks. Therefore, I could either increase the number of simulated electrons, or reduce the volume of creation. It can be at first thought that increasing the number of electrons in the simulation slows it down, but reducing the creation volume doesn't. This is not true because by reducing the volume, the electron trajectories are closer and their mutual Coulomb repulsion bigger. Being the force bigger we need a smaller time step to simulate correctly the trajectories, and we end up with a bottleneck: neither possibility is better than the other.

Of course this reasoning is rather qualitative and cannot be trusted. The computability of a problem has to be calculated in terms of amount of operations per cycle, and this is a function of the amount of electrons and the time step needed to correctly simulate the trajectories. Since I didn't want to enter into the exact dependencies, I just played around with both numbers: electron number and creation volume. I quickly realized that reducing the volume is much cheaper in terms of CPU times.

Because the Coulomb force for electron 'i' has to be calculated for every $j \neq i$, the number of operations' scaling is polynomial in N ($N(N-1)$), which is rather intuitive. The amount of operations is inversely proportional to h (time step), but h^2 must be inversely proportional to the applied forces in the problem. The Coulomb force goes as $1/d^2$ with d being a characteristic distance between particles, and $d \propto V^{\frac{1}{3}}$, so finally $h \propto V^{\frac{1}{3}}$. To sum up, increasing the number of electrons increases the number of operations polynomially, and decreasing the volume increases the operations number as $V^{-\frac{1}{3}}$. It has become clear that the best strategy is to reduce the volume.

I reduced the volume quite a lot: $A_\rho = R_1/35$ and $A_z = 0.025z_0$, which needs an amount of 4.7 electrons to reproduce the experimentally observed density. Hence, I used 5 electrons inside that tiny volume. Since I have reduced the

volume by a factor 587 with respect to the anharmonicity simulation, I need to reduce h by a factor $587^{1/3} \simeq 8.4$, then I must choose $h = 0.12 \times 10^{-12}$ [1].

I used $N_{stats.} = 40$ and a voltage configuration $V_1 = 0V$, $V_2 = 13.6V$ and $V_3 = -33.67$, i.e. the most harmonic configuration. The result is seen in figure 4.2.
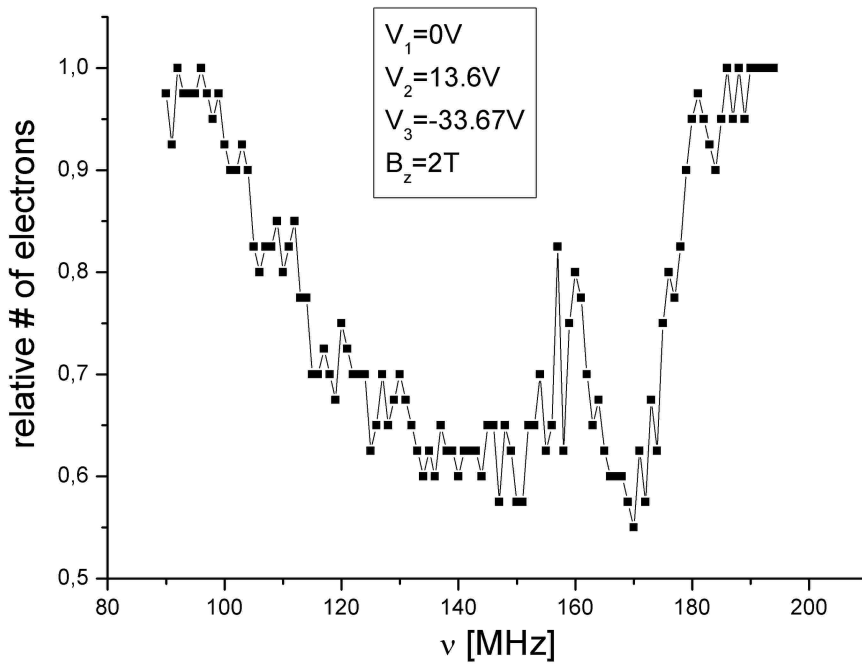

Figure 4.2: Resonance shape at twice the expected axial frequency. The COM peak (right), the individual peak(left) and a bistability zone in between, can be seen.

In fig. 4.2 it is seen that the individual resonance on the left is broad and has the expected trapezoidal shape. The region between this peak and the COM peak (right) shows a bistability, which means that electrons are oscillating at either the COM or individual frequencies with equal probability. In terms of an anharmonic

---

[1]A rather wonderful surprise came when I later found that with a time step 80 times bigger the same result was obtained.

driven oscillator, there's a frequency bifurcation at $\nu_{drive} \sim 158\text{MHZ}$.

The fact that the individual peak shows none of the peculiarities seen in the experiment, might point the lack of more abundant statistics on the experimental side.

A further comment on fig. 4.2 is that both peaks are overlapping (and hence the bistable region in between), whereas in experiment they were separated by about 10MHz.

It was seen in the experimental section that a voltage configuration which minimizes C_4 showed a dip in the middle of the individual peak. I ran a simulation with that configuration and no dip was seen. I fine tuned every possible parameter in the simulation but still no dip resulted. The conclusion is that either my simulation cannot resolve that subtle nonlinear effect, or that the dip is an experimental artifact. I rather believe in the first explanation, since I saw this dip in several runs of the experiment and under different conditions. A third possibility is that both evidences are correct, and therefore some hidden elements has not been included in the simulation.

4.3 Conclusions

The simulation has confirmed that despite the different concepts of eigenfrequency of an anharmonic oscillator and resonance curve of an anharmonic forced oscillator, the results are qualitatively very similar and that we can trust our simple theoretical derivation and predictions, at least regarding the compensation of anharmonicities of the potential.

The nonlinear effects of those anharmonicities plus the inclusion of the Coulomb perturbation in the simulation showed the expected individual+COM peaks behaviour, though not reproducing the surprising experimental curves. The deviation in experiment from the typical trapezoid-shaped individual peak's curve was not seen in the simulation, probably because of a lack of precision in the simulation[1].

---

[1]One could also argue that there is a lack of experimental data points.

4. NUMERICAL SIMULATION

It can also be hypothesized that some unknown element which was present in the experimental situation has not been included in the simulation. I would like to remind the reader that the simulation was done neglecting the magnetron motion, and any nonlinear effect related to this motion would not be seen, for example the effects of misalignment of the trap with respect to the magnetic field. Being this topic of no big importance for the development of the QUELE project it is left for future investigations.

Chapter 5

Conclusions

This thesis has been devoted to the investigation of confinement in a new type of trap, the planar Penning trap. The basis for this new concept is to be found in the well known and since long used Penning trap, which has been a rather useful tool for several decades. The development of this new kind of trap had a most definite purpose, the construction of a useful tool for quantum computing with trapped electrons, but may lead to other useful applications such as quantum information storage, studies of the decoherence caused by a conducting surface near a quantum system. It can further be used for typical high precision measurement such as that of masses or g-factors. Only the future can judge whether this new tool will prove useful or else be discarded as redundant.

In the chapter of theory I investigated the properties of this trap under the light of an easy theoretical approach, based on the cylindrical polynomial expansion of the potential. The potential was obtained for $\rho = 0$, and from there on properties such as the depth of the potential, position of the minimum, axial eigenfrequency and harmonic properties of the axial potential were studied. The amazingly simple expression for the potential along the z axis proved to be quite powerful and easy to handle.

Several proposals for the quantum communication between different qubits, qubits being stored in the axial degree of freedom of different singly-trapped electrons, were given and their rates calculated. This showed the feasibility of using those methods for a coherent control of the quantum states and quantum operations between them.

5. CONCLUSIONS

An experimental confirmation of those properties was given in chapter 3 and also a comparison with the theoretical model. A good qualitative agreement with the theory was shown. Quantitatively, the theory proved to be a good approximation, further approaching the actual experimental results when "equivalent" electrode sizes were used, showing that compensation of potential's anharmonicity could be compensated with a correction voltage very close to the theoretically predicted one. Further, a good storage time was found for a magnetic field of 2 Tesla, proving that confinement is sufficiently stable even at room temperature and a quite improvable vacuum condition.

The possibility of a double well configuration was theoretically shown and experimentally hinted, leaving the perfection and manipulation of such configuration for future researchers which might be interested.

In chapter 4 I tried to link the experiment and the theory with a numerical simulation. The confirmation of the anharmonicity compensation behaviour was shown to agree rather well with theory. I also studied the shape of the $2\omega_z$ resonance curve to check for similarities with the shapes obtained in experiment. However, my simulation couldn't resolve those surprising experimental results proving that the simulation was not realistic enough, or that it may lack some important element. This side study, not very important for quantum computing, was therefore left for future researchers which might want to test the nonlinear effects involved in the formation of such newly found shapes, particularly the one where C_4 was minimized, i.e. with a basic anharmonicity coming from the C_3 term. Since the asymmetry of this trap under reflection in z axis lends itself to a natural maximization of the C_3 term, it might prove useful in future researches on comparing theoretical results for the hexapolar-perturbed Penning trap with experiments.

A briefer conclusion can be given: the planar Penning trap works, provides stable confinement, its anharmonicites can be compensated and it can be trusted in future implementations of quantum computing. What else can one ask for?!

Acknowledgements

The chain of causation is long, so long as the Universe. We should always first acknowledge the Universe for creating our solar system and the earth, then the evolution of the earth for giving birth to a human species, then to the whole chain of mankind till we arrive to our nearest ancestors: parents, grandparents,etc. In my particular case I should also thank several other offspring chains, mainly related with the appearance of human beings like Prof. Werth (in whose group I have been brought up in the art of experimental physics), and the rest of colleagues which have made my thesis possible. Among them, mainly Paula Fernández, with her infinite patience and inner energy, who pushed the experiment through until it was made to work. I would also thank the temporary, but intensively fruitful lab collaboration with Dr. Alexandros Drakoudis. In addition, I should thank Joseba Alonso, whose recommendation made me a candidate to work in Prof. Werth's group.

I wish to thank also fruitful discussions with other scientists, for example Dr. Stefan Stahl, Prof. G. Werth (most of all), Tristán Valenzuela, Rafael Ferrer, Joseba Alonso and Dr. Manuel Vogel, just to begin with. I've had also valuable information exchange with the rest of the former group, see photo in "www.physik.uni-mainz.de/werth/", and with the newly formed group of Prof. K. Blaum.

I want to thank also Prof. K. Blaum and Prof. J. Walz for allowing our experimental work to be done in their laboratory and with their superconducting magnet. In particular to Prof. J. Walz for the period of time when he led our

experiment.

Last, to close the loop, I thank again the Universe, with its many wonders and mysteries, which scientists are so fond of speculating about. Even if scientific discoveries were not to make humans more noble or wiser, it would still be so much fun.

Bibliography

[Cirac] J.I. Cirac and P. Zoller, Quantum computation with cold trapped ions, *Phys. Rev. Lett.* **74**, 4091-4 (1995) 1

[Gershenfeld] N.A. Gershenfeld and L.I. Chuang, Bulk spin-resonance quantum computation, *Science* **275**, 350-6 (1997) 1

[Kane] B.E. Kane, A silicon-based nuclear spin quantum computer, *Nature* **393**, 133(1998) 1

[Loss] Daniel Loss and David P. DiVincenzo, Quantum computation with quantum dots, *Phys. Rev. A* **57**, 120-126 (1998) 1

[Freedman] M. H. Freedman, A. Kitaev, Z. Wang, Simulation of topological field theories by quantum computers, *Commun.Math.Phys.* **227**, 587-603 (2002) 1

[Makhlin] Y. Makhlin, G. Schoen, A. Shnirman, Josephson-Junction Qubits with Controlled Couplings, *Nature* **398**, 305-307 (1999) 1

[Tombesi] G. Ciaramicoli, I. Marzoli, P. Tombesi, Realization of a quantum algorithm using a trapped electron, *Phys. Rev. A* **63**, 052307 1, 2.5

[Gödel] Kurt Gödel, Über formal unentscheidbare Sätze der Principia Mathematica und verwandter Systeme, *I. Monatshefte für Mathematik und Physik* **38**, 173-98 (1931) 1.1

BIBLIOGRAPHY

[Turing] Alan Turing, On computable numbers with an application to the Entscheidungsproblem, *Proceedings of the London Mathematical Society, Series 2*, **42**, 230-265 (1936) 1.1, 1.1.1

[Chaitin] Gregory J. Chaitin, *Scientific American* **259**, No. 1 80-85 (1988) 1.1

[Shannon] Claude E. Shannon, A Mathematical Theory of Communication, *Bell System Technical Journal* **27**, 379-423, 623-656 (1948) 1.1.1

[Bell] J.S. Bell, On the Einstein-Podolsky-Rosen paradox, *Physics* **1**, 195-200 (1964) 1.1.1

[Aspect] A. Aspect, J. Dalibard, G. Roger, Experimental test of Bell's inequalities using time-varying analyzers, *Phys. Rev. Lett.* **49**, 1804-7 (1982) 1.1.1

[Zeilinger] Anton Zeilinger,A Foundational Principle for Quantum Mechanics, *Foundations of Physics* **29**, No. 4 (1999) 1.1.1

[Benioff] Paul Benioff, The computer as a physical system: A microscopic quantum mechanical Hamiltonian model of computers as represented by Turing machines, *J. Stat. Phys.* **22**, 563 (1980) 1.1.1

[Deutsch] David Deutsch, Quantum theory, the Church-Turing principle and the universal quantum computer, *Proc. R. Soc. A* **400**, 97-117 (1985) 1.1.1

[Shor] Peter Shor, Polynomial-time algorithms for prime factorization and discrete logarithms on a quantum computer, *Proc. 35th Annual Symp. on Foundations of Computer Science*(Santa Fe,NM:IEEE Comp. Soc. Press) *Preprint* quant-ph/9508027 1.1.1

[Coppersmith] Don Coppersmith, An approximate Fourier transform useful in quantum factoring, *IBM Research Report* RC 19642 1.1.1

[Grover] Lov K. Grover, Quantum mechanics helps in searching for a needle in a haystack, *Phys. Rev. Lett.* **79**, 325-8 (1997) 1.1.1

[Kitaev] Alexei Yu. Kitaev, Quantum measurement and the Abelian stabilizer problem, *Preprint* quant-ph/9511026 1.1.1

[Werth] H. Häffner, T. Beier, N. Hermanspahn, H.-J. Kluge, W. Quint, S. Stahl, J. Verdú, and G. Werth, High-Accuracy Measurement of the Magnetic Moment Anomaly of the Electron Bound in Hydrogenlike Carbon, *Phys. Rev. Lett.* **85**, 5308-5311 (2000) 1.2, 1.3, 2.4.4

[Dyck] R. S. Van Dyck, Jr., S. L. Zafonte, S. Van Liew, D. B. Pinegar, and P. B. Schwinberg, Ultraprecise Atomic Mass Measurement of the alpha Particle and ^{4}He, *Phys. Rev. Lett.* **92**, 220802 (2004) 1.2

[Blaum] A. Herlert et al., Mass spectrometry of atomic ions produced by in-trap decay of short-lived nuclides, *New J. Phys.* **7**, 44 (2005) 1.2

[Gabrielse] S. Peil and G. Gabrielse, Observing the Quantum Limit of an Electron Cyclotron: QND Measurements of Quantum Jumps between Fock States, *Phys. Rev. Lett.* **83**, 1287-1290 (1999) 1.2.3, 1.3

[Wineland] D.J. Wineland, R.E. Drullinger and F.L Walls, Radiation-pressure cooling of bound resonant absorbers,*Phys. Rev. Lett.* **40**, 1639 (1978) 1.2.3

[Dehmelt] W. Neuhauser, M. Hohenstatt, P. Toschek and H. Dehmelt, Optical-sideband cooling of visible atom cloud confined in parabolic well, *Phys. Rev. Lett.* **41**, 233 (1978) 1.2.3

[Deutsch2] D. Deutsch, A. Barenco and A. Ekert, Universality in Quantum Computation, *Proc. R. Soc. A* **449**, 669-677 (1995) 1.2.3

[Wineland2] C. Monroe, D.M. Meekhof, B. E. King, W. M. Itano and D. J. Wineland, Demonstration of a fundamental quantum logic gate, *Phys. Rev. Lett.* **75**, 4714 1.2.3

[Blatt] F. Schmidt-Kaler, H. Häffner, M. Riebe, S. Gulde, G. P. T. Lancaster, T. Deuschle, C. Becher, C. F. Roos, J. Eschner and R. Blatt, Realization of the Cirac-Zoller controlled-NOT quantum gate, *Nature* **422**, 408-411 (2003) 1.2.3

[Tombesi2] G. Ciaramicoli, I. Marzoli, P. Tombesi, Trapped electrons in vacuum for a scalable quantum processor, *Phys. Rev. A* **70**, 032301 (2004) 1.3

BIBLIOGRAPHY

[Jackson] John David Jackson, *Classical electrodynamics*, 2nd edition (1975), ISBN 0-471-43132-X 2.2.1

[Sneddon] Ian Naismith Sneddon, *Mixed boundary value problems in potential theory*, Amsterdam : North-Holland Pub. Co., (1966) 2.2.2

[Sneddon2] I. N. Sneddon, *Proc. Glasgow Math. Soc.* **4**, 108 (1960) 2.2.2.1

[Galve] S. Stahl, F. Galve, J. Alonso, S. Djekic, W. Quint, T. Valenzuela, J. Verdú, M. Vogel and G. Werth, A planar Penning trap, *Eur. Phys. J. D* **32**, 139-146 (2005) 2.5

[Ciaramicoli] Giacomo Ciaramicoli, Fernando Galve, Irene Marzoli, Paolo Tombesi, Array of planar Penning traps as a nuclear magnetic resonance molecule for quantum computation, *Phys. Rev. A* **72**, 042323 (2005) 2.5, 2.5.2

[Sorensen] Anders.S. Sørensen, Caspar H. van der Wal, Lilian I. Childress, Mikhail D. Lukin, Capacitive Coupling of Atomic Systems to Mesoscopic Conductors, *Phys. Rev. Lett.* **92**, 063601 (2004) 2.5.1

[Wunderlich] Ch. Wunderlich, Ch. Balzer, T. Hannemann, F. Mintert, W. Neuhauser, D. Rei and P. E. Toschek, Spin resonance with trapped ions, *J. Phys. B: At. Mol. Opt. Phys.* **36**, 1063-1072 (2003) 2.5.2

[Galve2] Fernando Galve, Paula Fernández and Günter Werth, Operation of a planar Penning trap, *Eur. Phys. J. D* (2006), DOI: 10.1140/epjd/e2006-00152-9 1

[Paasche] P. Paasche, C. Angelescu, S. Ananthamurthy, D. Biswas, T. Valenzuela, and G. Werth, Instabilities of an electron cloud in a Penning trap, *Eur. Phys. J. D* **22**, 183-188 (2003) 3.2.1

[Desaintfuscien] J. Yu, M. Desaintfuscien, and F. Plumelle,Ion Density Limitation in a Penning Trap due to the Combined Effect of Asymmetry and Space Charge, *Appl. Phys. B* **48**, 51-54 (1989) 1.2.2, 3.2.3

[Valenzuela] P. Paasche, T. Valenzuela, D. Biswasa, C. Angelescu, and G. Werth, Individual and center-of-mass resonances in the motional spectrum of an electron cloud in a Penning trap, *Eur. Phys. J. D* **18**, 295-300 (2002) 1.2.2, 3.2.3, 3.19, 3.2.6, 3.27

[Tommaseo] G. Tommaseo, P. Paasche, C. Angelescu, and G. Werth, Subharmonic excitation of the eigenmodes of charged particles in a Penning trap, *Eur. Phys. J. D* **28**, 39-48 (2004)

[Blumel] R. Alheit, X. Z. Chu, M. Hoefer, M. Holzki, G. Werth and R. Blümel, Nonlinear collective oscillations of an ion cloud in a Paul trap, *Phys. Rev A* **56**, 4023 (1997) 4.1

BIBLIOGRAPHY

Curriculum Vitae

Fernando Galve Conde

Born the 19th of May of 1979, Valencia (Spain)

Nationality: Spanish

Family status: Single

Actual residence: Mainz

Education

1983-1993 Ground studies, Colegio Salesianos D. Juan Bosco, Valencia, Spain

1993-1996 High School, Colegio Salesianos D. Juan Bosco, Valencia, Spain

1996-1997 "COU+Selectividad" (Pre-universitary studies), Instituto S. Vicente Ferrer, Valencia, Spain

1997-2001 Physics career, Universitat de Valéncia, Burjassot(Valencia), Spain

2001-2002 Last year of Physics Career (as Erasmus student), Johannes Gutenberg Universitaet, Mainz, Germany

2002-2003 Diplomarbeit in Physik, Prof. R. Schilling's research group in condensed matter, Institut fuer Physik, Johannes Gutenberg Universitaet, Mainz, Germany

2003-2006 Doktorarbeit in Physik, Prof. G. Werth's research group (trap physics), Johannes Gutenberg Universitaet, Mainz, Germany

Titles

2002 "Licenciado en Fsica" (Spanish equivalent of Diplom Physiker)